FATE1: CONTRIBUTOR TO TUMOR CELL FITNESS AND EXAMPLE OF AN ONCOGENE-ACTIVATED CANCER TESTIS ANTIGEN

Patrick J. Taus

A dissertation submitted to the faculty of the University of North Carolina at Chapel Hill in partial fulfillment of the requirements for the degree of Doctorate of Philosophy in the Department of Pharmacology, School of Medicine.

Chapel Hill
2016

Approved by:

Angelique Whitehurst

John Sondek

Ian Davis

Mohanish Deshmukh

Lee Graves

ABSTRACT

PATRICK J TAUS: FATE1: Contributor to Tumor Cell Fitness and Example of an Oncogene-activated Cancer Testis Antigen
(Under the direction of Angelique Whitehurst)

Cancer Testis Antigens (CTAs) are a group of genes defined by their unique expression pattern, normally expressed nearly exclusively in gametogenic tissues they are also found aberrantly expressed in malignant tissues throughout the body. As a result of the immune-privileged nature of their normal site of expression in the testis, CTAs are capable of eliciting an immune response when expressed within tumors. As a result of their antigenicity, CTAs have been the intense studied as potential immunotherapy targets since their discovery in the early 1990s; however, in this time their possible functional contributions to tumorigenesis have been woefully under investigated. Here, we undertook the first comprehensive approach to define the functional contribution of CTAs to tumorigenesis. This screen identified numerous CTAs that support aspects of tumorigenesis. Further studies demonstrated that the uncharacterized CTA Fetal and Adult Testis-Expressed 1 (FATE1) is a major contributor to tumor cell fitness across multiple cancer lineages. We found that FATE1 is a mitochondrial protein that interacts with Mitochondrial Fission Factor (MFF) a mediator of mitochondrial fission and that expression of FATE1 is capable of altering mitochondrial morphology. Within the transformed cellular background, we find that FATE1 regulates protein levels of the tumor suppressor, Bcl-2 Interacting Killer (BIK), a pro-apoptotic member of the Bcl-2 protein family. We also found that BIK protein is degraded by the FATE1-interactor RNF183 a previously uncharacterized E3-

ligase. We found further in vitro and clinical data that supports the hypothesis that FATE1 and RNF183 form a functionally relevant complex within tumors.

Like their functional roles, the mechanisms by which CTAs are activated within tumors is currently unclear. Although demethylation plays a large role, epigenetic alterations alone are not sufficient to drive expression of all CTAs indicating that trans-acting factors are required. Here we find that FATE1 is a direct target of chimeric transcription factor EWS-FLI1, the oncogene responsible for the pediatric bone and soft tissue tumor Ewing sarcoma. FATE1 expression is required for short and long term viability of Ewing sarcoma derived cell lines. By leveraging a previously published EWS-FLI1 ChIP-seq dataset we nominate three additional CTAs (BORIS, MAGE-A4, and SPATA19) as EWS-FLI1 targets, two of which, MAGE-A4 and SPATA19 are required to maintain Ewing sarcoma cell viability. The results of these studies argue that not only do CTAs function to support tumor cell fitness but as targets of oncogenes they may potentially be key functional drivers in the early stages of tumorigenesis.

ACKNOWLEDGEMENTS

First and foremost I would like to thank my mentor, Dr. Angelique Whitehurst. Angelique has always been supportive of my current work and my future career as a physician-scientist. While writing this thesis I have been reminded of many things Angelique taught me, and I'm sure that will continue throughout my days as a scientist.

I would like to thank my committee including my chair, Dr. John Sondek, and members Dr. Ian Davis, Dr. Mohanish Deshmukh, and Dr. Lee Graves for the critical analysis they have given my project and their helpful insights at my committee meetings. I would also like to specifically thank Dr. Davis for serving as my clinical mentor while I was at UNC and Dr. Deshmukh for co-sponsoring my F30 grant application and helping to solve the administrative nightmare it became.

At UT-Southwestern I would like to thank Dr. James Amatruda for not only allowing me to round with him on the pediatric oncology service but also for his advice on the Ewing sarcoma chapter of my thesis. I would also like to thank Eunice Webb and Kathy Mercer for all their work keeping the department and lab running smoothly.

I would like to thank the members of the Whitehurst lab, past and present. Especially, Dr. Kimberly Maxfield, Dr. Becky Sinnott, and Josh Wooten with whom I made the "move". I would also like to thank the UTSW-crew: Dr. Ashly Pavlovsky, Brandt Nichols, and Jennifer

Macion, all of whom have made the lab a wonderful environment over the last two and a half years.

Last, but not least, I would also like to thanks my friends and family who have supported me for years, especially Mom, Dad, and Kathleen.

TABLE OF CONTENTS

LIST OF TABLES

LIST OF FIGURES

LIST OF ABBREVIATIONS AND SYMBOLS

Abbreviation/Symbol	Definition
Δ	Deletion
5-aza	5-aza-2'-deoxycytidine
AIRE	Autoimmune Regulator
AMPK	Adenosine monophosphate-activated protein kinase
APO	Apo-ONE Homogenous Caspase-3/7 Assay
ATAD2	ATPase Family, AAA Domain Containing 2
BAGE	B Melanoma Antigen
BH	Bcl-2 Homology Domain
BORIS	Brother of the Regulator of Imprinted Sites
CC	Coiled-coil
CD	Cluster of Differentiation
cDNA	Complementary DNA
COX6BII	Cytochrome c oxidase subunit 6BII
CTA	Cancer Testis Antigen
CTCFL	CCCTC-Binding Factor Like
CTRL	Control
EdU	5-ethynyl-2′-deoxyuridine
ETS	E26 transformation-specific
EWS	EWS RNA-Binding Protein 1
EWS-FLI1	EWS-FLI1 chimeric transcription Factor

FATE1	Fetal and Adult Testis Expressed 1
FLI1	Friend Leukemia Virus Integration 1
GAGE	G Antigen 1
HECT	Homologous to the E6-APCarboxyl Terminus
HIF	Hypoxia Inducible Factor
HORMAD1	HORMA Domain Containing 1
HR	Hazard Ratio
KM	Kaplan-Meier
LDHC	Lactate Dehydrogenase Isoform C
MAGE	Melanoma Antigen
MARCH2	Membrane-Associated Ring Finger (C3HC4) 2
MARCH5	Membrane-Associated Ring Finger (C3HC4) 5
MFF	Mitochondrial Fission Factor
MHC	Major Histocompatibility Complex
mTEC	Medullary Thymic Epithelial Cells
NF-κB	Nuclear Factor Kappa-Light-Chain-Enhancer of Activated B Cells
NSCLC	Non-small Cell Lung Cancer
NUMA1	Nuclear Mitotic Apparatus Protein 1
NY-ESO-1	New York Esophageal Squamous Cell 1
PBMC	Peripheral Blood Monocyte
PRAME	Preferentially Expressed Antigen In Melanoma
RING	Really Interesting New Gene

SEREX	Seriological Analysis of Expression cDNA Libraries
siRNA	Small Interfering RNA
SMAC	Second Mitochondrial-derived Activator of Caspases
SPATA19	Spermatogenesis Associated 19
SPO11	SPO11 Meiotic Protein Covalently Bound To DSB
SSX	Synovial Sarcoma, X Breakpoint
SYCE1	Synaptonemal Complex Central Element Protein 1
SYCP1	Synaptonemal Complex Protein 1
TCR	T Cell Receptor
TET	TLS, EWSR1, TAFII68
TEX15	Testis Expressed 15
TGFβ	Transforming Growth Factor Beta
TM	Transmembrane
TOM20	Translocase of Outer Membrane 20
TRIM	Tripartitie Motif
Ub	Ubiquitin
UPS	Ubiquitin Proteasome System
WCL	Whole Cell Lysate

CHAPTER I: INTRODUCTION

Similarities between cancers and germline tissues were first noted over one hundred years ago by British developmental biologist John Beard who proposed the Trophoblastic Theory of Cancer which proposed that cancer was the result of aberrantly localized trophoblast cells throughout that body [1]. Although the major tenets of this theory were disproven, numerous similarities between tumorigenesis and germ cell development were noted in the following century (Figure 1). In the last twenty-five years the similarities between tumors and germ cells have been demonstrated on a profound genetic level following the identification of genes highly expressed in those two entities. This group of genes, known collectively as Cancer Testis Antigens (CTAs), affords unique therapeutic opportunities through their immunologic potential and the potential novel insights they may functionally afford into tumor biology. As the work described herein focuses on Cancer Testis Antigens a review of their discovery, biology, and the current state of their therapeutic utility will be presented.

The Search for Tumor Antigens

Cancer is a disease of unchecked cellular proliferation within the body. In many instances cancer is treated with chemotherapeutic drugs and/or surgery; however, physicians and scientists have long sought to harness the body's own immune system against this disease. The potential of the immune system in cancer treatment was first recognized over 120 years ago by William B. Coley who treated inoperable cancers by injecting them with suspensions of live or dead bacteria

Although dangerous, in many cases these injections led to shrinkage of the tumors presumably do to immune system activity. Later in the 20th century, a second line of evidence that tumors were vulnerable to immune destruction emerged. In 1943 Gross and colleagues found that mice in which tumors were chemically induced and then resected were able to reject the same tumor cells upon subsequent inoculation [2].

Several decades later in the 1970s the prominent role of T cells in tumor rejection was realized. This knowledge, coupled to the discovery of how to select and expand cytotoxic T lymphocyte clones *in vitro* would allowed for the identification of tumor antigens targeted by cytotoxic T cells through immunoscreening assays in the following decades [3-5]. In 1988 Boon and colleagues found that *in vitro* mutagenesis of a mouse tertacarcinoma cell line led to the expression of novel antigens that were the targets of cytotoxic T cells [2]. Using these T cell clones to screen cDNA libraries obtained from the vulnerable tumor cell clones the Boon group identified the first three tumor antigens, each being a mutated version of an ubiquitously expressed protein [6-8]. Subsequently, the first non-mutated antigen was identified using the parental cell line, this antigen was derived from a gene of unknown function, *Trap1a* [9]. The antigenicity of *Trap1a's* protein product was due its restricted expression, the only normal tissues where it was detected were mouse spermatogonia cells and placental trophoblasts. Uniquely, both of these cell types lack major histocompatibility complex (MHC) class I molecules and therefore cannot present *Trap1a*-derived peptides to T cells [9].

Discovery of Cancer Testis Antigens

In the early 1990s, Thierry Boon's group utilized autologous typing to identify the first human tumor antigens [10]. In this technique cDNA libraries from a patient's tumor and normal

cells are screened against their own T cells to identify reactive T cell clones and the corresponding MHC Type I-loaded antigens they recognize. Using this method the Boon group discovered that expression of the gene MAGE-A1 rendered melanoma cells sensitive to destruction by autologous cytotoxic T-cells [10, 11]. It was subsequently discovered that among normal tissues the expression of MAGE-A1 was restricted to male germ cells and trophoblasts of the placenta [11]. Further analysis revealed that MAGE-A1 was a member of a large gene family consisting of over 40 proteins that contain a full or truncated MAGE homology domain [12]. The MAGE family can be divided into two categories: Group I MAGEs (-A, -B, -C) which are encoded on the X-chromosome and whose expression are restricted to the testis and Group II MAGEs (-D, -E, -F, -G, and –H) that are expressed throughout the body and are encoded for throughout the genome [12]. Autologous typing was used to identify additional CTAs including BAGE and GAGE which were identified using cytotoxic T-cells derived from the same patient in whom MAGE-A1 was discovered [13, 14]. In the mid-90s the identification of CTAs was further advanced by Serial analysis of cDNA expression libraries (SEREX), a technique in which cDNA expression libraries are screened with antibodies in lieu of T-cells [15]. Utilization of this technique led to the discovery of several CTAs including SSX, SCP1, and NY-ESO-1, the latter of which is a highly immunogenic CTA that is currently being targeted using multiple immunotherapy approaches [15-19].

Classification of CTAs

The application of large-scale expression analysis and proteomics has greatly expanded the number of genes classified as Cancer Testes Antigens; however, unlike the earlier techniques of autologous typing and SEREX in which the antigenicity of the CTAs was a requisite to their

discovery, little is known about the immunogenic potential of many CTAs discovered solely through differential expression analysis. Large scale expression analysis also made clear that many CTAs are expressed at low but detectable levels in somatic tissues [20]. Based on these observations, the current criteria for designation as a CTA is as follows: a protein must be expressed within tumors, the testis and/or placenta, and no more than two somatic tissues [21]. CTAs can be further defined into three groups by the stringency of their expression profile: 1) testis restricted – found only in the testis, 2) testis-brain restrictive – expressed in both the testis and central nervous system, 3) testis selective – expressed in the testis and no more than two somatic tissues at lower levels than in the testis [20].

In addition to classification based on their expression profile, CTAs can also be divided into two groups based on their location within the genome. Nearly half of the currently annotated CTAs are located on the X-chromosome and are designated as CTA-X genes. CTA-X genes tend to display a testis-restricted profile, are more antigenic than CTAs located on the autosomes, and are frequently composed of large, highly homologous families such as the previously discussed MAGE family [22]. Many CTA-X families are thought to be the result of recent evolutionary expansion due to their proximity to other family members and the paucity of orthologues in lower species [22]. In addition, members of CTA-X families are either expressed in groups or not at all, suggesting a common mechanism of activation for the family [23]. Within normal testis the CTA-X genes are typically expressed in the proliferating spermatogonia germ cells [24]. On the other hand, CTAs located on the autosomes share little sequence homology, are rarely members of gene families, and tend to be expressed during the later stages of spermatogenesis [19].

Immunogenicity of CTA antigens

Like all intracellular proteins CTAs are presented in MHC class I molecules on the cell surface, where, if recognized as foreign by circulating T cells, they can evoke an immune response (Figure 2). Initially, cancer testes antigens were discovered due to their antigenicity using autologous typing and SEREX techniques; however, with the recent reliance on gene expression analysis and large scale proteomic approaches to identify CTAs, the antigenicity of many newly identified CTAs is unknown. Which CTAs are immunogenic and why some CTAs can elicit varying degrees of immune responses amongst patients are critical questions whose answers will have significant repercussions on the use of CTAs as targets for immunotherapy. Here, the factors governing the antigenicity of CTAs and the current state of CTA-based immunotherapy will be discussed.

Male germ cell differentiation, and pregnancy in the case of trophoblasts, begins many years after the establishment of a competent immune-system. As a result of these late onsets, many of the proteins specifically expressed during these processes would be considered ‘foreign’ by the developed immune systems. Fortunately, multiple immune-suppressive mechanisms are in place to prevent potential auto-immune reactions against these tissues. Failure to maintain this immune-privileged state can have disastrous consequences, such as to auto-immune infertility which accounts for 5 – 10 % of male infertility in the developed world [25]. One unique physiological property of germ cells that prevents induction of autoimmunity is their lack of MHC Class I receptors. MHC Class I receptors are responsible for the presentation of peptides derived from cytosolic proteins to T cells. Without these receptors, any potential antigenic peptides within germ cells are shielded from the immune system and potential autoimmune reactions are avoided [26].

Another major contributor to the immune-privileged environment of the testis are Sertoli cells. Sertoli cells are somatic cells within the seminiferous tubule that support the development of male germ cells into spermatids [27]. Sertoli cells physically prevent infiltration of immune cells via specialized tight junctions that form the blood-testes barrier on the outside of the seminiferous tubules [28]. Although the blood-testes barrier is a significant barrier to immune cell infiltration into the seminiferous tubule it does not completely isolate the seminiferous tubule as ingress is possible through the straight tubules and the rete testis [25].

In addition to the physical barrier they create, Sertoli cell produce an immunosuppressive chemical environment within the testis. Multiple immunoregulatory cytokines are produced by Sertoli cells including transforming growth factor-β (TGF-β), activin A, FAS ligand, and inhibitors of both complement and granzyme B [25]. In addition to Sertoli cells, the Leydig cells of the seminiferous tubules also contribute to the immunosuppressive cytokine milieu through secretion of macrophage-migratory-inhibitor factor which can inhibit cell lysis mediated by cytotoxic T-cells and Natural Killer cells [29-31]. The resulting immunosignaling environment of the testes promotes a “type II” immunoregulatory, tolerant response in preference to “type I” cell-mediated immunity response [25].

Even with the various immunosuppressive barriers in place to prevent recognition of testis expressed proteins by the central immune system, tolerance to such antigens can develop. This occurs through expression of otherwise testis-restricted antigens by autoimmune regulator (AIRE) transcription factor within the medullary thymic epithelial cells (mTECs) during negative selection of T-cells during immune development [32]. Expression of the MAGE-A1 and NY-ESO-1 has been documented within mTECs which may explain the lack of antigenicity of certain CTAs or the differential immune responses to the same CTAs amongst patients [33].

Variability degree of tissue-specific gene expression within mTECs leading to varying levels of central tolerance has been reported for MART-1, a non-CTA melanoma antigen, and such variations may also contribute to the variation of CTA antigenicity [34].

Activation of Cancer Testes Antigens

The mechanism(s) by which CTAs are aberrantly activated within tumors is unclear but has major implications for their potential therapeutic exploitation. There is variation in CTA expression across tumor types. Some cancers such as bladder, non-small cell lung, and melanomas express numerous of CTAs, while others such as renal and colon express few [21]. CTAs also demonstrated a heterogeneous expression pattern within tumors themselves as immunohistochemistry has revealed focal expression patterns for several CTAs [24, 35]. Undoubtedly alterations in DNA methylation are major contributors to the aberrant expression of CTAs within tumors. Multiple studies have demonstrated activation of CTAs following treatment with DNA-Methyltransferase inhibitors such as 5-aza-2'-deoxycytidine (5-aza) [36, 37]. Interestingly, changes in DNA methylation may explain the focal nature of CTA expression within tumors as microdissection of ovarian tumors based on immunohistochemical staining for NY-ESO-1 demonstrated an inverse correlation between intratumoral NY-ESO-1 expression and DNA methylation [38]. Further epigenetic alterations such as histone post-translational modifications through inhibition of histone deacetylases or H3K9 methyltransferases, augment CTA expression following treatment with DNA methyltransferase inhibitors; however neither histone modification alone is sufficient to upregulate CTAs in these systems [39, 40].

DNA demethylation alone is sufficient to activate a number of CTAs; however, rarely does demethylation alone lead to wholesale activation of the entire CTA cohort. Furthermore,

studies have demonstrated differential activation of CTAs between tumor-derived and normal cell lines showing similar levels of demethylation [41]. Together these observations clearly demonstrate that mechanisms aside from DNA demethylation are required to activate specific CTAs. A few examples of such mechanisms have been previously described. For example expression of MAGE-A1 were found to be driven in large part by members of the ETS transcription factor family following promoter demethylation [42], while NY-ESO-1 activation is dependent on the binding of SP1 within its promoter [43]. Interestingly, SP1 is recruited to the NY-ESO-1 promoter by BORIS/CTCFL, which competes for NY-ESO-1 promoter occupancy with its paralog CTCF [43, 44]. BORIS, itself a CTA activated by hypomethylation, has been shown to activated a number of other CTAs in overexpression studies in both normal and transformed cellular contexts [45-49]; however, activation of BORIS/CTCFL alone is not sufficient to drive expression of CTAs in all cellular backgrounds [50, 51]. In total these data suggest the trans-acting factors are necessary and perhaps even sufficient to drive CTA-expression in the proper cellular backgrounds. Identification of such trans-acting factors may open therapeutic windows in the genetic backgrounds in which they are active.

Function of CTAs within spermatogenesis

The broad expression range of CTAs, throughout spermatogenesis from spermatogonia stem cells to implantation of the fertilized egg cell, as well as their genetic diversity suggests a vast array of functions for this group [22]. Numerous CTAs have been knockout in mouse models in efforts to characterize their roles in spermatogenesis. Many of these models develop normally aside from focal defects in male fertility, suggesting that while essential for spermatogenesis, CTAs have few, if any impacts on the development and function of non-

gametogenic tissues [22]. Not surprisingly, CTAs contribute significantly to the germ-cell specific processes of meiosis during the primary and secondary spermatocyte stages. The CTA SPO11 initiates homologous recombination during meiosis by introducing DNA double strand breaks through its transesterase activity [52]. Several CTAs: SYCE1, SYCP1, and HORMAD1, are members of the synaptonemal complex that ultimately resolves the DNA breaks via homologous recombination; while another CTA, TEX15 is required for proper loading of repair proteins at the break sites [53-56].

Interestingly, several CTAs promote mitochondrial function, possibly to compensate for the high metabolic demands of spermatozoa motility [57]. These CTAs include COX6BII a sperm-specific isoform of a Complex IV subunit in the electron transport chain; LDHC, a sperm specific subunit of the lactate hydrogenase tetramer; and SPATA19, a mitochondrial adhesion protein that supports mitochondrial distribution, abundance, and respiratory capacity [58, 59]. Although examples have yet to be described, the functions of CTAs described above would potentially allow a tumor cell to counter increased burdens of DNA damage (Meiotic CTAs) or metabolic demand (Mitochondrial CTAs). As the functional spectrum of CTAs within the testis far exceeds the examples described here, their possible functional utility to tumors through isomorphic or neomorphic functions is immense.

CTA-based therapeutic strategies

The antigenicity of the first CTAs to be discovered directed a large volume of the subsequent research involving CTAs into their potential utilization as immunotherapeutic targets in cancer. Numerous vaccines targeting several CTAs have reached phase II or III clinical trials. NY-ESO-1 is a frequent target of these vaccines with dozens of ongoing clinical trials. Earlier

results are encouraging as a recombinant NY-ESO-1 vaccine demonstrated a clinical benefit in patients with melanoma or ovarian cancer [60]. In addition to traditional vaccine approaches, recombinant NY-ESO-1 was used in the first study to elicit dendritic cell-induced T cell activity by fusing recombinant NY-ESO-1 to a monoclonal antibody specific for a dendritic cell receptor. In Phase I trials, this approach was well tolerated and six of eight patients who also received immune-checkpoint inhibitors had objective tumor regression [61]. In a murine model, vaccination with dendritic cells pre-loaded with a truncated form of BORIS inhibited tumor growth, metastasis, while increasing tumor infiltration by CD4 and CD8 T cells in a murine 4T1 mammary tumor implantation model, further demonstrating the potential use of CTA in non-traditional vaccination approaches [62].

In addition to their use in vaccine-based approaches CTAs have also been targeted using adoptive T cell therapy. In this approach, a patient's T cells are extracted and then engineered *in vitro* to expressed T cell receptors (TCRs) against tumor antigens, expanded, and then reintroduced into the patient. An adoptive T cell approach targeting NY-ESO-1 led to clinical responses in 55 % and 61 % of patients with metastatic melanoma or synovial sarcoma, respectively [63, 64] . Unfortunately, in one study in which peripheral blood monocytes (PBMCs) were transduced with a MAGE-A3-targeted TCR, significant toxicity and even death occurred due to cross reactivity with MAGEA-12 within brain tissue [65]. In a second study, using PBMCs that were also transduced with a MAGE-A3-targeted TCR, two people experienced cardiac arrest due to cross reactivity with the protein titin within cardiac muscle [66]. These studies illustrate the critical need for target specificity especially when utilizing exogenous T cell receptors which are not subject to any *in vivo* selection against potential cross reactive self-antigens.

Functional contributions of CTAs to tumorigenesis

To date the majority of research regrading CTAs focused on their potential roles as targets of immunotherapy and until the late 2000s functional studies into potential pro-tumorigenic roles for CTAs were few and far between. The first clues that CTAs may contribute to tumorigenesis include several studies around the turn of the century that showed overexpression of MAGE and GAGE genes contributed to tumor cell resistance to biological factors such as tumor-necrosis factor and FAS-ligand, chemotherapeutics such paclitaxel and doxorubicin, and γ-irradiation [67-69]. Further suggesting that CTAs functionally contribute to tumorigenesis were the results of an unbiased genome wide screen which identified a significantly enriched cohort of CTAs among genes that promote tumor cell resistance to the anti-mitotic chemotherapy drug paclitaxel [70]. Further studies demonstrated that one of the CTAs identified in that cohort, Acrosin Binding Protein, prevents disruption of microtubule dynamics and centrosomal clustering by negatively regulating levels of aberrantly expressed NUMA1 [71].

In the last decade, research into potential functional roles for CTAs in tumorigenesis has increased dramatically and shed light onto the fact that CTAs impact multiple aspects of tumorigenesis. The CTA ATAD2 was shown to alter pro-tumorigenic gene expression by stimulating the transcriptional activity of c-myc [72]. The CTA Preferentially expressed in melanoma (PRAME) was found to antagonize retinoic acid signaling and thereby block retinoic acid-induced differentiation, growth arrest, and apoptosis within melanoma [73]. Several pro-tumorigenic functions have been identified for multiple members of the MAGE family. In 2010, the MAGE Homology Domain's ability to regulate activity of TRIM family E3-ligases was uncovered by Doyle and colleagues who demonstrated MAGE-C2 targeted TRIM28 to the tumor

suppressor p53 leading to its degradation [74]. Further studies from the Potts lab showed that AMPK is degraded in a cancer-specific manner by a MAGE-A3/6-TRIM28 complex [75]. Although, several pro-tumorigenic roles for CTAs including the examples described here have been identified, no comprehensive approach has been taken to examine potential functional roles for the entire collection of CTAs.

Summary of Dissertation

The goal of this project was to identify CTAs that functionally support tumorigenesis. To that end, we undertook a comprehensive screening approach to define the functional contribution of annotated CTAs to several aspects of tumorigenesis including cell viability, survival, proliferation and activity of five pro-tumorigenic signaling pathways (Chapter III). The results of these screens identified the uncharacterized CTA Fetal and Adult Testis Expressed 1 (FATE1) as a major mediator of tumor cell viability and survival. To begin a functional characterization of FATE1 we determined that FATE1 is a mitochondrial protein that interacts with a core component of the mitochondrial fission machinery, Mitochondrial Fission Factor (MFF). Additionally, we found that FATE1 expression is capable of altering mitochondrial morphology, a process that impacts cellular metabolism and susceptibility to apoptosis. In Chapter IV, owing to the potent activation of the programmed cell death pathway following the depletion of FATE1 we further defined FATE1's role in regulation of this pathway. We find that FATE1 interacts with and regulates levels of the pro-apoptotic tumor suppressor Bcl-2 Interacting Killer (BIK). Additionally, we find that a FATE1 binding partner RNF183, an uncharacterized E3-ligase, also functions to suppress BIK levels, and find evidence supporting a functional FATE1-RNF183 complex. In Chapter V, FATE1 is identified as a target of the chimeric transcription factor EWS-

FLI1, the oncogenic driver of the pediatric malignancy Ewing sarcoma. Using multiple cell viability assays we demonstrate that FATE1 is required for the short and long term viability of Ewing sarcoma cells. Additionally, by leveraging a previously published EWS-FLI1 ChIP dataset we nominate three additional CTAs: BORIS, MAGE-A4, and SPATA19, as potential EWS-FLI1 transcriptional targets, two of which, MAGE-A4 and SPATA19 are necessary for maintenance of Ewing sarcoma cell viability.

Overall these studies highlight the ability of cancer cells to utilize aberrantly expressed genes to overcome the biologic consequences of cellular transformation. The potency and penetrance of FATE1 depletion on tumor cell viability indicates it may be a general mechanism utilized by tumor cells to overcome transformation-induced stress. The finding that an oncogenic-specific transcription factor (EWS-FLI1) activates several CTAs not only demonstrates a novel mechanism of CTA activation within tumors but it also provides several new lines of investigation for Ewing sarcoma-specific vulnerabilities.

Figure 1: Phenotypic similarities between gametogenesis and tumorigenesis.

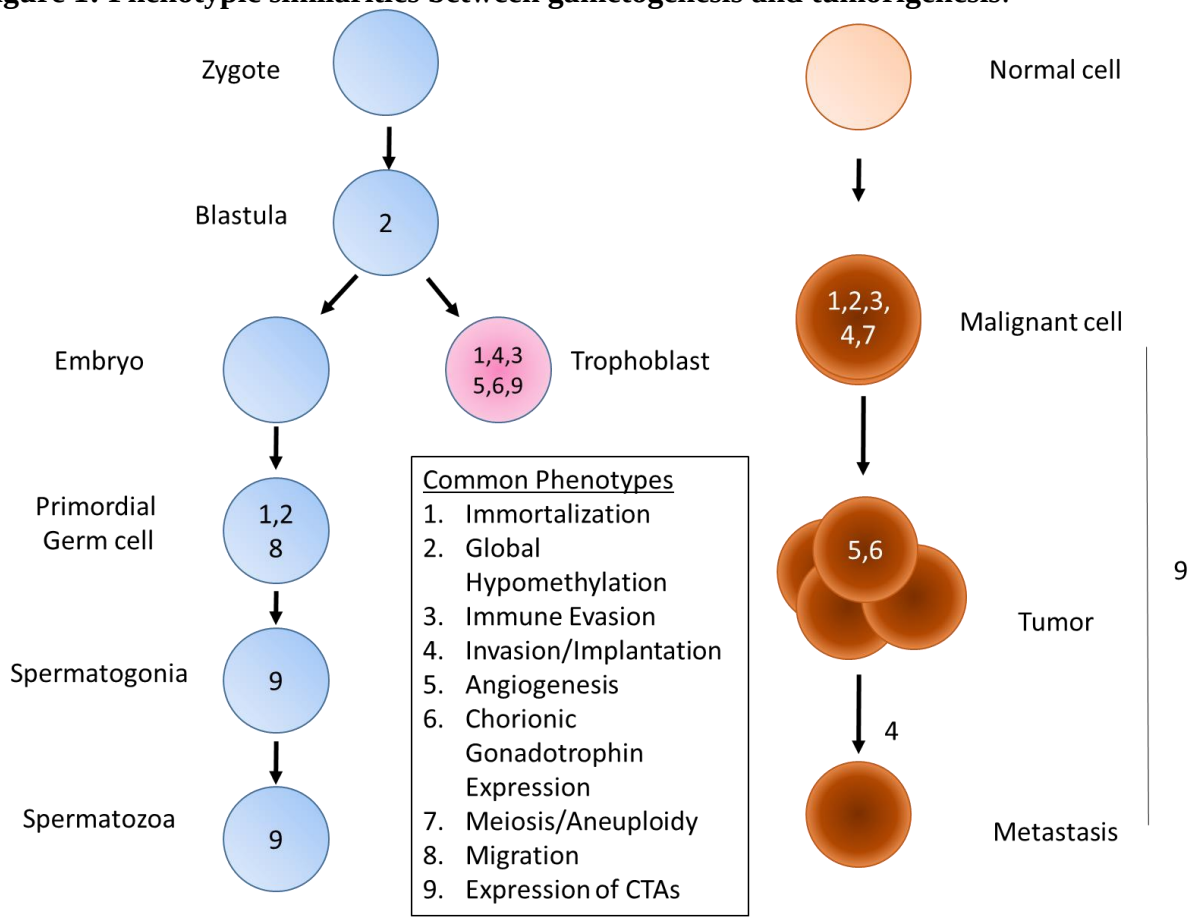

Figure 1: Phenotypic similarities between gametogenesis and tumorigenesis. Similarities at different stages of gametogenesis (left) and tumorigenesis (right) are indicated by number. Numbers correspond to phenotypes listed in the embedded table. Adapted from Simpson AJ et al., 2005 [19].

Figure 2: Cancer Testis Antigen presentation to cytotoxic T cells

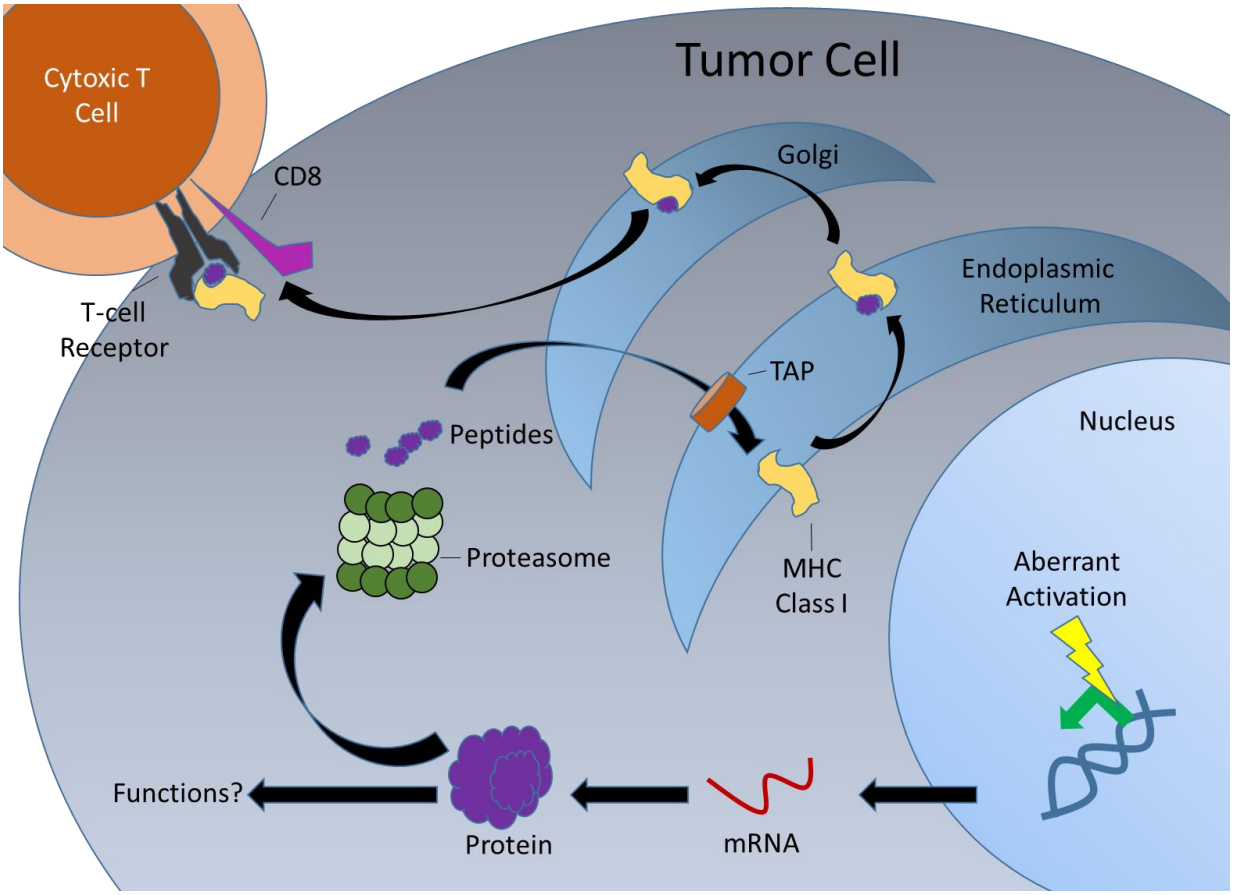

Figure 2: Cancer Testis Antigen presentation to cytotoxic T cells. Within tumor cells, aberrantly expressed proteins are subject to proteasome-mediated degradation. The resulting peptides are transported through the transporter associated with antigen processing (TAP) into the endoplasmic reticulum. In the endoplasmic reticulum, antigens are loaded onto major histocompatibility (MHC) class I molecules that transported through the Golgi apparatus and displayed on the cell surface. On the cell surface, antigens recognized as foreign by cytotoxic T cells can activate an immune response. To date, few specific mechanisms governing the aberrant activation of CTAs have been elucidated while potential pro-tumorigenic functional contributions for a large majority of CTAs have yet to be interrogated. Adapted from Coulie PG et al., 2014 [2].

CHAPTER II: MATERIALS AND METHODS

Cell lines. Cell lines were obtained from American Tissue Type Collection (ATCC) or John Minna (UT-Southwestern (UTSW)) except for: TC-32 (Children's Oncology Group), SK-MEL-2 (National Cancer Institute); hMPro™ Mesenchymal Progenitor Cells (Aruna Biomedical); SK-MEL-37 and SK-OV-6 (Lloyd Old, Ludwig Institute); SUM159, SUM229, and SUM149 (Asterand); HuMEC (Charles Perou, University of North Carolina at Chapel Hill, (UNC)); HME50-hTERT, Fibroblasts (BJ) (Jerry Shay, UTSW); WHIM12 (Matthew Ellis, Baylor College of Medicine); ES-2 (Rolf Brekken, UTSW); PEO1 and U2OS (Michael White, UTSW); HEK293GP and HCC1806 (Gray Pearson, UTSW); RCC4 (William Kim, UNC); HCT116 (Cyrus Vaziri, UNC); HCT116-BAX$^{-/-}$BAK$^{-/-}$ DKO (Bert Vogelstein, Johns Hopkins University)**;** EWS502, EWS894, RD-ES, SK-ES-1, MHH-ES-1, A673, and SK-N-MC (Ian Davis, UNC). All cell lines were cultured in provider's recommended medium. Because SK-OV-6 is on the ICLAC list of misidentified cell lines, Short Tandem Repeat (STR) profiling was used to validate the line used in this study [76, 77]. SK-OV-6 was used because it has previously been demonstrated to express a number of CTAs [78]. Cells were evaluated for mycoplasma contamination by DAPI stain for extra-nuclear DNA.

Antibodies. Antibodies used for immunoblotting were as follows: Santa Cruz Biotechnology: GAPDH (sc-51907; 1:1000), HA (sc-805; 1:500 and sc-7392; 1:500), TOM20 (sc-11415; 1:500), BIK (sc-10770; 1:500 and sc-1710; 1:250), c-Myc (sc-40; 1:1000 and sc-789; 1:500), ERK1/2 (sc-93; 1:1000), Ubiquitin (sc-8017; 1:250), ACTIN (sc-8432, 1:2500), and FATE1 (sc-101220;

1:1000); Sigma: FATE1 (HPA034604; 1:2000), and RNF183 (SAB2106627; 1:1000); Cell Signaling Technology: Cleaved Caspase-3 (9661; 1:500), PARP1 (9532; 1:1000), and BCL-xL (2764; 1:5000); Abcam: FATE1 (ab111486; 1:1000); V5 (R960; 1:1000; Life Technologies); FLI1 (554266; 1:500; BD Biosciences). Antibodies for immunofluorescence were as follows: c-Myc (sc-40; 1:100; Santa Cruz Biotechnology), TOM20 (sc-11415; 1:500; Santa Cruz Biotechnology), GM130 (ab31561; 1:100; Abcam), Cytochrome c (556432; 1:200) and ; BD Biosciences), HA (MMS-101R; 1:100; Covance), Catalase (219010; 1:1000; Calbiochem), V5 (R960; 1:300; Life Technologies), Calnexin (ADI-SPA-860; 1:100; Enzo), COX IV (4850; 1:125; Cell Signaling Technology), and β-tubulin (T5293; 1:100; Sigma), and FLAG (F1804, Sigma).

Reagents. Pan-caspase inhibitor, (3S)-5-(2,6-difluorophenoxy)-3-[[(2S)-3-methyl-2-(quinoline-2-carbonylamino)butanoyl]amino]-4-oxopentanoic acid (Q-VD-OPh) was purchased from Sigma. siRNAs were obtained from GE Healthcare (siGENOME siRNA) or Sigma (Mission® siRNA). Control (CTRL) siRNAs were either non-targeting control (GE Healthcare) or targeted genes DLNB14, FNDC3B, or APOL6. CellTiter-Glo® (CTG), Apo-ONE® Homogenous Caspase-3/7 (APO), ONE-Glo™ Luciferase Assay System, and Dual Glo® Luciferase Assay System were purchased from Promega. Lipofectamine® RNAiMAX was purchased from Thermo Fisher Technologies. DharmaFECT™ reagents and DharmaFECT™ Duo were purchased from GE Healthcare Life Sciences. Opti-MEM® was obtained from Thermo Fisher Scientific. MitoTracker® Red CMXRos (C32H32Cl2N2O) was purchased from Thermo Fisher Scientific.

Expression Plasmids and Mutagenesis. Full-length FATE1 cDNA in pRK5 (a gift from Michael White, UTSW), was subcloned into pCMV-myc (Clontech) and pcDNA3 (Thermo Fisher Scientific) between SalI and NotI, and EcoRI and NotI, respectively. Myc-FATE1 cDNA was from pCMV-myc-FATE1 was subcloned into pLPCX (Clontech) between BglII and NotI. Full-length RNF183 cDNA was obtained in pLX304 from the CCSB-Broad lentiviral ORF collection housed at UNC and cloned into pCMV-HA (Clontech) between SalI and NotI. Full-length BIK cDNA was obtained from pEGFP-BIK (Addgene plasmid #10952). HA-RNF183-C13A/C59A and BIK-L61G, which has limited toxicity as compared to wild-type[79], were generated using site-directed mutagenesis. BCL-xL cDNA (a gift from Mohanish Deshmukh, UNC) was cloned into pCMV-myc between SalI and NotI and then myc-BCL-xL cDNA was subcloned into pLPCX between BglII and NotI. eGFP cDNA (a gift from Michael White, UTSW) was subcloned into pLPCX between BglII and NotI. Viral packaging plasmids, pCMV-dr8.91 and pCMV-VSV-G, were a gift from Bill Hahn, Harvard). pRL-CMV (a gift from Deborah Chapman, University of Pittsburgh). EWS-FLII cDNA (a gift from Ian Davis, UNC) was cloned into pCMV-HA between SalI and NotI. 3xFLAG-tagged EWS-FLI1 cDNA in a Gateway Entry vector (a gift from James Amatruda, UTSW) was inserted into pLX304 via the Gateway LR clonase reaction**..** pFATE1-Luc was produced by amplifying a 1606 bp fragment -1634 to -29 bp upstream of FATE1 translational start site from HCT116 genomic DNA with KpnI and HindIII extensions. The insert was then ligated into pTA-Luc (Clontech) thereby removing minimal TA-promoter and placing the FATE1 promoter directly upstream of the *luc* gene from *Photinus pyralis*. pFATE1ΔEF1-Luc was produced by amplifying the 1268 bps on the 3'-prime end of the FATE1-promoter insert in pFATE1-Luc with KpnI and HindIII extensions and then inserting it into pTA-Luc as described for pFATE1-Luc.

siRNA screen and data processing. Transfection conditions for each cell line were optimized using the CTG assay and the formula: Transfection Efficiency = 1-(Luminescence^{siUBB}/Luminescence$^{siCTRL)}$. A custom siGenome SMART pool siRNA library (Dharmacon/GE Healthcare Life Sciences) was purchased in 96-well plate format and resuspended as described [70]. siRNAs were diluted to 250 nM in serum free medium and 30 µL of this solution (8.3 pmoles of siRNA) was mixed in well with appropriate transfection reagents in 9.8 µL Opti-MEM® and incubated for 20 minutes. Then, 60 µL or 80 µL of cells in growth medium were added for cell biological and signaling assays respectively. Cell biological screens were performed 96 hours post plating using 20 µL CTG (ATP; viability), 90 uL APO (caspase-3/7 activity; survival), or the Click-iT® EdU Alexa Fluor® 488 Imaging Kit (DNA synthesis; proliferation) assay systems according to manufacturers' protocols. CTG and APO assays were read with a Pherastar Plus or Pherastar FS (BMG Labtech) plate reader. siRNA pools with z-scores > 2 in the apoptosis screen or < -2 in the viability and proliferation screens were considered outliers. Only siRNA pools that exhibited statistically significant change ($P \leq 0.05$ by unpaired Student's t-test) were considered. For the HIF, NF-κB, Wnt, and TGFβ reporter screens, siRNA pools that reduced reporter activity by either > 60 % in a single cell line or > 30 % in more than 2 cell lines were considered positives. For the NF-κB, Wnt, and TGFβ signaling screens, both basal and ligand-induced values were considered.

Transfections. For siRNA transfection, cells were trypsinized and plated into medium containing 50-100 nM siRNA complexed with RNAiMAX™ in Opti-MEM® and incubated as indicated in the figure legends. For cDNA transfections, HeLa, H1155 and H1299 cells were transfected using Lipofectamine 2000™ (Thermo Fisher Scientific) and HEK293T cells were

transfected using FuGENE 6® or the calcium phosphate method[80]. All manufacturers' protocols were followed.

Generation of stable cell lines. Cell lines stably expressing shRNAs were created via lentiviral-mediated gene transduction through co-transfection of HEK293T cells with viral expression and packing plasmids (pCMV-VSV-G and pCMV-dr8.91). For FATE1 studies, stable lines were created via retroviral-mediated gene transduction through co-transfection of HEK293GP cells with pLPCX expression plasmids and pCMV-VSV-G. Virus conditioned media was used to infect target cells in the presence of polybrene and stable populations were selected using appropriate antibiotics.

Luciferase assays. Indicated luciferase reporters (100 ng), Renilla reporter (pRL-CMV, 2 ng) and 100 ng indicated cDNAs were transfected into HEK293T using FuGENE 6®. Forty-eight hours later, luciferase activity was measured using the Dual-Glo® Luciferase Assay System.

Colony formation assay. At indicated incubation times following siRNA transfection, cells were replated at limiting dilution, fed twice a week and stained with Geimsa (Sigma).

Soft Agar Assays. 48 hours after lentiviral-mediated transduction of shRNAs, cells were suspended in 1 mL of 0.35 % bacto-agar in appropriated media over a 1 mL base layer of 0.7 % bacto-agar in appropriate media. One mL of media was added to the top of each well and exchanged twice weekly for three weeks. At the end of three weeks colonies were stained with Giemsa and counted.

Gene expression. RNA was isolated using or an RNA isolation kit (Sigma) and reverse transcribed using the High-Capacity cDNA Reverse Transfection Kit (Thermo Fisher Scientific) according to manufacturer's instructions. An Applied Biosystems Real-Time PCR system and either Solaris™ (Dharmacon), SYBR® Green or TaqMan® Real-Time PCR (Thermo Fisher Scientific) gene expression assays were used. Gene expression assays were multiplexed with RPL27 as a control assays. Relative expression values were calculated using the comparative $2^{-\Delta\Delta CT}$ method [81].

Immunoblotting. Whole cell lysates were prepared in 2x Laemmli sample buffer and resolved using Sodium Dodecyl SulFATE1 Polyacrylamide Gel Electrophoresis (SDS-PAGE). Gels were transferred to Immobilon® PVDF (Millipore) or nitrocellulose (Bio-Rad Laboratories) membranes, blocked in tris-buffered saline containing 0.1 % Tween20 (TBST) and blocked in 5 % non-fat dry milk, bovine serum albumin (BSA), or Odyssey® (LI-COR Biosciences) blocking buffer followed by incubation with indicated primary antibodies for 1 hour or overnight. After washes in TBST, appropriate HRP-coupled secondary antibodies (Jackson Immunoresearch) or IRDye® antibodies (LI-COR Bioscience) were used for chemiluminescence or fluorescence detection (Odyssey®), respectively. Coomassie stain (Genlantis) was incubated with SDS-PAGE gels for 30 minutes followed by destain for 4 hours.

Immunofluorescence. Cells plated on glass coverslips were fixed with 3.7 % formaldehyde and permeabilized with 0.5 % Triton X-100 for ten minutes. For calnexin staining, cells were permeabilized with ice-cold methanol for 10 minutes. Cells were blocked and washed in 1 %

BSA, 0.1 % Tween-20 in 1X Phosphate Buffered Saline (PBS) (PBTA). Cells were incubated with primary antibodies for 1 hour followed by three washes in PBTA. Coverslips were then incubated with Alexa Fluor®-conjugated secondary antibodies (Thermo Fisher Scientific) for 30 minutes followed by 3 washes in PBTA and a wash in H_2O. MitoTracker was added for 30 minutes prior to fixation. Prolong® Gold Antifade reagent with DAPI (Thermo Fisher Scientific) was used to mount slips on glass slides and images were acquired on either a Leica DM55000 B upright microscope or a Zeiss LSM510 confocal microscope.

Viability Assays. Cells were reverse transfected with RNAiMAX™ in Opti-MEM® with 50-100nM siRNA in 96 well format. 120 hours post-transfection (unless otherwise indicated), CTG was used to quantitate total ATP using a Pherastar Plus plate reader.

Immunoprecipitation. Unless otherwise indicated, cells where lysed on ice for 30 minutes in non-denaturing lysis buffer (NDLB): 50 mM HEPES pH 7.4, 1.0 % Triton X-100, 0.5 % Sodium Deoxycholate, 150 mM NaCl, 1 mM $NaVO_4$, 25 mM β-Glycerophosphate, 1 mM EthyleneDiaminetetraacetic Acid (EDTA), 1 mM Ethylene Glycol Tetraacetic Acid (EGTA), plus protease-inhibitor cocktail (Sigma)). Lysates were clarified at 12,000*g* for 10 minutes. Then, 10% of each clarified lysate was set aside as an input loading control and the remainder was immunoprecipitated for 4 hours at 4 °C with antibodies coupled to Protein A/G beads. Unless otherwise indicated, beads were washed two times in high salt (350 mM NaCl) NDLB, once in NDLB, and then resuspended and boiled in 2X Laemmli sample buffer.

Autoubiquitination Assays. For *in vitro* autoubiquitination assays, HEK293T were transfected

with pCMV-HA-RNF183 or pCMV-HA-RNF183-CC/AA. Twenty-four hours after transfection, cells were lysed on ice in non-denaturing lysis buffer (NDLB): 50 mM HEPES, pH = 8, 1.0 % Triton X-100, 0.5 % Deoxycholate, 150 mM NaCl, 1 mM NaVO4, 25 mM β-Glycerophosphate, 1 mM EDTA, 1 mM EGTA, plus protease-inhibitor cocktail, clarified at 12,000g for 10 minutes and then immunoprecipitated for 4 hours with anti-HA antibody (Covance) and Protein A/G beads (Life Technologies). Beads were then washed 3 times in NDLB with 350 mM NaCl and two times in ligase buffer: 50 mM Tris pH 7.5, 150 mM KCl, 1 mM MgCl2. After the final wash, beads were resuspended in ligase buffer containing 100 nM recombinant E1 (Enzo Life Sciences), 1 µM recombinant UbcH5b (Enzo Life Sciences), 5 µM ubiquitin from bovine erythrocytes (Sigma), plus or minus 5 mM Mg2+-ATP and incubated for 1.5 hours at 37 °C.

GST-183 Purification. BL21(DE3) E. coli transformed with pGEX-4T-1-RNF183 were induced with 1 mM IPTG in the presence of 100 nM $ZnCl_2$ and incubated for 4 hours at 37 °C. Bacteria were pelleted and then flash frozen. The next day the pellet was thawed on ice and resuspended in 30 mL of ice cold lysis buffer (50 mM Tris-HCl pH = 7.7, 150 mM KCl, 0.1 % Triton X-100, 1 mM DTT, and protease inhibitor cocktail). Lysozyme was added to a final concentration of 1 mg/mL and the lysate was rocked on ice for 30 minutes and then sonicated seven times for 15 seconds at 70 % power and 50% cycle. The lysates was then centrifuged for 1 hour at 12,000 rpm at 4 °C. The resulting supernatant was transferred to a fresh conical and incubated with glutathione agarose beads for 2 hours at 4 °C. Beads were collect by centrifugation at 2,000g for 2 minutes and then washed five times with 20 mL of lysis buffer. After the final wash beads were eluted into six 2 mL fraction of elution buffer (50 mM Tris-HCl pH 7.7, 150 mM KCl, 1 mM DTT, and 10 mM reduced glutathione). Samples of all fractions were blotted using

coomassie blue and those with GST-RNF183 bands were dialyzed overnight into protein storage buffer (50 mM Tris-HCl pH 7.7, 100 mM KCl, 10 % glycerol, 1 mM DTT).

***In vitro* ubiquitination assay.** The Enzo® Ubiquitinylation kit was used to evaluate GST-RNF183 for E3-ligase activity towards 6xHis-BIK (Abnova). Briefly, 100 nM ubiquitin activating enzyme (E1), 100 nM ubiquitin conjugation enzyme UbcH5b (E2),1 mM recombinant GST-RNF183, 100 nM 6xHIS-BIK, and 5 mM bovine ubiquitin (Sigma) were incubated in 1 x Ligase Buffer (50 mM Tris-HCl pH 7.5, 150 mM KCl, 1 mM $MgCl_2$, 1 mM DTT), with 5 mM Mg^{++}-ATP. The reaction mixture was incubated at 37 °C for 90 minutes and then quenched by addition of 2x Laemelli buffer. Negative control reactions were performed in the absence of Mg^{++}-ATP.

GREAT analysis. Genomic binding coordinated from Patel el al 2012 were converted to GRCh37 and subjected to GREAT 3.0.0 analysis using the basal plus extension gene regulator definition with the following parameters: Proximal- 5.0 kb upstream and 1.0 kb downstream, plus Distal up to 1000 kb.

Oncomine™ Analysis. For Oncomine™ BIK mRNA tumor/normal analysis, the follow studies were used: GSE165151, GSE25142, and The Cancer Genome Atlas (TCGA) Research Network (http://cancergenome.nih.gov/) [82-85].

Survival Analysis The overall survival and clinicopathological data sets were GSE8894, Lung Adenocarcinoma and Colorectal TCGA (downloaded from cBioPortal) [85, 86]. Samples were

placed into groups based on a median cutoff, with the exception of the colorectal patients in Figure 4f, where a z-score cutoff of expression > 1.5 was used. The distributions of time-to-event outcomes were estimated using the method of Kaplan and Meier. P values and hazard ratios were calculated using a Cox regression model.

CHAPTER III: FATE1 IS A MITOCHONDRIAL CTA THAT SUPPORTS TUMOR CELL VIABILITY[1]

Introduction

Recently, pro-tumorigenic functional roles for CTAs have begun to be defined; however, these studies have been confined to only a few CTAs or CTA gene families. Aside from several CTA gene families whose members have extensive homology, there is little sequence homology between CTAs. Additionally, the known functions of CTAs in spermatogenesis are quite diverse, impacting processes at each step of male cell differentiation up to and including implantation. The diversity of protein sequences and known functions within sperm suggests the spectrum of potential functions for CTAs in tumorigenesis may be quite large. To assess this in a comprehensive manner we interrogated the impact of expression of individual CTAs on tumor cell viability, survival, and proliferation, as well as five signaling modules implicated in tumorigenesis (NF-κB, HIF, TGF-β, Retinoic Acid, and Wnt). These assays were carried out in a panel of 11 tumor-derived cell lines from diverse cancer lineages chosen to provide maximal representation of annotated CTAs. The results of the viability and survival arms of this screen identified the uncharacterized CTA Fetal and Adult Testis Expressed 1 (FATE1) as a major contributor to tumor cell viability and therefore I will briefly summarize the previously published literature regrading FATE1.

[1] Elements of the work referenced in this chapter are published in: Kimberly E. Maxfield and Patrick J. Taus, Kathleen Corcoran, Joshua Wooten, Jennifer Macion, Yunyun Zhou, Mark Borromeo, Rahul K. Kollipara, Jingsheng Yan, Yang Xie, Xian-Jin Xie, and Angelique W. Whitehurst. Comprehensive Functional Characterization of Cancer-Testis Antigens Defines Obligate Participation in Multiple Hallmarks of Cancer. Nat Commun. 2015 Nov 16

FATE1

The FATE1 transcript was first identified in a 2001 study that sought to map transcripts with enriched testicular expression to the breakpoints of chromosome translocations in infertile men [87]. The same year, a follow up study cloned FATE1 from fetal tissue and identified its gene structure consisting of 5 exons spanning 7 kb on the X chromosome [88]. In 2003, FATE1 mRNA expression was detected in samples from patients with hepatocellular (66 %) and colorectal carcinomas (21 %). Of note, three patients with hepatocellular carcinomas positive for FATE1 expression had reactive sera against recombinant FATE1 protein indicating FATE1's antigenic potential *in vivo* [89]. In 2005, immunohistochemical analyses detected FATE1 protein within the testis in spermatogonia, primary spermatocytes, and Sertoli cells but failed to detect its presence in other normal tissues [35]. No functional role for FATE1 within normal tissues or cancers had been described prior to following studies.

Results

Functional Analysis of CTAs

We designed an experimental platform to allow for broad-scale investigation of the mechanistic contribution of CTAs to tumor cell autonomous behaviors (Figure 3A). One hundred forty CTAs with documented expression in solid tumors were selected for this study (Table 1). Given the notorious heterogeneity of CTA expression among tumors, we used quantitative expression profiling to identify 11 tumor-derived cell lines providing maximal representation of our CTA panel (135 CTAs) (Figure 3B) [78]. These cell lines were derived from prostate, breast, ovarian, skin, non-small cell lung cancer (NSCLC), and bone tumors. Each cell line within this 'testbed' exhibited a distinct pattern of CTA expression; however, most CTAs were present in >

2 cell lines and 20 % were expressed in all 11 cell lines (Figure 3B).

To annotate tumorigenic CTAs, we individually depleted each CTA in each of the 11 cell lines and measured the consequences on viability, apoptosis and proliferation. In addition, we measured the consequences of CTA depletion on the Hypoxia Inducible Factor (HIF), Wnt, TGFβ, and Nuclear Factor Kappa-light-chain-enhancer of activated B cells (NF-κB) signaling pathways in a subset of cell lines using luciferase reporters. These pathways were chosen because they are classic tumorigenic signaling cascades that are also essential during development and therefore, we reasoned were most likely to be affected by CTAs in tumor cells. Importantly, each luciferase signaling reporter exhibited a broad dynamic range upon ligand-mediated stimulation in at least 5 testbed cell lines, providing an opportunity to examine CTA influence in multiple genetic backgrounds. Raw data from each screen were normalized to internal non-targeting controls and a z-score was calculated for all CTAs in each assay and cell line (Figure 3C).

Multiple CTAs are essential for tumor cell viability

siRNA pools targeting 17 CTAs that significantly affected apoptosis, viability or proliferation (defined as > 1.5 standard deviations from the mean of all CTAs) were retested using individual siRNAs. Fourteen pools contained 2 or more active siRNAs, suggesting on-target activity (Figure 3D-F). The CTA that exhibited the most potent viability dependency in multiple genetic backgrounds was Fetal and Adult Testis Expressed 1 (FATE1) ($P = 0.0011$, Kolmogorov-Smirnov test) (Figure 4A and B). FATE1 mRNA was detectable in all 11 testbed cell lines and its depletion led to a > 30 % reduction of viability in melanoma, breast, prostate and sarcoma settings (Figure 4B). Importantly, 3 of the 4 siRNAs in the original screening pool

were sufficient to recapitulate the activity of the FATE-targeted siRNA pool (Figure 3F). We also returned FATE1 as essential for viability in a previous genome-wide loss of function screen in H1155 cells, a NSCLC cell line [70]. Given the penetrance of siFATE-induced viability defects in our testbed cell lines, we further evaluated tumor cell dependency on FATE1 by expanding our analysis to additional cell lines derived from colorectal, ovarian, sarcoma, breast, cervical and NSCLC cancers. While all cell lines were sensitive to FATE1 depletion, we identified a subset (HCT116, WHIM12, U2OS, HeLa, ES-2, PEO1, SUM159, A549, LNCaP), which exhibited an almost complete loss of viability 120 hours post transfection with siFATE1 (Figure 4C). These observations corresponded with a potent loss in viability as assessed by colony formation assays in multiple tumorigenic backgrounds (Figure 4D). Looking at patient expression data we found that among colorectal cancer patients, a dataset chosen because of FATE1 significant impact on viability of the colorectal carcinoma cell line HCT116 cells, those patients with high expression of FATE1 had a significantly poorer outcome compared to those with low FATE1 expression, indicating FATE1 may play a clinically relevant role within tumors (Figure 4E).

FATE1 is a mitochondrial protein

Owing to the critical role of FATE1 expression on tumor cell viability we sought to characterize potential functional roles for FATE1. We began by analyzing FATE1's primary sequence which indicated a largely disordered protein with potential coiled-coil and transmembrane domains in its C-terminus (Figure 5A). A BLASTP search of FATE1's primary amino acid sequence showed significant homology between FATE1 and Mitochondrial Fission Factor (MFF). This area of homology spanned MFF's C-terminal coiled-coil (CC) and

transmembrane domains (TM), which exhibit 29 % identity and 55 % similarity to the corresponding regions of FATE1 (Figure 5B) [90]. MFF is a mitochondrial resident protein that functions during mitochondrial fission to recruit the mechanical effector of mitochondrial fission, Dynamin-related protein 1, to the mitochondrial outer membrane surface [91, 92]. Together these data suggest a domain map of FATE1 shown in Figure 5C.

Consistent with its homology to MFF's mitochondrial-targeting transmembrane and coiled-coil domains, myc-FATE1 localized to the mitochondria with limited presence in other organelles (Figure 6A) [91]. We then assessed the requirement of FATE1's putative coiled-coil and transmembrane domains on FATE1 localization. Both domains are required for FATE1 to localized to the mitochondria, deletion of the transmembrane domain localized FATE1 to the cytoplasm and nucleus and deletion of the coiled-coil domain localized FATE1 to the endoplasmic reticulum. (Figure 6B and C). Coiled-coil domains frequently mediate protein-protein interactions so we assessed a possible interaction between FATE1 and MFF. We found that the two protein interact within cells, and that this interaction requires FATE1's coiled-coil domain (Figure 7A and B). We also assessed the requirement for MFF in localizing FATE1 to the mitochondria. Using mouse embryonic fibroblasts harboring a MFF-/- deletion we assessed the localization of wild-type FATE1 and found that it maintained its mitochondrial localization in the absence of MFF expression (Figure 7C).

As MFF is a critical mediator of mitochondrial morphology we assessed whether FATE1 impacted mitochondrial morphology [90]. Stable expression of FATE1 led to basal alterations in mitochondrial shape within both immortalized fibroblasts and H1299 lung adenocarcinoma cells. Within BJ-fibroblasts FATE1 expression led to balloon-like mitochondrial structures (compared to a thin, reticular mitochondrial network in control cells expressing Histone H2B-GFP) (Figure

8A). In H1299 cells FATE1 condensed the mitochondrial network into a perinuclear aggregate. Interestingly, this phenotype was also observed H1299 cells depleted of MFF, suggesting the two proteins may have opposing functions (Figure 8B). Additionally, the FATE1-induced perinuclear aggregation was attenuated when cells were depleted of the mitochondrial fusion-effector, Mitofusin 1 (MFN1) [93] (Figure 8B). Importantly, the H1299 cell lines used showed no differences in proliferation rates indicating the mitochondrial phenotypes were not due to alterations in cell cycle (Figure 8C).

Discussion

Intriguing correlative associations between gametogenesis and tumorigenesis have been noted for over 100 years (Figure 1). For example, tumor cells can produce trophoblastic hormones at sufficient levels to be used as a serum marker for tumor detection and recurrence [94]. Additionally, gene products whose expression is otherwise restricted to reproductive tissues are frequently re-expressed in a range of tumor types. However, despite widespread activation in tumors, a global investigation into the contribution of these genes to neoplastic behaviors has been lacking. Here, by integrating findings from a multi-faceted, comprehensive platform we find that CTAs engage divergent mechanisms in the tumorigenic regulatory network to promote cancer.

We uncovered multiple CTAs that are essential for tumor cell viability. These CTAs have a diversity of known functions within sperm and therefore likely buttress different aspects of the tumorigenic platform. Among the CTAs impacting tumor cell viability, the previously uncharacterized CTA FATE1 had the most potent impact across the testbed of tumor cell lines used in our analyses. We found that FATE1 localizes to mitochondria and can alter mitochondrial morphology. Control of mitochondrial morphology can impact multiple aspects of

cell viability including the effectiveness of mitochondrial respiration and its sensitivity to outer membrane premeabilization in response to apoptotic stimuli [95-97]. Mechanistically FATE1 may be influencing mitochondrial morphology by antagonizing the function of MFF, a mitochondrial membrane protein critical to the mitochondrial fusion process [90]. We identified an interaction between the two proteins and found that expression of the two has opposing effects on mitochondrial morphology, evidence that taken together supports a possible functional relationship (Figure 7A and Figure 8B). The FATE1-MFF interaction depended on the proteins' homologous coiled-coil domain (Figure 7B), a domain that is also required for FATE1's mitochondrial localization but in a MFF-independent manner (Figure 7C). Due to the coiled-coil's importance in the mitochondrial localization of FATE1, elaboration of the mechanisms governing this localization may also inform aspects of MFF regulation due to the shared homology within this region.

Table 1. Screened Cancer Testis Antigens

Description	*Location*	*Gene Name*	*Antigenic*
Acrosin binding protein	12p13.31	ACRBP	Y
Actin-like 8	1p36.2-p35	ACTL8	
ADAM metallopeptidase domain 2	8p11.2	ADAM2	
A kinase (PRKA) anchor protein 3	12p13.3	AKAP3	
Armadillo Repeat Containing 3	10p12.31	ARMC3	Y
ATPase family, AAA domain containing 2	8q24.13	ATAD2	
B melanoma antigen 1-5	21p11.1	BAGE1-5	Y
Bromodomain, testis-specific	1p22.1	BRDT	
Calcium binding tyrosine-(Y)-phosphorylation regulated	18q11.2	CABYR	Y
Cancer antigen 1	6p24.3	CAGE1	Y
Calreticulin 3	19p13.11	CALR3	
Coiled-coil domain containing 110	4q35.1	CCDC110	Y
Coiled-coil domain containing 62	12q24.31	CCDC62	Y
Cytochrome c oxidase subunit VIb polypeptide 2 (testis)	19q13.42	COX6B2	
Cysteine-rich secretory protein 2	6p12.3	CRISP2	
Chondrosarcoma associated gene 1	Xq28	CSAG1	
CSAG family, member 2	Xq28	CSAG3	Y
Cancer/testis antigen family 45 (8 members)	Xq26.3	CT45A1-6	Y
Cancer/testis antigen family 47 (4 members)	Xq24	CT47A1-6,8-11	
Cancer/testis antigen 1B	Xq28	CTAG1B	Y
Cancer/testis antigen 2	Xq28	CTAG2	Y
Cutaneous T-cell lymphoma-associated antigen 1	18p11.2	CTAGE1	
CCCTC-binding factor (zinc finger protein)-like	20q13.31	CTCFL	Y
Chromosome X open reading frame 48	Xq26.3	CXorf48	
Chromosome X open reading frame 61	Xq23	CXorf61	Y
DEAD (Asp-Glu-Ala-Asp) box polypeptide 43	6q12-q13	DDX43	
DEAD (Asp-Glu-Ala-Asp) box polypeptide 53	Xp22.11	DDX53	Y
Dickkopf-like 1 (soggy)	19q13.33	DKKL1	
Developmental pluripotency associated 2	3q13.13	DPPA2	Y
Family with sequence similarity 46, member D	Xq21.1	FAM46D	Y
Fetal and adult testis expressed 1	Xq28	FATE1	Y
Fragile X mental retardation 1 neighbor	Xq28	FMR1NB	Y
Ferritin, heavy polypeptide-like 17	Xp21	FTHL17	
G antigen 1,2,3,4,5,6,7,8,12B,12E,12C,12D,12E,12F,12G,12H,12I,12J,13 (19 members)	Xp11.23	GAGE1-8,2A, 12B-J,GAGE13	Y

Table 1, continued. Screened Cancer Testis Antigens

Description	*Location*	*Gene Name*	*Antigenic*
HORMA domain containing 1	1q21.3	HORMAD1	Y
Insulin-like Growth Factor 2 mRNA Binding Protein 3	7p11	IGF2BP3	Y
Immunoglobulin superfamily, member 11	3q13.32	IGSF11	Y
Interleukin 13 receptor, alpha 2	Xq13.1-q28	IL13RA2	
Lactate dehydrogenase C	11p15.1	LDHC	
LEM domain containing 1	1q32.1	LEMD1	
Lipase, member I	21q11.2	LIPI	
Leucine zipper protein 4	Xq23	LUZP4	Y
Lymphocyte antigen 6 complex, locus K	8q24.3	LY6K	Y
Melanoma antigen family A, 8	Xq28	MAGEA8	
Melanoma antigen family A, 9	Xq28	MAGEA9	Y
Melanoma antigen family B, 1	Xp21.3	MAGEB1	Y
Melanoma antigen family B, 2	Xp21.3	MAGEB2	Y
Melanoma antigen family B, 3	Xp21.3	MAGEB3	
Melanoma antigen family B, 4	Xp21.3	MAGEB4	
Melanoma antigen family B, 5	Xp21.3	MAGEB5	
Melanoma antigen family B, 6	Xp21.3	MAGEB6	
Melanoma antigen family C, 1	Xq26	MAGEC1	Y
melanoma antigen family C, 2	Xq26	MAGEC2	Y
Melanoma antigen family C, 3	Xq26	MAGEC3	
MORC family CW-type zinc finger 1	3q13	MORC1	
Nuclear RNA export factor 2	Xq22.1	NXF2	
Outer dense fiber of sperm tails 1	8q22.3	ODF1	
Outer dense fiber of sperm tails 2	9q34.11	ODF2	Y
Outer dense fiber of sperm tails 3	11p15.5	ODF3	Y
Opa interacting protein 5	15q15.1	OIP5	
P antigen family, member 2 (prostate associated)	Xp11.21	PAGE2	Y
P antigen family, member 4 (prostate associated)	Xp11.21	PAGE4	Y
P antigen family, member 5 (prostate associated)	Xp11.21	PAGE5	
PAS domain containing 1	Xq28	PASD1	Y
Piwi-like 2 (Drosophila)	8p21.3	PIWIL2	
Placenta-specific 1	Xq26	PLAC1	Y
POTE ankyrin domain family B,C,D (3 members)	8p11.1,15q11.2,21q11.2	POTEB-D	
Preferentially expressed antigen in melanoma	22q11.22	PRAME	Y
Sarcoma antigen 1	Xq26	SAGE1	Y

Table 1, continued. Screened Cancer Testis Antigens

Description	*Location*	*Gene Name*	*Antigenic*
Solute Carrier Organic Anion Transporter Family, Member 6A1	5q21.1	SLCO6A1	Y
Sperm autoantigenic protein 17	11q24.2	SPA17	Y
Sperm associated antigen 9	17q21.33	SPAG9	Y
SPANX family, member A1,A2,C,D, E2 (5 members)	Xq27.1	SPANX	Y (B)
SPANX family, member N5	Xq27.1	SPANXN5	
Spermatogenesis associated 19	11q25	SPATA19	
SPO11 meiotic protein covalently bound to DSB homolog (S. cerevisiae)	20q13.31	SPO11	
Synovial sarcoma, X breakpoint 1	Xp11.23	SSX1	
Synovial sarcoma, X breakpoint 2	Xp11.23	SSX2	Y
synovial sarcoma, X breakpoint 4	Xp11.23	SSX4	Y
Testis Specific, 10	2q11.2	TSGA10	Y
Protease, Serine, 50	3p21.31	TSP50	
Testis specific protein, Y-linked 1 (3 members)	Yp11.2	TSPY1	
X antigen family, member 1B, E (2 members)	Xp11.22	XAGE1B; XAGE1E	Y
X antigen family, member 2	Xp11.22	XAGE2	
Zinc finger protein 165	6p21.3	ZNF165	Y

Figure 3: Platform for a multidimensional screen to interrogate CTA function.

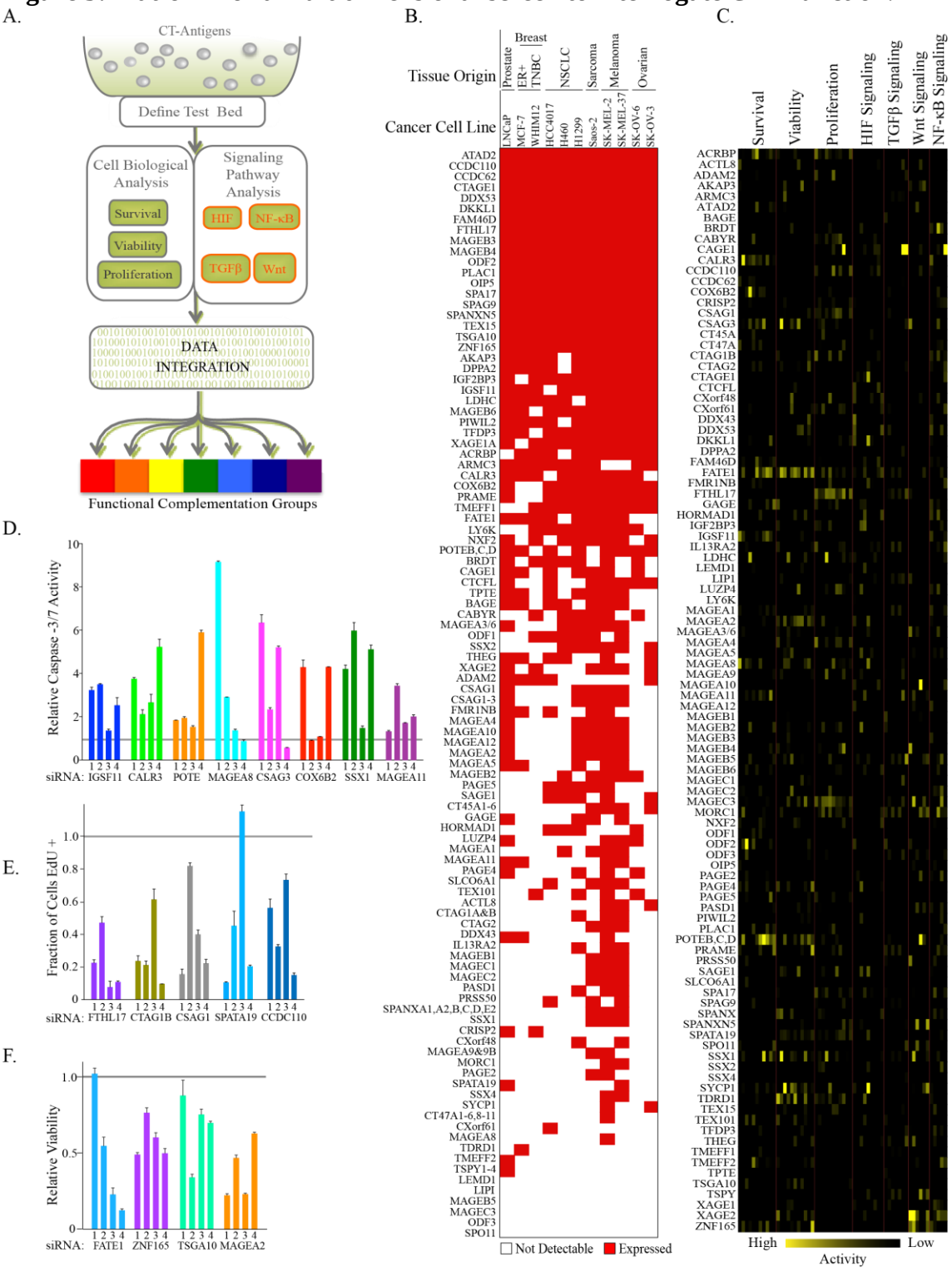

Figure 3: Platform for a multidimensional screen to interrogate CTA function. (A) Workflow for siRNA screen. (B) Presence (red) and absence (white) calls for all CTAs in indicated cell lines based on quantitative mRNA expression analysis. (C) Z-scores for each screen were calculated and plotted for each CTA (left) for each assay and cell line (top, cell lines are hidden). (D-F) siRNAs were transfected into cell lines and 96 hours post transfection, APO (D), EdU (E) and CTG (F) assays were performed. Bars represent mean (n = 2) ± range. Grey line indicates activity of control siRNA. Numbers indicate independent siRNA sequences.

Figure 4: FATE1 supports tumor cell viability

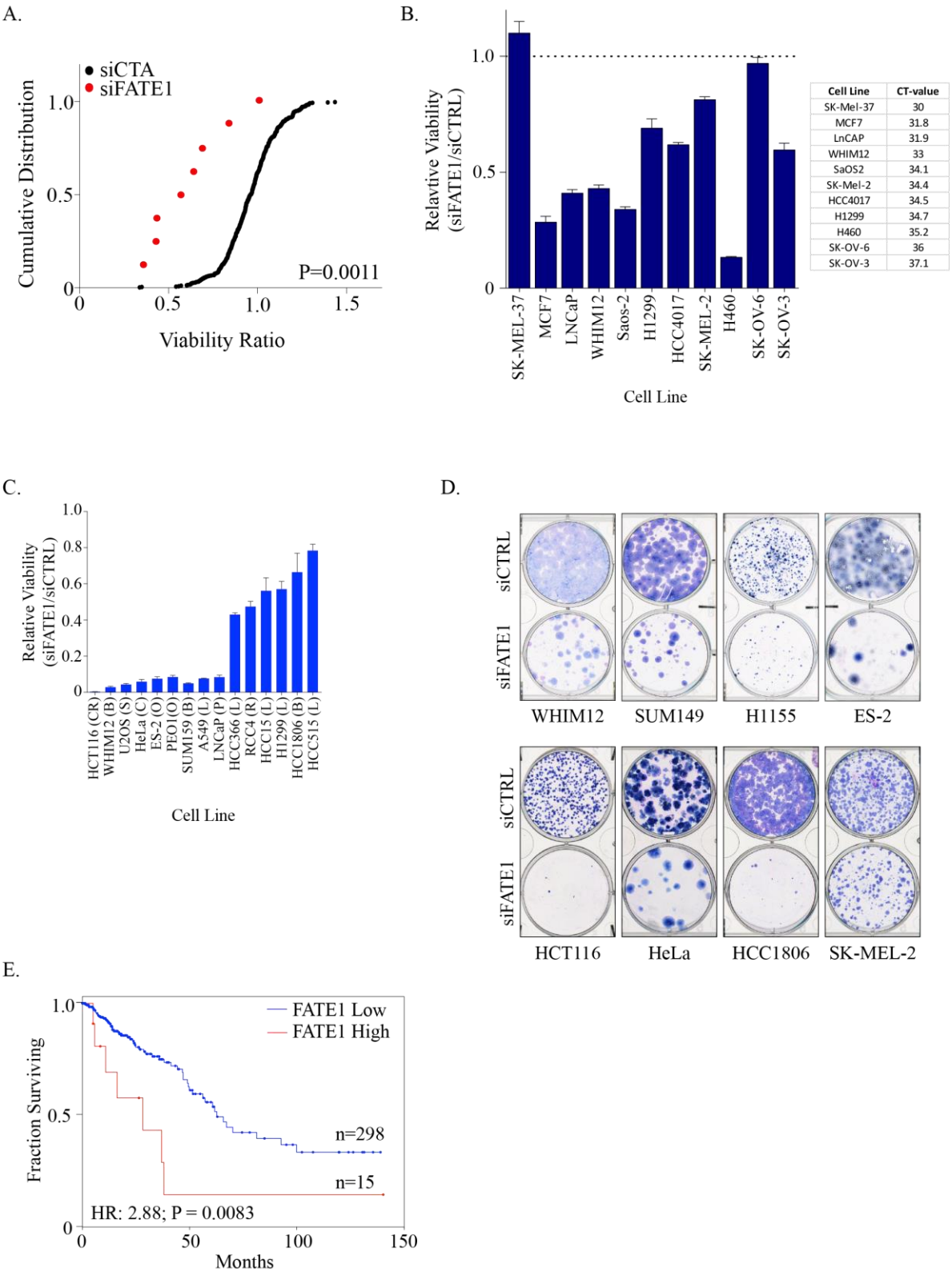

Figure 4: FATE1 supports tumor cell viability. (A) Distribution of siFATE1 viability ratios versus all other siCTAs in testbed cell lines where FATE1's mRNA expression value was a CT value < 35. Points represent mean of at least 2 independent assays. P value calculated by Kolmogorov-Smirnov test. (B) Left: Viability (relative to non-targeting control) in all testbed cell lines 96 hours after siFATE1 transfection. Bars represent mean ($n \geq 2$) ± range. Right: mRNA (CT) expression values of FATE1 in test bed cell lines. (C) Viability assay in indicated cell lines 120 hours post siRNA transfection. Bars represent mean viability relative to siCTRL ($n = 4$) ± standard error of the mean (SEM). CR: Colorectal, B: Breast, S: Osteosarcoma, C: Cervical, O: Ovarian, L: Lung, P: Prostate, R: Renal. (D) Colony formation assays were performed 48 (HCT116) or 72 hours after siRNA transfection. Data representative of 2 independent assays. (E) Kaplan-Meier (KM) survival curves from TCGA colorectal adenocarcinoma patients. HR and P value calculated by Cox Regression Analysis.

Figure 5: FATE1 domain structure.

A.

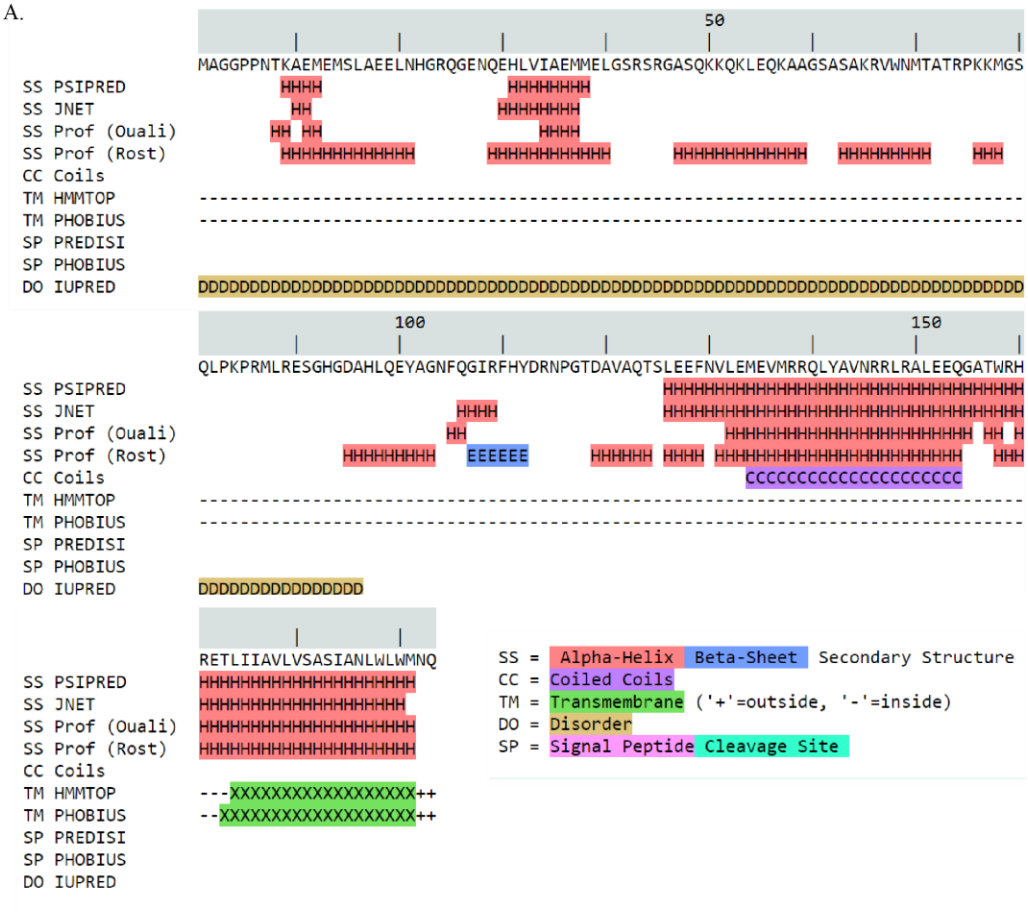

B.

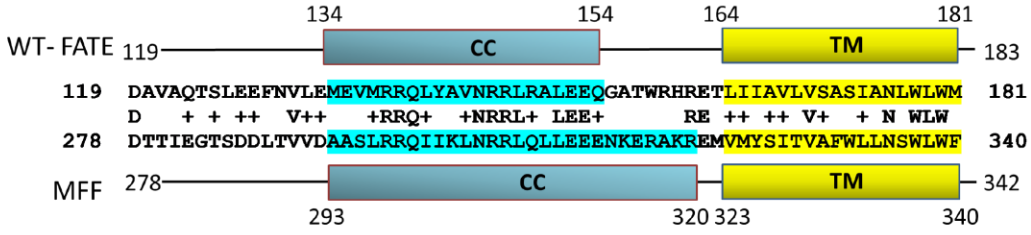

Score = 43.1 bits (100), Expect = 9e-10, Method: Compositional matrix adjust.
Identities = 19/63 (30%), Positives = 36/63 (57%), Gaps = 0/63 (0%)

C.

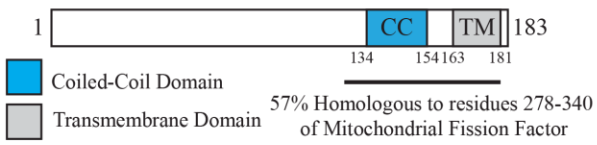

Figure 5: FATE1 domain structure. (A) Quick2D protein motif output for FATE1 amino acid sequence. Potential transmembrane domain in green and coiled-coil domain in purple. (B) Protein-Blast search of FATE1's amino acid sequence identified homology between the C-termini of FATE1 and Mitochondrial Fission Factor. (C) Domain map of FATE1. CC: Coiled Coil; TM: Transmembrane.

Figure 6: FATE1 is a mitochondrial protein.

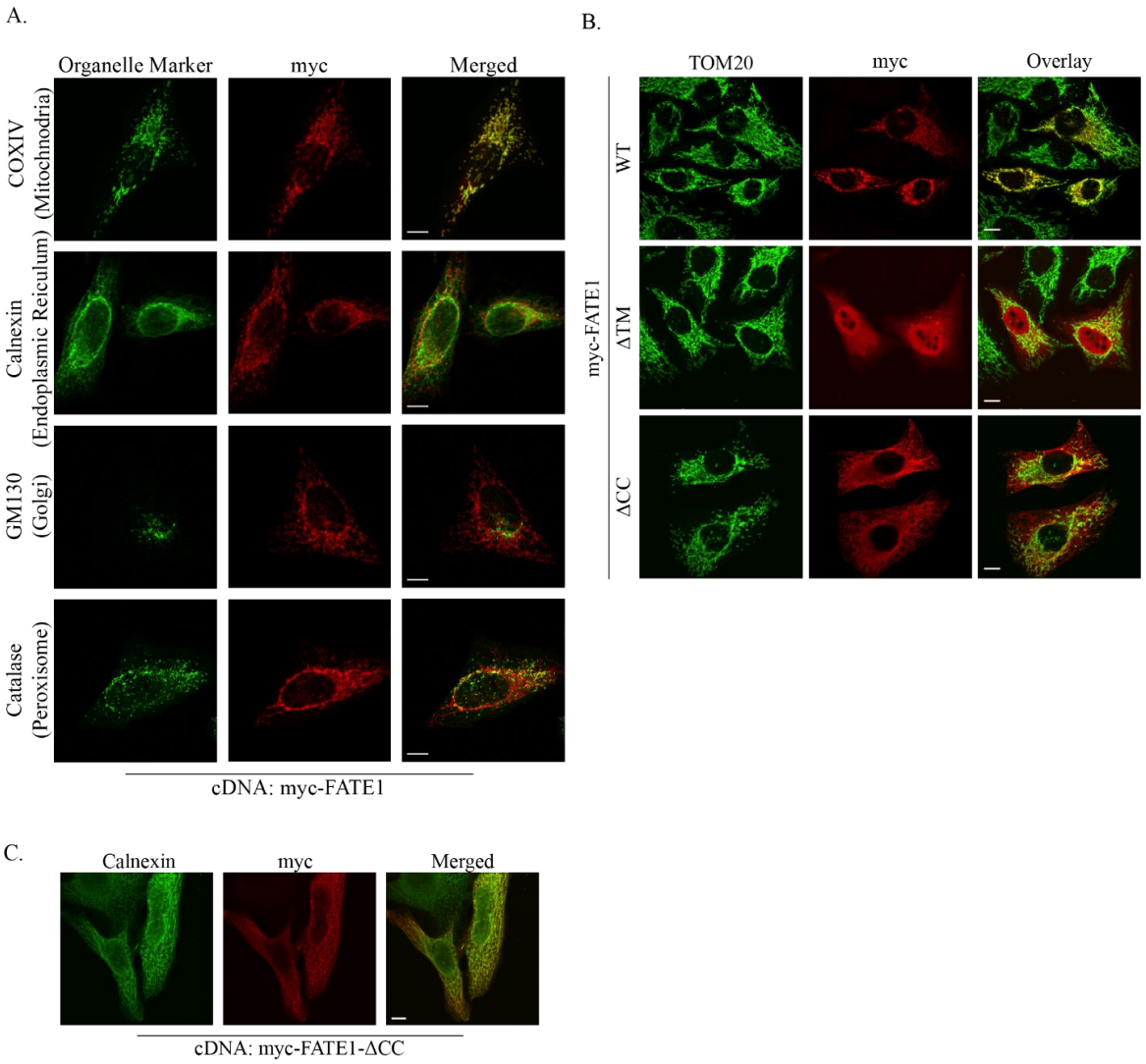

Figure 6: FATE1 is a mitochondrial protein. (A) HeLa cells transfected with indicated cDNAs for 24 hours were fixed, immunostained with indicated antibodies (top), and imaged with confocal microscopy. WT: Wild-type, ΔTM: Transmembrane Deletion, ΔCC: Coiled-Coiled deletion. Scale bars represent 10 μm. Data representative of 2 independent assays. TOM20 was used to visualize the mitochondria. (B) HeLa cells transfected with myc-FATE1 for 24 hours were fixed, stained with indicated antibodies, and imaged with confocal microscopy. Data representative of 2 independent assays. Scale bars represent 10 μm. Organelles (left) are in green, myc-FATE1 is in red. (C) HeLa cells transfected with myc-FATE1ΔCC cDNA for 24 hours was fixed and permeabilized in ice cold methanol and then processed for immunofluorescence with myc (red) and calnexin (green) antibodies. Scale bar represents 10 μm.

Figure 7: FATE1 interacts with Mitochondrial Fission Factor.

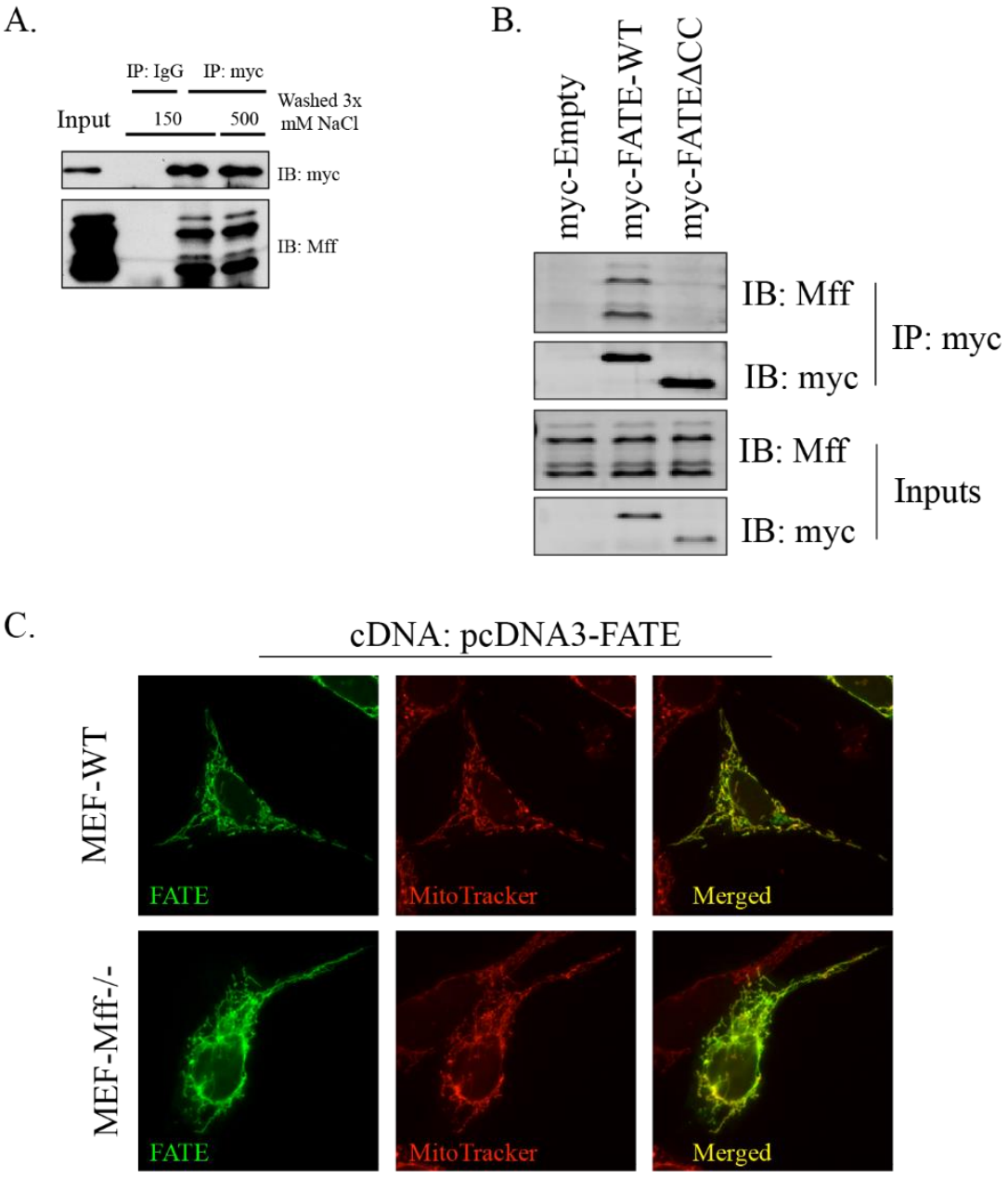

Figure 7: FATE1 interacts with Mitochondrial Fission Factor. (A) Lysates from H1299 cells stably expressing indicated cDNAs were immunoprecipitated with anti-myc antibody, washed three times with normal (150 mM) or high (500 mM) salt-lysis buffer, and then immunoblotted as indicated. (B) Lysates from H1299 cells expressing indicated cDNAs were immunoprecipitated and then immunoblotted as indicated. IP: immunoprecipitated, IB: immunoblotted. (C) Wild-type or Mff-knockout mouse embryonic fibroblasts on glass coverslips were transfected with FATE1 cDNA. 24 hours later, cells were incubated with MitoTrackerRed CMXRos for 30 minutes, fixed, and processed for immunofluorescence with anti-FATE1 antibody.

Figure 8: FATE1 alters mitochondrial morphology.

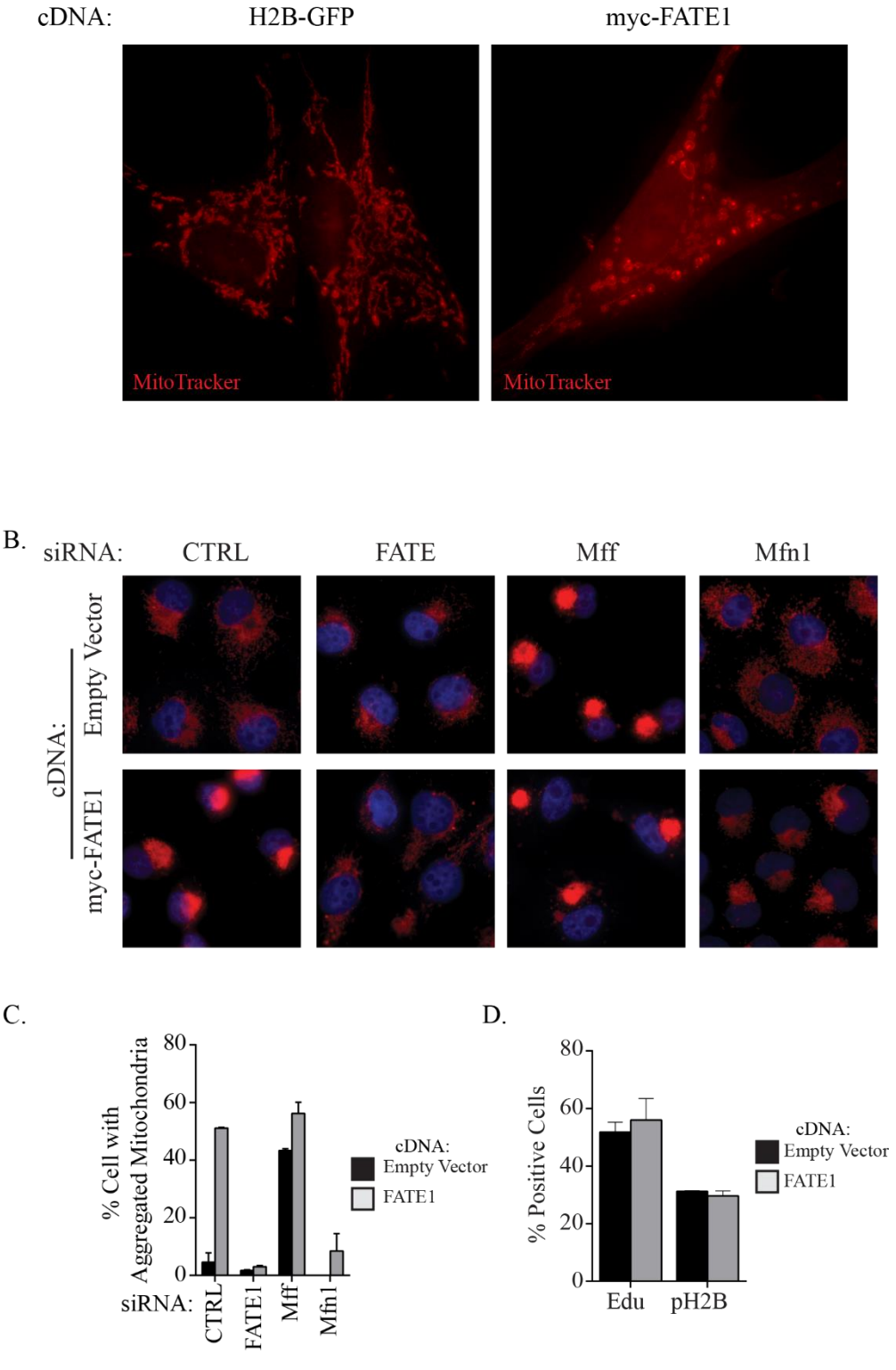

Figure 8: FATE1 alters mitochondrial morphology. (A) BJ-Fibroblasts stably expressing indicated cDNAs were incubated with MitoTracker RedCMXRos for 30 minutes, fixed, and then imaged. (B) H1299 stably expressing indicated cDNAs were reverse transfected with indicated siRNAs. 48 hours after siRNA transfection, cells were incubated with MitoTracker RedCMXRos for 30 minutes, fixed, and processed for immunofluorescence. (C) Mitochondrial morphology of cells in (B) was manually quantitated in > 200 cells per condition in two independent experiments. Bars represent mean (n = 2) ± range. (D) H1299 cells transfected as in (b) were stained with indicated antibodies and more than > 200 cells per condition in two independent experiments were counted. Bars represent mean (n = 2) ± range.

CHAPTER IV: FATE1 MODULATES PROGRAMMED CELL DEATH WITHIN TUMOR CELLS[2]

Introduction

A defining hallmark of malignant cells is the ability to resist signals arising from both internal (e.g. oncogenic stress, DNA damage) and external (e.g. hypoxia) sources that would otherwise activate the process of programmed cell death, apoptosis [98, 99] . Tumor cells employ a number of mechanisms to overcome these insults, including: upregulation of anti-apoptotic proteins, and loss or suppression of proteins that activate apoptosis (e.g. p53) or suppress pro-survival signaling (e.g. PTEN) [100, 101]. Targeting the dysregulated apoptotic pathway within tumors has proven effective in early phase clinic trials using navitoclax, an anti-apoptotic Bcl-2 family inhibitor; however, side effects including anemia and other cytopenias, infection, and gastrointestinal distress were common [102, 103]. The identification and targeting of tumor-specific mechanisms of deflecting cell death signals would significantly reduce such side effects while maintaining clinical efficacy.

Cancer Testes Antigens represent a cohort of genes that could deflect cell death in a nearly tumor-specific fashion. In our comprehensive analysis of CTAs (Chapter III) we found that depletion of multiple CTAs led to a significant cellular apoptotic activity within cells. The

[2] Elements of the work referenced in this chapter are published in: Kimberly E. Maxfield and Patrick J. Taus, Kathleen Corcoran, Joshua Wooten, Jennifer Macion, Yunyun Zhou, Mark Borromeo, Rahul K. Kollipara, Jingsheng Yan, Yang Xie, Xian-Jin Xie, and Angelique W. Whitehurst. Comprehensive Functional Characterization of Cancer-Testis Antigens Defines Obligate Participation in Multiple Hallmarks of Cancer. Nat Commun. 2015 Nov 16

studies presented here in Chapter IV will elaborate the role of FATE1 in antagonizing apoptosis. To begin I will discuss the regulation of the apoptotic pathway as mediated by members of the Bcl-2 protein family as well as the post-translational mechanisms that can alter levels of this protein family and in doing so alter cellular sensitivity to apoptosis itself.

Regulation of Apoptosis

Apoptosis or programmed cell death is a cellular process that allows cellular destruction in a controlled, inflammatory-free manner that is critical for development and tissue homeostasis. Apoptosis plays a critical role in proper male germ cell development as loss of Bcl-2 family members BAX, BCL-W, or simultaneous loss of BIM and BIK lead to defects in spermatogenesis resulting in infertility [104-106]. On a molecular level, the apoptotic pathway is regulated by members of the Bcl-2 protein family. This family is define by the presence of four Bcl-2 Homology domains (BH1-BH4) and can be divided into three functional groups: 1) the pro-apoptotic mitochondrial pore-forming members, BAX and BAK, 2) the anti-apoptotic members (BCL-2, BCL-xL, and MCL-1) that antagonize activity of the pro-apoptotic members, and 3) the third group, called BH3-only members due to their possession of only a BH3 domain, that serve as apical sensors of the pathway and transduce discrete cellular stress signals to the other family members (Figure 9) [107]. Activation of the pore-forming members leads to the release of pro-apoptogenic factors such as cytochrome c and SMAC from the mitochondrial and a nearly irreversible apoptotic cascade resulting in cellular destruction through the activity of cellular caspases, cysteine-aspartic proteases that target proteins throughout the cell leading to its demise [108, 109].

Post-translational regulation of the apoptotic pathway

Apoptosis is regulated in part by the balance of pro- and anti-apoptotic Bcl-2 members. These levels can be controlled on transcriptional, translational, and post-translational levels [110-112]. For the purposes of the results discussed in this chapter, an overview of the current body of work concerning the post-translational regulation of Bcl-2 family members through the actions of the ubiquitin-proteasome systems (USP) will be presented at this time.

The UPS along with autophagy are the major mechanisms by which cells degrade intracellular proteins. While autophagy degrades proteins and macromolecules wholesale at an organelle level, the UPS targets individual proteins for degradation through conjugation of ubiquitin chains onto lysine residues within the target protein or onto a target protein's free N-terminal α-amino group through the N-rule pathway [113, 114]. Tight ubiquitin-mediated degradation of numerous members of the Bcl-2 protein family is required to maintain cellular homeostasis [115]. The necessity of this regulation can be seen in the clinic as multiple Bcl-2 family members including BIK, NOXA, and BIM drive tumor cell death following treatment with Bortezomib a proteasome inhibitor which is used clinically under the name Velcade® for treatment of multiple myeloma and relapsed mantle cell lymphoma [116, 117].

The conjugation of ubiquitin molecules onto target proteins is carried out sequentially through the action of three distinct classes of ubiquitin conjugating enzymes: E1s, E2s, and E3s. E1 enzymes activate ubiquitin in an ATP-dependent process that conjugates the ubiquitin directly onto an E1 cysteine via a thioester linkage [118]. The activated ubiquitin is transferred onto a cysteine (via a thioester linkage) within an E2-conjugating enzyme [118]. Finally, ubiquitin is transferred to the final substrate through the activity of E3-ligases [118]. Eukaryotes have two main forms of E3-ligases defined by either RING (Really Interesting New Gene) or

HECT (Homologous to the E6-AP Carboxyl Terminus) domains that interact with E2 enzymes. RING domains facilitate the direct transfer of the charged ubiquitin from the E2 onto the target lysine while HECT domain-containing proteins form a thioester with the ubiquitin before transferring it to the substrate [118, 119].

E3-ligases are targeted to their substrates either directly or through additional binding partners that serve as scaffolding/adaptor proteins [118]. The activity of E3-ligases is also regulated by post-translation modifications of the substrates including phosphorylation (the most prominent), glycosylation and proline hydroxylation [113]. The activity of E3-ligases can also be regulated by the E3-ligase itself through self-ubiquitination which can occur in both substrate-independent, and substrate-dependent fashions [120]. Within the cell, the activity of E3-ligases is also regulated by the activity of deubiquitinases, proteases that cleave ubiquitin chains which serve to fine tune or even reverse ubiquitin modification on substrates and E3-ligases alike [121].

Results

Depletion of FATE1 activates programmed cell death

In our cellular survival screen (Chapter III) depletion of FATE1 l elevated the activity of executioner caspases greater than 2-fold in 5 of the 8 lines in which it was expressed (Figure 10A). This induction of the apoptotic pathway was also detectable by immunoblot in a range of tumorigenic settings and suggests that depletion of FATE1 potently induces the programmed cell death pathway (Figure 10B and C). Importantly, while FATE1 protein was detectable in all tumor-derived cell lines, it was low or undetectable in telomerase immortalized, non-tumorigenic fibroblasts and lung epithelial cells, where siFATE1 did not lead to cleavage of caspase-3 (Figure 10C). Taken together, these data suggest that reactivation of FATE1 may be required to

suppress apoptosis specifically in the transformed cellular environment irrespective of disease site.

siFATE1-induced apoptosis requires the core apoptotic machinery

Given the potent induction of the apoptotic pathway following depletion of FATE1 and FATE1's localization to the mitochondria, a critical signaling hub in apoptotic signaling, we further analyzed the role of the key regulators of mitochondrial premeabilization siFATE1-induced death. Depletion of FATE1 in HCT116 cells induced cleavage of PARP1 and cytochrome c release, a phenotype that was absent in BAX/BAK null HCT116 cells (Figure 11A). Overexpression of the anti-apoptotic Bcl-2 family member, BCL-xL, also rescued cell death following siFATE1 (Figure 11B). Consistent with a general role in deflecting apoptosis, we found that cells overexpressing FATE1 exhibited attenuated PARP1 cleavage following staurosporine (STS) challenge (Figure 11C).

FATE1 regulates stability of the BH3-only tumor suppressor BIK

To further elaborate the mechanisms of FATE1's anti-apoptotic function, we examined FATE1 interacting partners reported by large-scale proteomics studies (Figure 12A) [122, 123]. Among the dozen interactors was the founding member of the pro-apoptotic BH3-only family, BCL-2 Interacting Killer (BIK) [124-126]. Since its discovery it has been noted that the BIK locus is found deleted or silenced in several forms of cancer including renal cell carcinomas, gliomas, colorectal, head and neck, and lymphomas suggesting it can function as a tumor suppressor [127-131]. BIK can be induced transcriptionally by genotoxic stress, E2F stimulation, cytokines (IFNγ and TGFβ), IgM ligation and estrogen starvation and BIK mRNA is frequently

found upregulated in tumors compared to normal tissues (Figure 12B) [132-138]; however, BIK protein is expressed at low to undetectable levels indicating that tumor cells adapt mechanisms to prevent BIK protein accumulation [116, 117, 125, 139, 140]. These mechanisms likely consisted of augmented proteasome-mediated turnover as inhibition of this pathway or attenuation of BIK ubiquitination leads to its accumulation [134, 141]. Accumulation of BIK correlates with the induction of apoptosis following treatment with Velcade ® (Bortezomib) a proteasome inhibitor approved for clinical use [116, 117]. We verified that FATE1 and BIK interact within mammalian cell (Figure 12C) and found that upon depletion of FATE1, BIK protein was stabilized within cancer cells (Figure 12D). Significantly, depletion of BIK rescued siFATE1-induced apoptotic signaling (Figure 12E), leading us to hypothesize that FATE1 may be involved in the regulation of BIK stability.

Within a cell, targeted degradation of proteins is mediated by the ubiquitin-proteasome system which is initiated via the conjugation of poly-ubiquitin chains to proteins destine for destruction. Conjugation of ubiquitin to target molecules is carried out by E3-ligases. While FATE1 does not have any identifiable E3-ligase domains, yeast 2-hybrid studies have identified several FATE1 binding partners with potential E3 ligase activity [142, 143]. Among this cohort, depletion of RNF183 led to stabilization of BIK (Figure 13A and B). RNF183 is uncharacterized protein with a C3HC4-RING domain whose expression may be a biomarker for endometrial carcinoma in uterine aspirates (Figure 13C) [144]. We found that RNF183 localized to the endoplasmic reticulum (Figure 13D). We confirmed that FATE1 and RNF183 interact within mammalian cells and confirmed the RNF183 possess E3-ligase activity which is dependent on its canonical RING domain cysteine residues (Figure 13E and 13F) [118].

In gain of function experiments, overexpression of wild-type RNF183, but not RNF183

lacking E3-ligase activity, reduced expression of exogenous BIK, indicating that RNF183's E3-activity negatively regulates BIK protein accumulation (Figure 14A). We also verified RNF183's ability to directly ubiquitinate BIK using a reconstituted *in vitro* system (Figure 14B). Given its potent effect on the stabilization of BIK, we evaluated the consequences of RNF183 depletion on cell viability. We observed a striking correlation between siFATE1 and siRNF183 sensitivity in a panel of tumor derived cell lines (Figure 14C and D). Furthermore, we found that BIK interacted with RNF183 along with FATE1 in intact cells (Figure 14E). These findings indicate that FATE1 and RNF183 may collaborate to restrain BIK protein levels and promote cellular escape from otherwise lethal apoptotic signaling.

We then examined a potential role for FATE1 and RNF183 cooperativity within patient tumors. In NSCLC, patients with tumors expressing high levels of both FATE1 and RNF183 were at highest risk for poor survival (hazard ratio (HR) = 2.80; $p < 0.0001$) as compared to those with high expression of only FATE1 (HR = 1.73, $p = 0.0124$) or RNF183 (HR = 1.62, $p = 0.0004$) (Figure 14F). In a separate NSCLC data set, the majority of tumors with high FATE1 expression exhibited elevated RNF183 expression, and high expression of both genes predicted shortened overall survival time (HR = 2.529, $p = 0.0004$) (Figure 14G). The frequency of co-expression of RNF183 and FATE1 along with their correlation with poor outcome reinforces the notion that these proteins are functioning in human tumors to promote survival.

Discussion

In this chapter we elucidate the ability of FATE1 to promote tolerance to cellular stress, which would otherwise lead to cellular demise. Successful tumorigenesis requires the circumvention of otherwise fatal fail-safe mechanisms and/or an adaption to unfavorable

physiological conditions. Prototypical examples include thwarting oncogene-induced pro-apoptotic signaling, DNA damage stress, toleration of proteotoxic stress due to aneuploidy, and buffering of oxidative stress resulting from altered mitochondrial function [145-147]. FATE1 may represent one mechanism by which tumor cells overcome these barriers by promoting the degradation of second messengers in this signaling system.

We also found that RNF183, a novel E3-ligase, associates with FATE1 and BIK, and is capable of regulating BIK protein levels. Several lines of evidence support the notion that FATE1 and RNF183 may function in a molecular complex that has clinical consequences. Possible roles for FATE1 in this interaction include modulation of RNF183 activity, substrate targeting, or processivity of ubiquitination, or regulating RNF183 protein levels by preventing its auto-ubiquitination. As FATE1 is also reported to interact with several other E3-ligases, it may have similar effects on these ligases although at this time potential targets for such complexes are unknown; however, in additional to BIK, FATE1 has also been found to interact with two additional tumor suppressive BH3-only proteins, BNIP3 and BNIP3L both of which should be high priority candidates for future studies into FATE1's anti-apoptotic activity [148, 149].

Figure 9: Overview of Bcl-2 family.

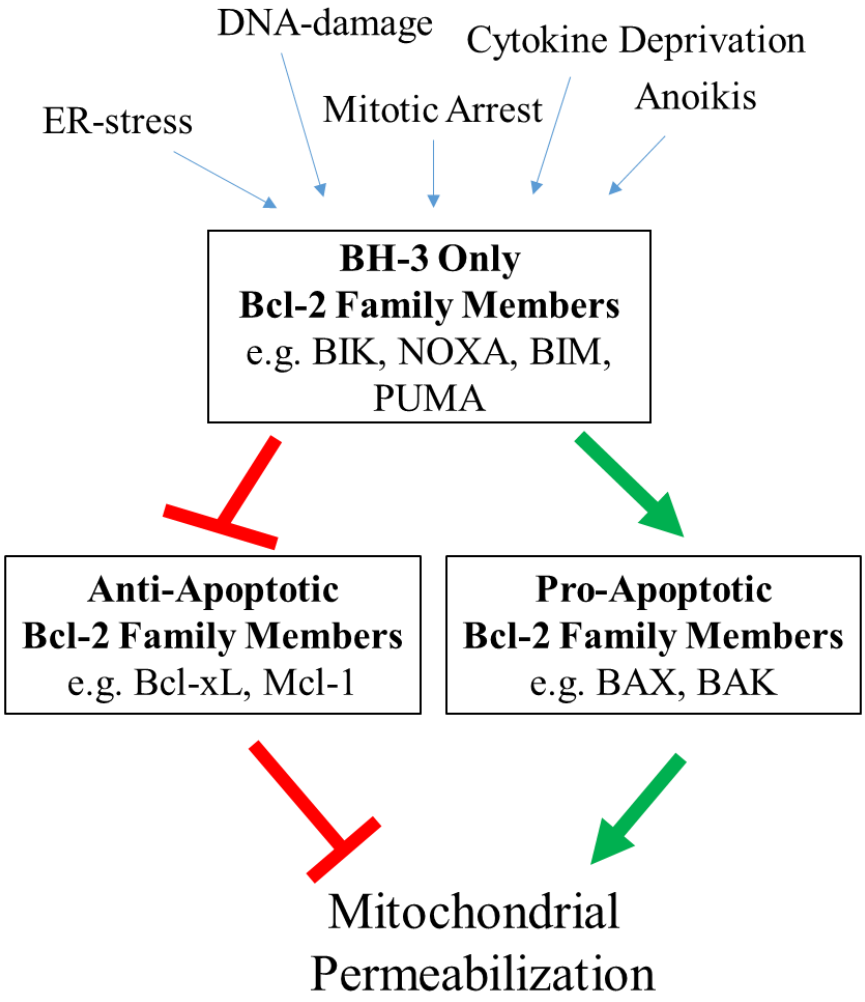

Figure 9: Overview of Bcl-2 family. BH3-only family members transduce a variety of cellular stress signals to the pro- and anti-apoptotic members of the Bcl-2 family. BH3-only members can either directly activate pro-apoptotic members or indirectly activate them by disrupting the sequestering activity of anti-apoptotic family members. Once active, BAX and BAK form pores within the mitochondrial outer membrane releasing pro-apoptogenic factors (e.g. cytochrome c and SMAC) into the cytosol initiating the apoptotic cascade culminating in cell death.

Figure 10: Loss of FATE1 induces programmed cell death.

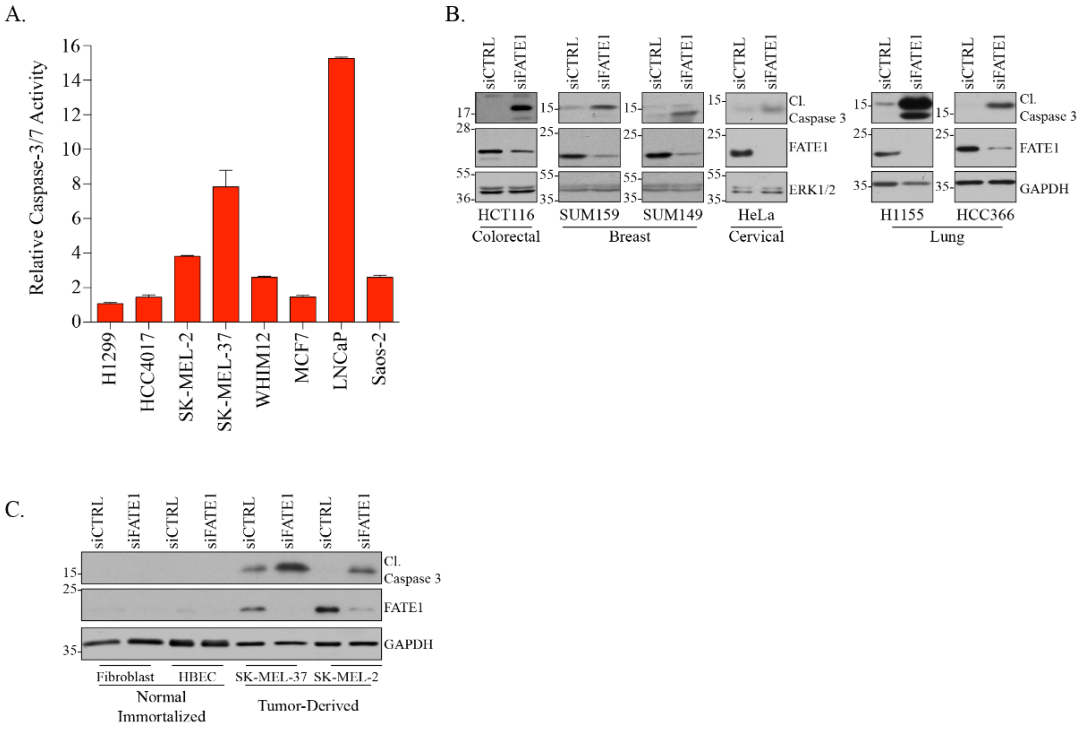

Figure 10: Loss of FATE1 induces programmed cell death. (A) Relative (to non-targeting control) cleaved caspase- 3/7 activity in testbed cell lines exhibiting detectable FATE1 expression 96 hours after siFATE1 transfection. (B) Whole cell lysates (WCLs) from indicated cell lines transfected with siCTRL or siFATE for 48 (HCT116), 72 (SUM159, SUM149, H1155) or 96 hours (HeLa, HCC366) were immunoblotted with indicated antibodies. Data representative of a minimum of 2 independent assays. (C) WCLs from indicated cell lines were immunoblotted as indicated 96 hours after siRNA transfection. Data representative of 2 independent assays.

Figure 11: FATE1 depletion engages the activity of Bcl-2 protein family.

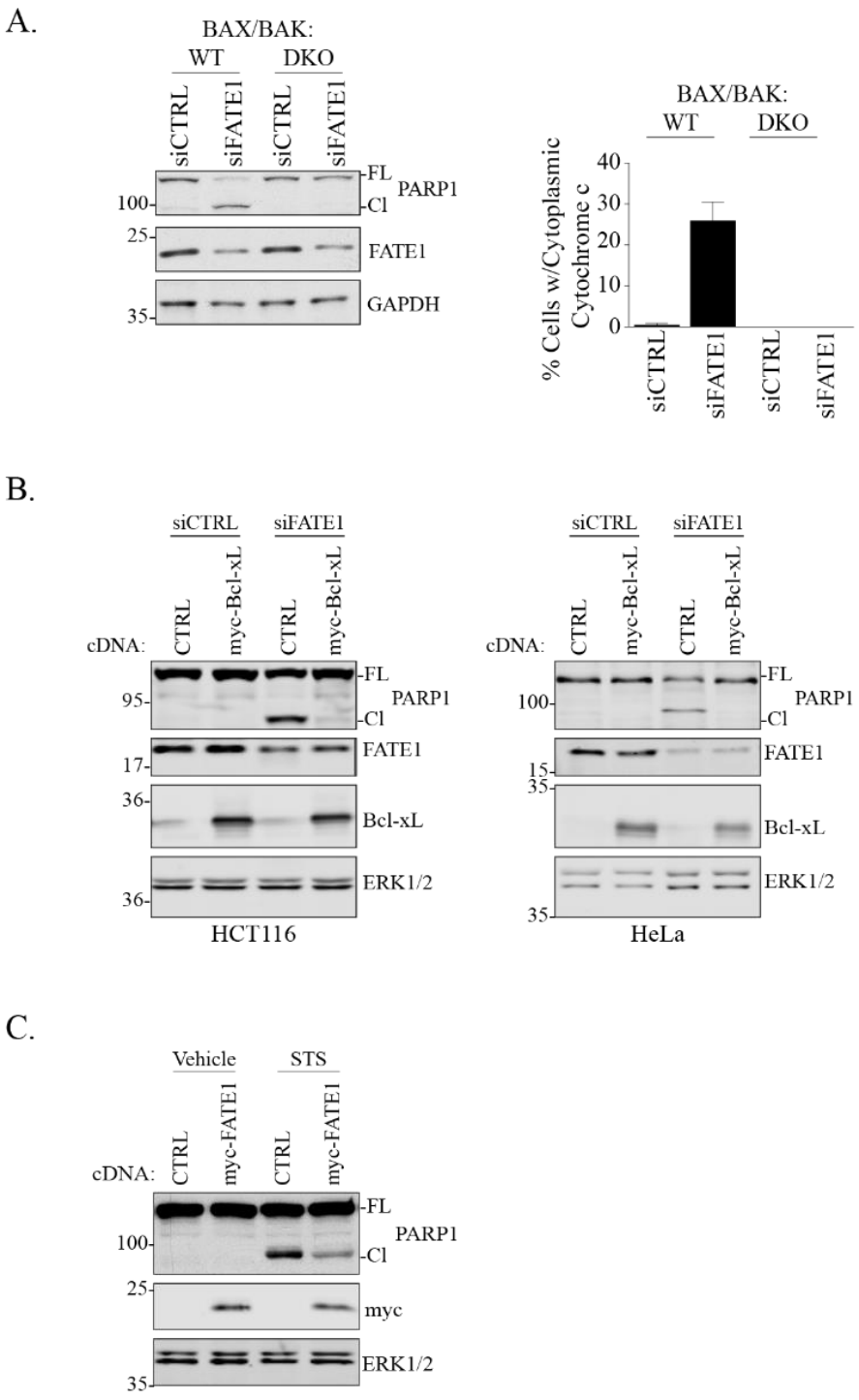

FATE1 depletion engages the activity of Bcl-2 protein family. (A) Left: 48 hours after siRNA transfection, WCLs from indicated HCT116 cells (DKO: Double Knockout) were immunoblotted with indicated antibodies. Data representative of 2 independent assays. Right: HCT116 cells were transfected and exposed to 10 μM Q-VD-OPh for 48 hours, fixed, and immunostained for cytochrome c and TOM20. Cytoplasmic cytochrome C was quantitated manually for ≥ 200 cells per experiment for each condition. Bars represent mean (n = 3) ± SD. FL = full length PARP1, Cl = cleaved PARP1. (B) WCLs from HCT116 or HeLa cells stably expressing a control construct (HCT116: empty vector; HeLa: pLPCX-GFP) or myc-BCL-xL were immunoblotted with indicated antibodies 48 (HCT116) or 72 hours (HeLa) post siRNA transfection. (C) H1299 cells stably expressing empty vector or myc-FATE1 were exposed to vehicle or 1 μM STS for 6 hours. WCLs were immunoblotted with indicated antibodies. Data representative of 3 independent assays.

Figure 12: FATE1 regulates BIK protein levels.

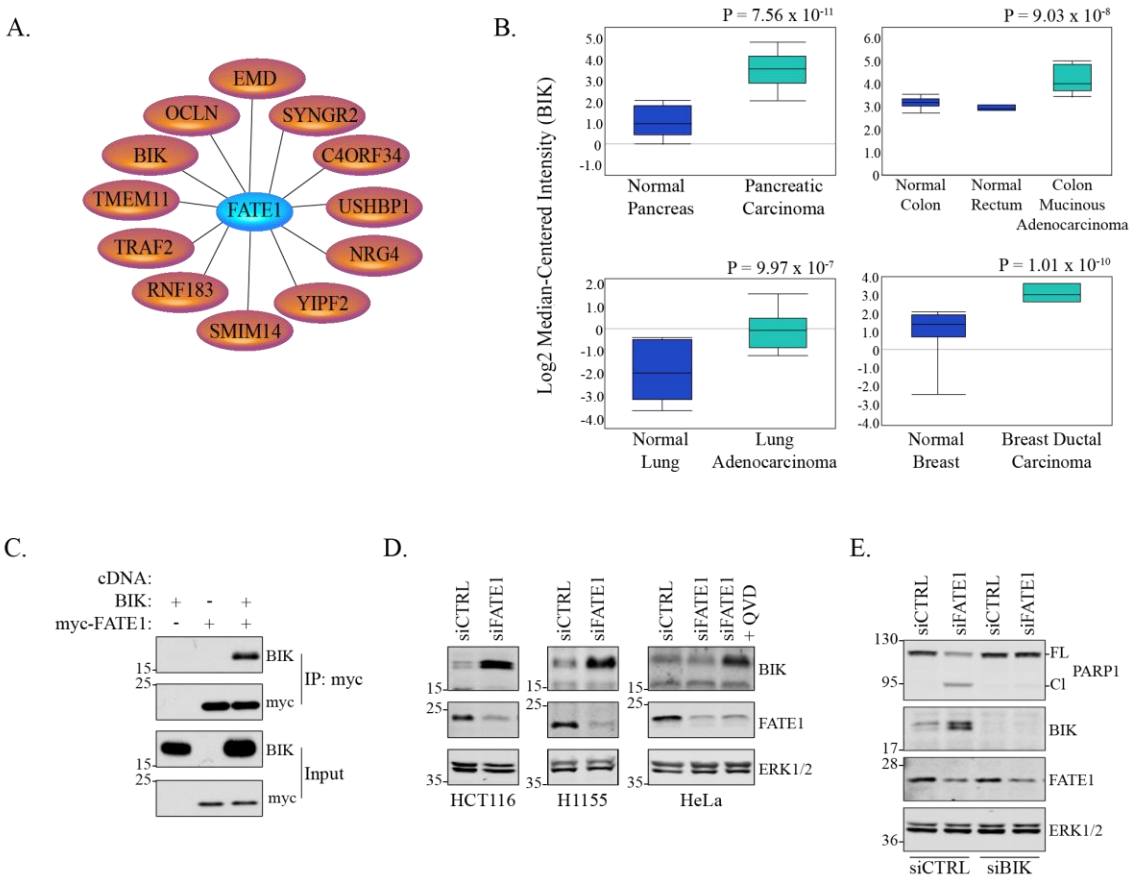

Figure 12: FATE1 regulates BIK protein levels. (A) Interaction data for FATE1 based on yeast two-hybrid proteomics analyses. (B) Expression of BIK mRNA in indicated tumor tissues [82-85]. Graphs generated by Oncomine™. (C) Sixteen hours after transfection in HEK293T cells, lysates (pH 8.0) were incubated with myc antibodies, washed in NDLB and immunoblotted with indicated antibodies. Data representative of 3 independent assays. (D) WCLs were collected 48 (HCT116) or 72 hours (H1155 and HeLa) following siRNA transfection and immunoblotted as indicated. +QVD: Cells were exposed to 10 μM of the pan-caspase inhibitor Q-VD-OPh for the duration of the experiment. Data representative of at least 2 independent assays. (E) HCT116 cells were transfected for 24 hours with siCTRL or siBIK then transfected with siCTRL or siFATE for an additional forty-eight hours. WCLs were collected and immunoblotted as indicated. Data representative of 3 independent assays.

Figure 13: FATE1 interactor RNF183 possesses E3-ligase activity.

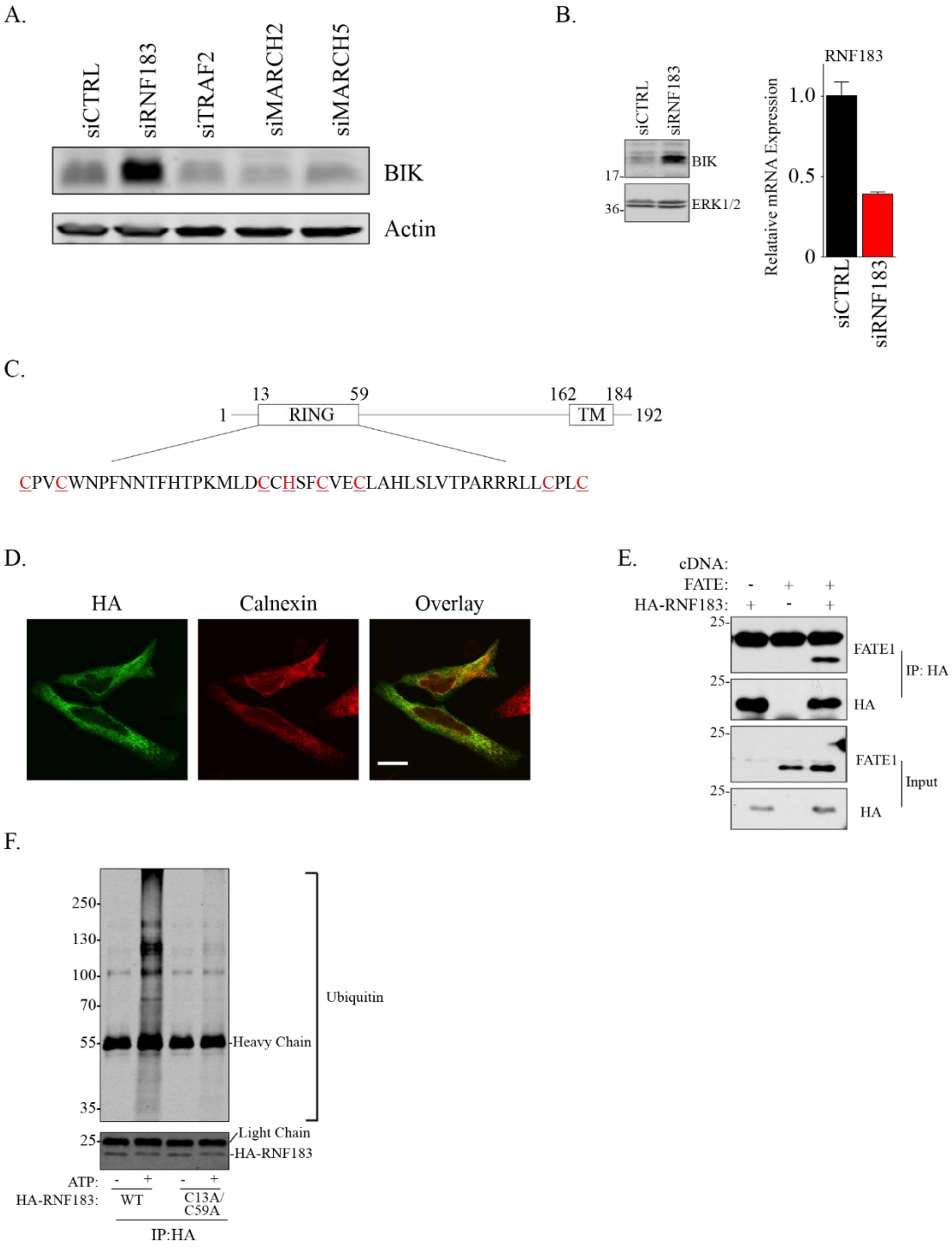

Figure 13: FATE1 interactor RNF183 possesses E3-ligase activity. (A) Seventy-two hours after transfection with indicated siRNAs, WCLs from HCT116 were immunoblotted as indicated. (B) Left: Seventy-two hours after transfection with indicated siRNAs, WCLs from HCT116 were immunoblotted as indicated. Right: RNA was collected from parallel samples was used to measure RNF183 mRNA expression. Bars represent mean (n = 2) ± range. (C) RNF183 domain structure based on the Human Protein Reference Database (HPRD). Conserved Zn++ -coordinating residues are underlined in red. RING: Really Interesting New Gene; TM: Transmembrane. (D) Twenty-four hours after transfection with pCMV-HA-RNF183, HeLa cells were fixed, immunostained with indicated antibodies, and imaged using confocal microscopy. Data representative of 2 independent assays. Scale bars represent 10 μm. Green is HA, Calnexin (red) is used to visualize the ER. (E) HEK293T cells were transfected with indicated plasmids for 24 hours, lysates prepared (pH 8.0) and then immunoprecipitated with anti-HA and immunoblotted as indicated. Data are representative of 3 independent assays. (F) HEK293T cells transfected with indicated cDNAs for 24 hours were immunoprecipitated and subjected to an autoubiquitination assay as described in Materials and Methods. Data representative of 2 independent assays.

Figure 14: RNF183 impacts the stability of the apoptotic effector BIK.

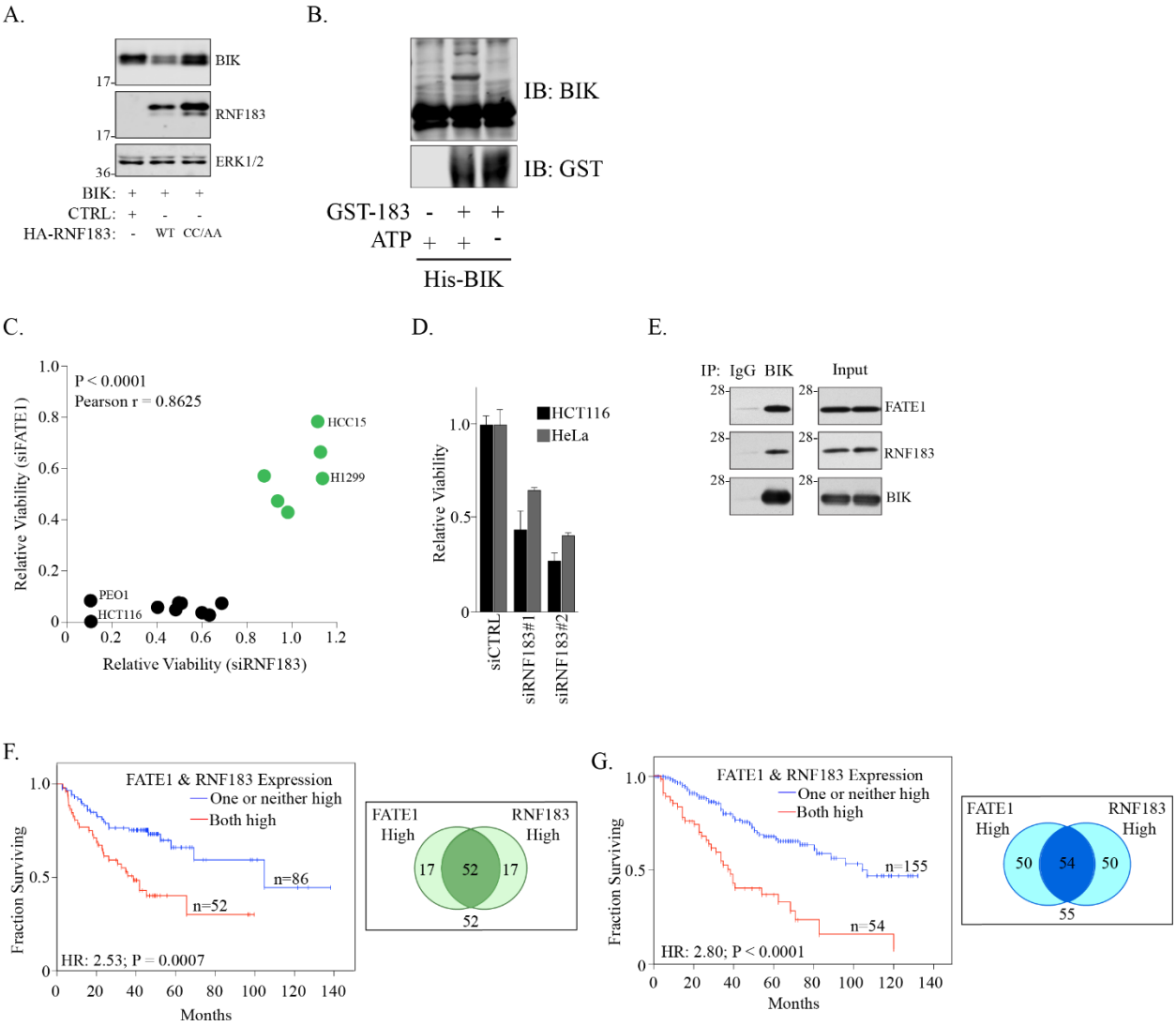

Figure 14: RNF183 impacts the stability of the apoptotic effector BIK. (A) WCLs from H1299 cells transfected with indicated cDNAs for 24 hours were immunoblotted as indicated. WT: Wild-type. CC/AA: C13A/C59A. Data representative of 3 independent assays. (B) An *in vitro* ubiquitination assay was performed as described in Materials and Methods using recombinant GST-RNF183 and 6xHis-BIK (C) Cell lines from Fig. 4c were transfected for 120 hours with siFATE (y-axis) or siRNF183 (x-axis) and cell viability was measured via CTG. Dots represent mean of 4 independent assays. (D) Viability assays was performed 96 hours after siRNA transfection in indicated cell lines. #'s = independent siRNA pools. Bars represent mean (n = 3) ± SD. (E) Twenty hours post transfection with BIK-L61G, FATE, and HA-RNF183 cDNAs, HEK293T cells were lysed in NDLB, immunoprecipitated and immunoblotted as indicated. Data representative of 2 independent assays. (F) Kaplan-Meier survival curves of patients from GSE42127 as a function of high FATE1 and RNF183 expressing tumors. Venn diagram represents proportion of patients in each group. HR and P value calculated by Cox Regression Analysis. (G) as in (F) with patients from GSE8894.

CHAPTER V: EWS/FLI1 DRIVES EXPRESSION OF MULTIPLE FUNCTIONAL CANCER TESTIS ANTIGENS

Introduction

The mechanisms by which CTAs are aberrantly activated within cancers has not been fully elucidated. Although alterations in DNA methylation are a significant driver of CTA expression, rarely do these alterations lead to induction of the entire CTA group, arguing that in certain cases additional transcriptional factors are involved. A potential role for tumor-specific transcription factors driving the activation of CTAs has yet to be explored. In this Chapter, studies examining the role of EWS-FLI1, a chimeric transcription factor that underlies the molecular pathology of Ewing sarcoma, in activation of FATE1 will be presented. To begin, I will discuss Ewing sarcoma, including its underlying biology, clinical management, and the current state of ongoing efforts to improve outcome for patients with the disease.

Ewing sarcoma

Ewing sarcoma is the second most common bone and soft tissue malignancy within adolescences with an incidence of roughly 10 cases per 1,000,000 adolescents. Under current treatment protocols patients presenting with localized disease have a five-year event free survival (EFS) of 73 %. Unfortunately, twenty-five percent of patients present with metastatic disease which has a five-year EFS of only 22 % [150, 151]. Furthermore, roughly 30 to 40 % of patients treated for local disease eventually develop recurrent disease which has a five-year survival rate

under 15 % [150, 152, 153]

Molecular pathology of EWS-FLI1

Ewing sarcoma is driven by an oncogenic transcription factor resulting from a genomic translocation [154]. In roughly 90 % of cases this chimeric transcription factor contains the C-terminus of EWS, a TET family transcription factor, and the N-terminus of FLI1, a member of the ETS transcription factor family member [155]. The fusion, which is under control of the constitutively active EWS-promoter, couples the transactivation activation domain of EWS to the DNA-binding domain of FLI1 [154, 156, 157]. Within Ewing sarcoma cells the fusion is essential for proliferation and tumorigenesis and aside from its causative translocation, the genetic landscape of Ewing sarcoma tumors is nearly devoid of additional chromosomal abnormalities [158, 159]. The resulting chimeric transcription factor can up and down regulate genes and examples of each have been shown to contribute to the survival and proliferation of Ewing sarcoma cells and xenografts [155]. EWS-FLI1 can bind conventional ETS motifs but also acquires the ability to bind GGAA repeats [160]. The ability of EWS-FLI1 to bind GGAA repeats was discovered while investigating the regulation of *NR0B1*. These study found a series of 25 GGAA repeats with the in *NR0B1* that were necessary and sufficient for EWS-FLI1 driven transcription of NR0B1 [160].

The majority of EWS-FLI1 GGAA-repeat binding sites were located within intergenic DNA, typically at great distances (> 200 kb) from transcription start sites [161]. These intergenic sites overlap with enhancer elements defined by the canonical enhancer marks H3K4me1 and H3K27ac marks [162]. The impact of EWS-FLI1 on enhancer activity is determined by the nature of the EWS-FLI1 binding site contained within [162]. Enhancers with four or more

GGAA-repeats were found to be activated by EWS-FLI1 (as measured by enhanced p300 recruitment) while enhancers containing conical ETS motifs were repressed [162]. As microsatellite regions are known to be highly polymorphic, variations at such sites may underlie the ethnic differences in susceptibility to the disease [163, 164].

To date, the study of Ewing sarcoma oncogenesis has been hampered by a lack of biologically relevant model systems. Early studies demonstrated that immortalized murine fibroblasts (NIH3T3 cells) were transformed by expression of EWS-FLI1 [165]; however, recently the value of this as a model for Ewing sarcoma oncogenesis has come into question due to differences in expression profiles of these cells with tumor samples from patients and differential requirements of EWS-FLI1 regulated genes for cell survival in murine and human cell lines [166, 167]. A potential explanation for differences observed between mouse and human systems is the different microsatellite composition of each species' genome [155]. These discrepancies suggest that production of a mouse model of Ewing sarcoma reflective of the human condition will be difficult. Also, the cell of origin of the diseases is unknown further adding to the difficultly of studying the oncogenesis of Ewing sarcoma. Several recent studies support mesenchymal progenitor cells as a strong candidate as the potential cell of origin for Ewing sarcoma; however while expression of EWS-FLI1 within mouse mesenchymal stem cells has induced transformation, transformation of human mesenchymal stem cells by EWS-FLI1 has yet to be demonstrated [168-170].

Current Treatment of Ewing sarcoma

Treatment of Ewing sarcoma consists of both local (surgery and/or radiation) and systemic chemotherapy. In the United States, the current standard of care chemotherapy regimen

consists of alternating courses of vincristine-cyclophosphamide-doxorubicin with ifosfamide-etoposide every three weeks for roughly one year [150]. Recently, an intensified protocol for patients presenting with localized disease in which chemotherapy was administered every two weeks increased event-free survival to 73 % (compared to 65 % in the standard arm, P = 0.48) [151]. Surgery is the first choice for local control of Ewing sarcoma tumors, however, radiation is considered for unresectable tumors, cases were potential functional morbidity from surgery is deemed too high or as adjuvant therapy in surgical cases in which negative margins are not obtained [171, 172]. Radiation in a preoperative setting in which clean margins are unlikely has led to tumor shrinkage and clear margins following subsequent surgery [173].

Ongoing clinical trials in Ewing sarcoma

Currently, on-going phase III clinical trials in the United States are testing the benefit of the addition of a second topoisomerase inhibitor, topotecan, to the current five drug backbone chemotherapeutic regimen (COG-AEWS1031) in patients with localized disease. A phase II study in patients with newly diagnosed Ewing sarcoma is also evaluating the efficacy of the addition of the a second topoisomerase inhibitor, irinotecan, as well as an additional alkylating drug, temozolomide, and the cardioprotecitve agent dexrazoxane to the current five drug backbone (NCI-2013-01094). A phase II trial is testing the efficacy of cabozantinib-s-malate, a receptor tyrosine kinase inhibitor, in patients with relapsed osteosarcoma or Ewing sarcoma (NCI-2014-01927).

In addition to traditional chemotherapeutic approaches, several immunotherapeutic avenues are being explored for Ewing sarcoma. A recent phase I trial combining 5-Aza-2'-deoxycitadine and a dendritic cell peptide vaccine targeting three cancer testis antigens (MAGE-

A1, MAGE-A3, and NY-ESO-1) in children with relapse or refractory sarcomas (including Ewing sarcoma) found that the treatment was well tolerated and over half of the patients developed a response to the antigens over the course of treatment [174]. Preliminary *in vitro* studies have also demonstrated the effectiveness of Natural Killer cells against Ewing sarcoma derived cell lines [175]. Approaches targeting the novel breakpoint region of the EWS-FLI1 fusion demonstrated that while the native peptide had poor loading onto HLA-A2.1, modified peptides with enhanced MHC loading could be used to raise CTLs that then demonstrated potent killing of tumor cells expressing endogenous EWS-FLI1 and could prolong survival of mice with Ewing sarcoma xenografts [176]. Unfortunately, although immune-mediated mechanisms are showing promise, Ewing sarcomas lose expression of MHC class I molecules during disease progression thereby limiting the temporal window in which immune therapies may be effective in treating the disease [177].

Results

FATE1 is a target of EWS-FLI1

While defining the testbed cell lines used in our comprehensive assessment of CTAs to tumorigenesis (Chapter III) we found that a cell line derived from a Ewing sarcoma tumor (TC-32) expressed the highest level of FATE1 mRNA (Figure 15A). Looking at an expanded panel of cell lines we found that Ewing sarcoma-derived cell lines expressed significantly higher levels of FATE1 mRNA compared to cell lines derived from other cancer backgrounds (osteosarcoma, breast, lung, melanoma, ovarian, and colorectal cancers) (Figure 15B). Ewing sarcoma tumors are driven by a well-defined chimeric transcription factor EWS-FLI1 that activates an oncogenic transcription program. We hypothesized the high levels of FATE1 were due to activation by

EWS-FLI1. In support of this hypothesis, ChIP-seq analysis of EWS-FLI1-immunoprecipitated DNA revealed a EWS-FLI1 binding site within FATE1's proximal promoter that overlapped with a region of open chromatin (Figure 15C). Intriguingly, the ChIP'ed DNA sequence contained multiple inverted GGAA repeats in relation to the FATE1 promoter (Figure 15C).

Although not definitive, a growing body of evidence suggests that mesenchymal progenitor cells are the cell of origin for Ewing's Sarcoma [168-170]. Interestingly, within this cell type, the chromatin within the FATE1 promoter overlaying the EWS-FLI1 binding site is in an open confirmation and this region condenses a small extent following differentiation into osteoblasts and to a much larger degree within adipocytes (Figure 15D). To assess the importance of the EWS-FLI1 site within the FATE1 promoter we cloned the endogenous FATE1 promoter into a luciferase reporter construct and found a significant induction of luciferase activity following expression of EWS-FLI1. Critically, this induction was lost when a truncated fragment of the FATE1 promoter lacking the EWS-FLI1 binding site was substituted into the reporter (Figure 15E). In comparison to other tumor-derived and stem cell lines in the ENCODE dataset, the chromosome region required for FATE1 induction is significantly more open chromatin within EWS502 cells which may be reflective of maintenance of an open state from the tumor's cell of origin or EWS-FLI1-driven epigenetic alterations (Figure 15F) [178].

EWS-FLI1 mediates expression of FATE1

To assess whether EWS-FLI1 was required for expression of FATE1 we depleted endogenous EWS-FLI1 in a panel of Ewing sarcoma derived cell lines using a siRNA oligo specific for the breakpoint region of Type I EWS-FLI1 fusions [179]. Depletion of EWS-FLI1 led to a concomitant decrease in expression of FATE1 mRNA in all four cell lines tested (Figure

16A). Additionally, we found that depletion of EWS-FLI1 led to a decrease in FATE1 protein levels in A673 and TC-32 cells (Figure 16B). To test whether EWS-FLI1 was sufficient to drive expression of FATE1 we overexpressed EWS-FLI1 cDNA in HCT116 cells and found a potent induction of FATE1 mRNA (Figure 16C). In a non-tumor setting we found that stable expression of EWS-FLI1 in mesenchymal progenitor cells lead to a profound induction of FATE1 transcript and an accumulation of FATE1 protein at the mitochondria (Figure 16D). In total, these data support the sufficiency of EWS-FLI1 to drive expression of FATE1 in both tumor and normal cellular backgrounds.

FATE1 mediates Ewing sarcoma viability

Ewing sarcomas are dependent on the oncogenic transcriptional network activated by EWS-FLI1 and functional members of this network represent potential vulnerabilities within the tumor. Identification of the functional members that are potentially antigenic would make ideal targets for immunotherapy as evasion of the immune response by downregulation of the target would have negative consequences for tumor cell viability. We assessed the requirement for FATE1 in a panel of Ewing sarcoma derived cell lines and found that depletion of FATE1 led to a > 50 % reduction of cell viability in all four lines (Figure 17A and B). Additionally, depletion of FATE1 leads to a robust induction of apoptosis within the same cell lines (Figure 17C); however, we failed to detect an accumulation of BIK following FATE1 depletion (Figure 17D). Additionally, long term proteasome inhibition failed to induce BIK protein in TC-32 cells (Figure 17E) indicating that in the Ewing sarcoma oncogenic environment regulation of BIK may not be necessary and siFATE1-induced cell death results from a mechanism independent from the one described in Chapter III.

To assess the consequences of FATE1 depletion on the long-term survival of Ewing sarcoma cells we stably depleted FATE1 with two independent shRNA constructs and measured the ability of Ewing sarcoma cells to form colonies in soft agar (Figure 17F). Here, we found that depletion of FATE1 using either of two unique shRNAs led to a significant reduction in colony formation (Figure 17F). As we had previously implicated a FATE1-E3-ligase complex in support of tumor cell viability in colorectal carcinoma we asked whether any FATE1-E3-ligase binding partners are also required for Ewing sarcoma viability. Here we found that depletion of three, MARCH2, RNF183, and TRAF2, led to significant decreases in Ewing sarcoma cell viability (Figure 17G).

EWS-FLI1 regulates a cohort of CTAs

Given the regulation of FATE1 by EWS-FLI1 we wished to assess whether additional CTAs may be regulated by EWS-FLI1. To assess this possibility we performed a GREAT analysis on previously published EWS-FLI1 binding sites [178, 180]. This analysis identified 25 testis restricted CTAs associated with EWS-FLI1 binding sites, the majority of which were located 50 to 500 kb from the CTA's transcription start site (Table 1 and Figure 18A). To assess which of these CTAs could potentially be regulated transcriptionally by EWS-FLI1, we measured expression of those with commercially available qPCR probes following siRNA-mediated depletion of EWS-FLI1. Nine CTAs showed a significant reduction in expression following EWS-FLI1 depletion (Figure 18B). As this reduction in expression may be due to indirect mechanisms we next tested whether EWS-FLI1 is sufficient to drive expression of these CTAs in a gain of function setting. Overexpression of EWS-FLI1 in HCT116 cells was sufficient to drive expression of three members of this cohort in addition to FATE1 (BORIS, MAGEA4,

and SPATA19) (Figure 18C). The levels of induction of BORIS, MAGE-A4, and SPATA19 were much lower than FATE1, this may be due to the location of their associated EWS-FLI1 binding sites. While FATE1 has a EWS-FLI1 binding site within its proximal promoter, the EWS-FLI1 binding sites for BORIS (+43,090) , MAGE-A4 (-51623), and SPATA19 (+830093) are at much greater distances from their transcription start sites indicating EWS-FLI1 in likely influencing their expression via activity at enhancer elements and thus may require additional factors to achieve high levels of expression. To evaluate whether any of genes may make a functional contribution in Ewing sarcoma we assessed the contribution of each to cell viability in four Ewing sarcoma-derived cell lines. From this analysis we found that depletion of SPATA19 and MAGEA4 led to a significant reduction in viability in three or more of the lines tested (Figure 18D). Importantly, the loss of viability phenotype was recapitulated for each gene using a second, unique siRNA pool, greatly reducing the possibility that the effect are due to off-target siRNA activity (Figure 18E).

Returning to the small cohort of CTAs that we found responsive to EWS-FLI1 expression in HCT116 cells we sought to ask if epigenetic alterations would augment EWS-FLI1-induced expression of theses CTAs. The HCT116 cell line is a good model for such studies as it has a high level of basal genomic methylation compared to other tumor-derived cell lines (Figure 19A) and it undergoes significant demethylation following treatment with 5-aza-2'-deoxycitidine (5-aza) (Figure 19B). Within these cells 5-aza treatment alone induced robust expression of BORIS and MAGE-A4 while independently it had no impact on expression levels of FATE1 and SPATA19; however, 5-aza did synergize with EWS-FLI1 to drive expression of FATE1, while SPATA19 was induced to a minimal degree by EWS-FLI1 expression alone (Figure 19C). These data indicate that within the same genetic background CTAs have differential responses to

epigenetic changes and trans-acting factors, in some cases demethylation dominates gene regulation, in other it synergizes with trans-acting factors, and in some it has no impact on CTA expression.

Discussion

Ewing sarcoma oncogenesis is driven by the dysregulated transcription program induced by the chimeric EWS-FLI1 transcription factor. Here we have identified that FATE1 is a transcriptional target of EWS-FLI1 and importantly, it contributes to the viability of Ewing sarcoma cells. Although we have not yet defined the mechanism by which FATE1 supports the viability of Ewing sarcoma cells the finding that multiple FATE1-E3-ligase binding partners are required for Ewing sarcoma cell viability suggests FATE1 may modulate the activity of one or more of these partners in a pro-tumorigenic role within the disease. Previously, multiple reports have indicated that Ewing sarcoma cells are sensitive to engagement of cell receptor death pathways, as TRAF2 mediates signal transduction downstream of these pathways, a potential role for FATE1 in modulating the response to activation of these pathways within Ewing sarcoma should be assessed [181-184].

By leveraging a previously published EWS-FLI1 ChIP-seq data [178] and focused gene expression assays we were able to identified three additional CTAs as potential targets of EWS-FLI1: BORIS, MAGE-A4, and SPATA19. Unlike, FATE1, EWS-FLI1 likely activates these CTA through its activity at distant enhancer elements; however, further investigation will be required to confirm this hypothesis. We also demonstrated that within the same genetic background, CTAs show differential activation in response to epigenetic alterations and/or trans-acting factors. Functionally, depletion of two of the CTAs we nominated as potential EWS-FLI1-

targets MAGE-A4 and SPATA19 had significant impacts on Ewing cell viability and further characterization of their functional role within Ewing sarcoma is warranted. Several studies have shown that SPATA19 functions as a mitochondrial adhesion factor in developing sperm. Mice with a germ cell-specific conditional knockout of *Spata19* were infertile and showed disrupted mitochondrial morphology and significant deficits mitochondrial protein abundance and respiratory function [58, 59, 185]. No functional studies of SPATA19 within tumor cells have been conducted but based on its presumed function within germ cells, investigations into a possible role for SPATA19 in supporting tumor cell metabolism should be prioritized. Potential pro-tumorigenic functions for MAGE-A4 are more difficult to predict. Previously reported functions for MAGE-A4 are anti-tumorigenic including suppression of the oncoprotein gankyrin and induction of p53-dependent and p53-independent apoptosis by a peptide derived from the C-terminus of MAGE-A4 [186, 187]. How MAGE-A4 activity within the cellular background of Ewing sarcoma supports viability will likely require identification of novel MAGE-A4 molecular interactors and investigation into its post-translation processing within the disease.

Table 2: Cancer Testis Antigens associated with EWS-FLI1 binding sites.

CTA	Chromosome	Distance from TSS	Distance Category
BORIS/CTCFL	20	+43090	5-50
PRSS54	16	-36475	5-50
SPATA19	11	+830093	>500
ADAM2	8	+129615	50-500
ADAM29	4	+641268	>500
	4	798778	>500
LUZP4	X	+169138	50-500
MAGEA1	X	+59575	50-500
MAGEA4	X	-51623	50-500
ODF1	8	-99576	50-500
	8	-75881	50-500
	8	+25403	5-50
SYCP1	1	+26743	5-50
ZNF645	X	+584434	>500
ACTL8	1	+345926	50-500
DDX53	X	-142588	50-500
DPPA2	3	+128585	50-500
	3	+148679	50-500
FATE1	X	-1362	<5
	X	+7391	5-50
FTHL17	X	-704561	>500
	X	-123766	50-500
	X	+50223	50-500
SLCO6A1	5	-238290	50-500
TEKT5	16	+80004	50-500
CABYR	18	-249198	50-500
HORMAD2	22	-51019	50-500
	22	+68493	50-500
LEMD1	1	-73547	50-500
	1	-50503	50-500
	1	-22986	5-50
	1	-3345	<5
	1	-1951	<5
	1	+11275	5-50
MORC1	3	-69790	50-500
	3	-49696	5-50
	3	+84884	50-500
SPACA3	17	-43770	5-50
	17	+161106	50-500
	17	+277768	50-500
	17	+281678	50-500
TDRD1	10	-29466	5-50
TFDP3	X	-85526	50-500
	X	-13585	5-50

Figure 15: FATE1 is a target of the oncogenic transcription factor EWS-FLI1.

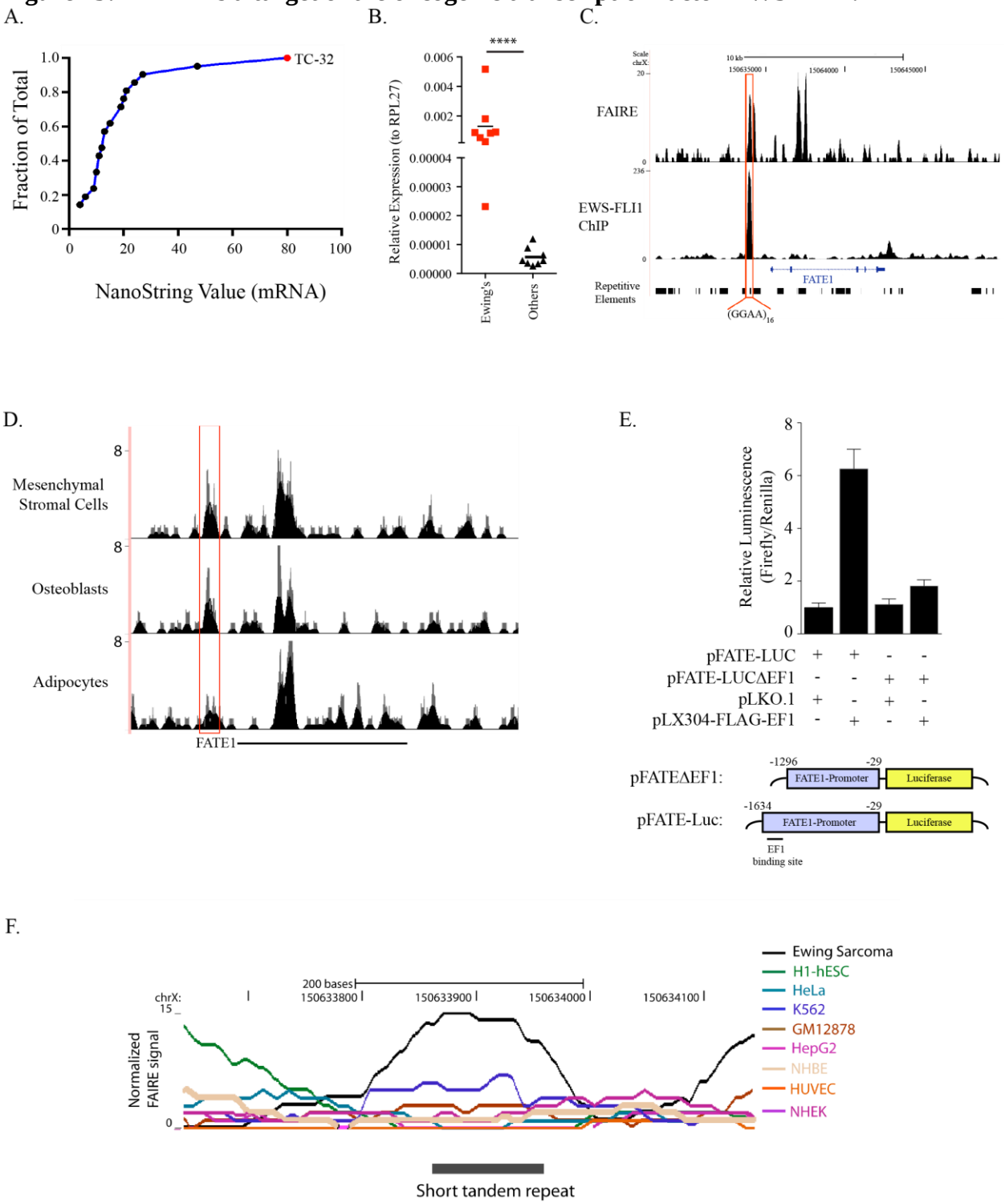

Figure 15: FATE1 is a target of the oncogenic transcription factor EWS-FLI1. (A) NanoString Expression values for FATE1 mRNA in candidate test bed cell lines (Chapter III). (B) Cell lines derived from Ewing sarcoma tumors (red) or cancers of various origins (black) were analysis for expression levels of FATE1. P = 0.0002 by Mann Whitney test. (C) Read counts at FATE1 loci following chromatin immunoprecipitation with HA-EWS-FLI1 ChIP (bottom) or Formaldehyde-Assisted Interrogation of Regulatory Elements (FAIRE) (top). (D) FAIRE signal at FATE1 loci in various stages of mesenchymal differentiation. (E) Luciferase activity was measured in HEK293T cells 48 hours after transfection with indicated plasmids. (F) FAIRE signal within the proximal FATE1 promoter in Ewing's derived EWS502 cells and ENCODE cell lines.

Figure 16: EWS-FLI1 drives expression of FATE1.

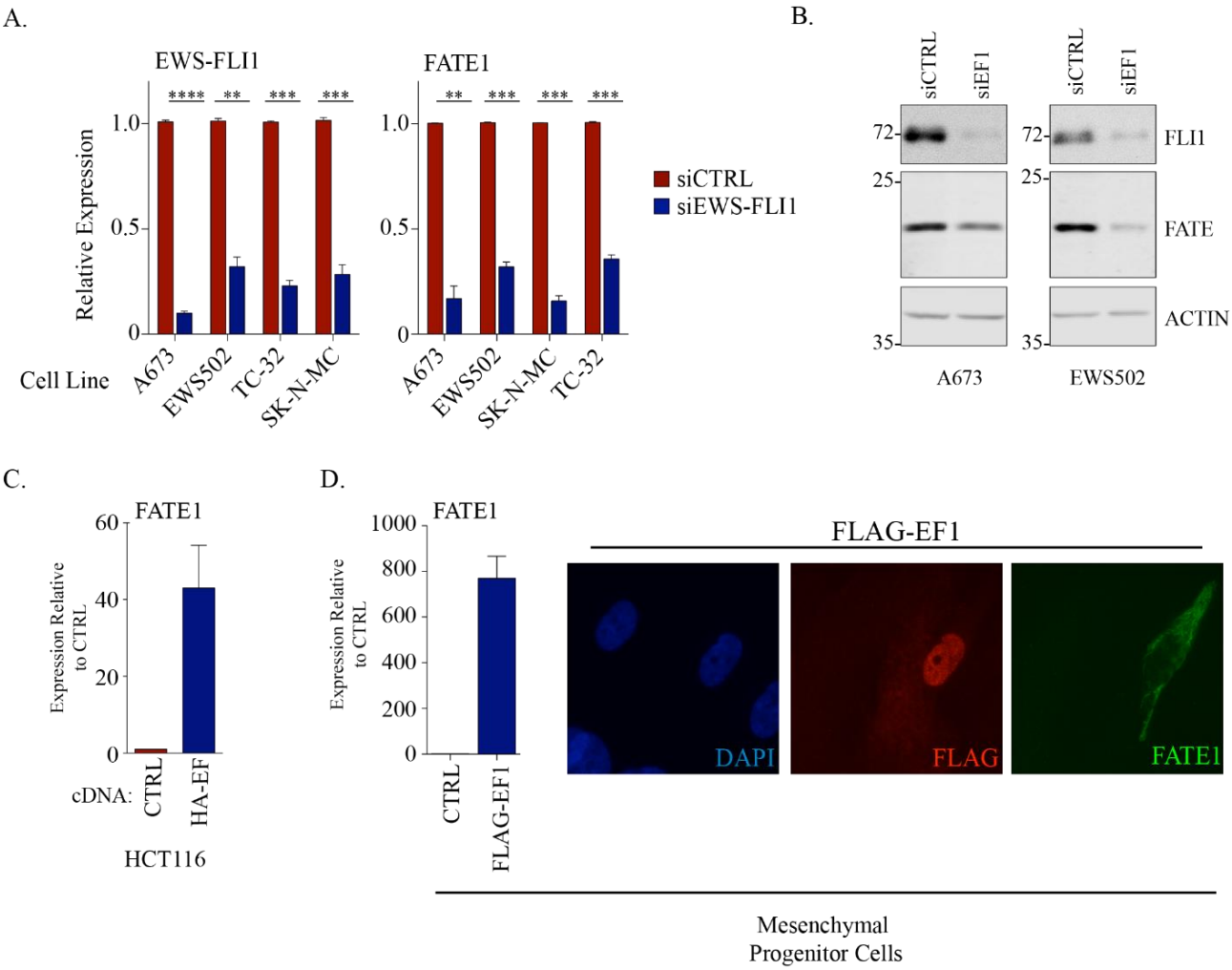

Figure 16: EWS-FLI1 drives expression of FATE1. (A) Forty-eight hours after transfection with indicated siRNAs, RNA was isolated from indicated cell lines and used for qPCR analysis of mRNA levels of indicated genes. Bars represent mean (n = 3) ± SEM. (B) Ninety-six hours after transfection with indicated siRNAs WCLs were collected from indicated cell lines and immunoblotted as indicated. (C) Forty-eight hours after transfection with indicated cDNA constructs, RNA was collected from HCT116 cells and used for qPCR analysis of FATE1 mRNA expression. Bars represent mean (n = 3) ± SEM. (D) Left: Ninety-six hours after infection with indicated lentiviral constructs RNA was collected from mesenchymal progenitor cells and used for qPCR analysis of FATE1 mRNA expression. Bars represent mean (n = 2) ± range. Right: Ninety-six hours after infection with indicated lentiviral constructs, mesenchymal progenitor cells were fixed and immunostained with indicated antibodies.

Figure 17: FATE1 supports Ewing sarcoma cell viability.

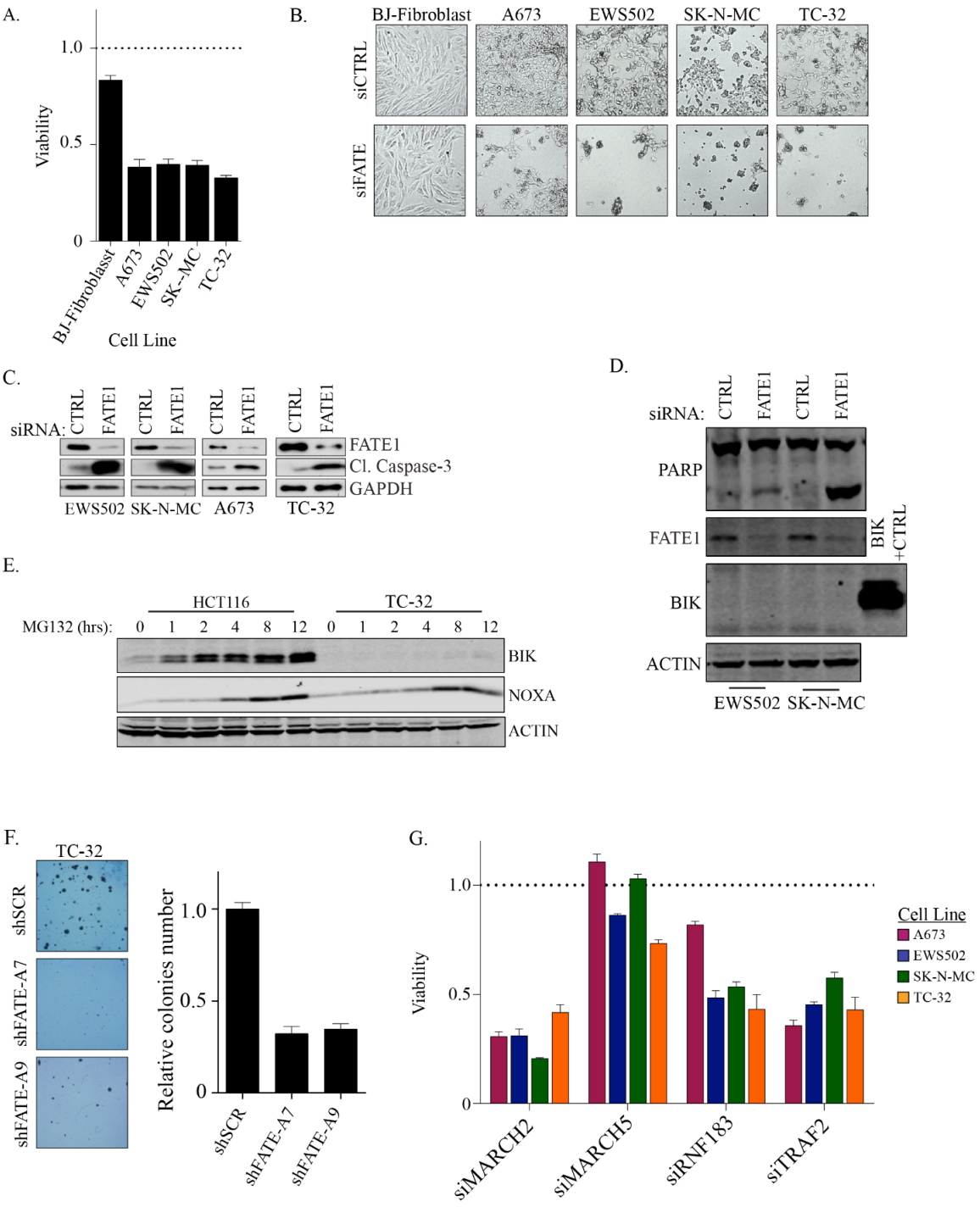

Figure 17: FATE1 supports Ewing sarcoma cell viability. (A) Viability of indicated cell lines 120 hours after transfection with indicated siCTRL or siFATE1. Bars represent mean (n = 4) ± SEM. (B) Bright-field images of cells assayed in (A). (C) Seventy-two hours after siRNA transfection, WCLs were collected from indicated cell lines and immunoblotted as indicated. (D) Seventy-two hours after siRNA transfection, WCLs were collected from indicated cell lines and immunoblotted as indicated. BIK-positive control is a HeLa cell lysate expressing BIK cDNA. (E) WCLs were collected from HCT116 or TC-32 cells treated with 20 μM MG132 for indicated incubation periods and immunoblotted as indicated. (F) Indicated cell lines were seeded in soft agar 48 hours after infection with indicated shRNAs. After three weeks colonies were stained overnight with Giemsa and then imaged and counted. (G) Viability of indicated cell lines 120 hours after transfection with indicated siRNAs. Bars represent mean (n = 4) ± SEM.

Figure 18: EWS-FLI1 regulates a cohort of CTAs.

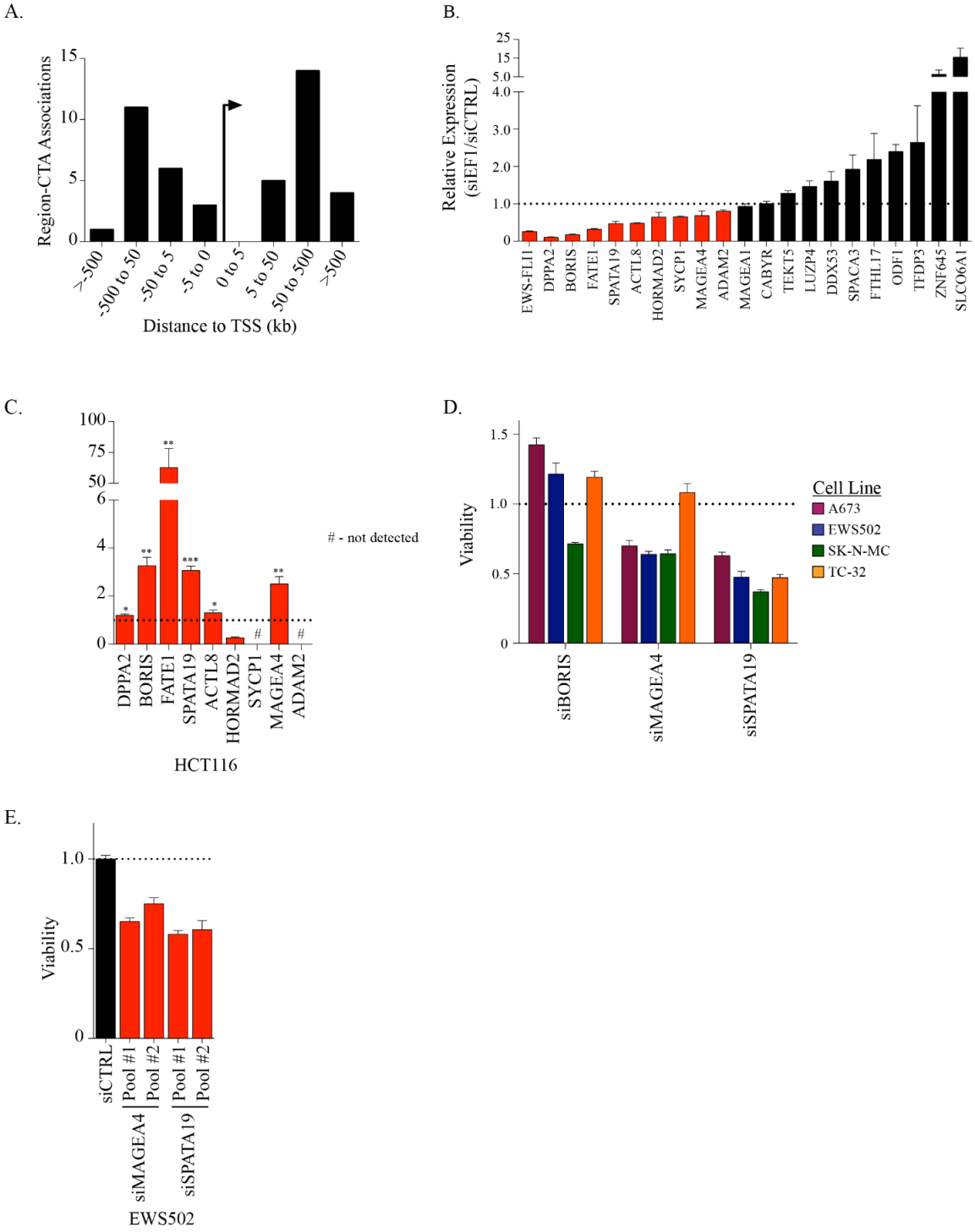

Figure 18: EWS-FLI1 regulates a cohort of CTAs. (A) Distribution of EWS-FLI1 binding sites in relation to CTA transcription start sites. (B) Forty-eight hours after transfection with indicated siRNAs, RNA was collected from EWS502 cells and used for qPCR analysis of mRNA levels of indicated CTAs. Bars represent mean (n = 3) ± SEM. (C) Forty-eight hours after transfection with indicated cDNAs, RNA was collected from HCT116 cells and used from qPCR analysis of mRNA levels of indicated genes. Bars represent mean (n = 3) ± SEM. (D) Viability of indicated cell lines was measured 120 hours after transfection with indicated siRNAs. Bars represent mean (n = 4) ± SEM. (E) Viability of EWS502 cells was measured 120 hours after transfection with either of two unique siRNA pools targeting SPATA19 or MAGEA4. Bars represent mean (n = 4) ± SEM.

Figure 19: Epigenetic and trans-acting mechanisms contribute to CTA expression.

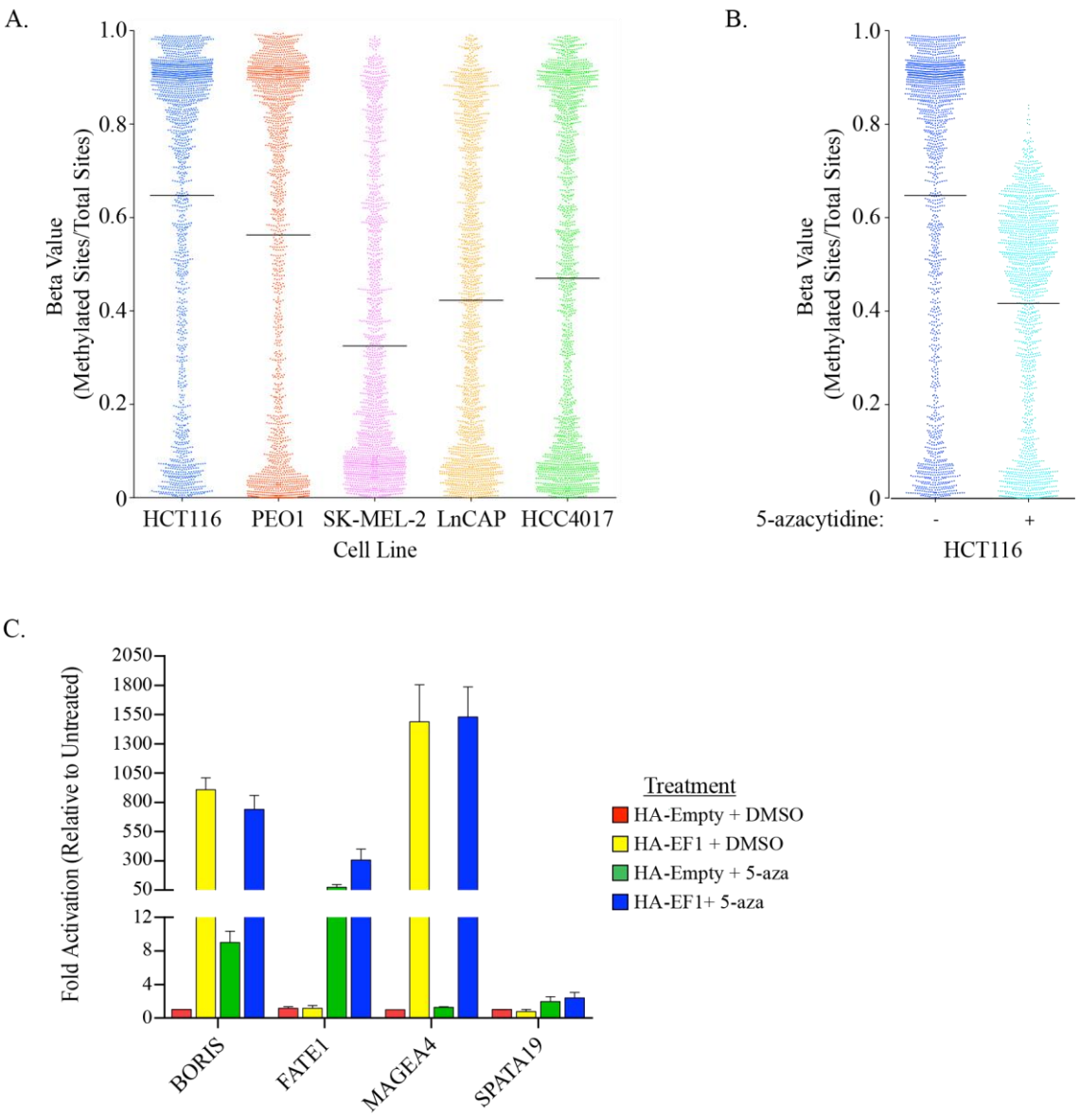

Figure 19: Epigenetic and trans-acting mechanisms contribute to CTA expression. (A) Beta-values in five tumor derived cell lines. (B) Beta-values in HCT116 following treatment with DMSO or 5-aza-2'-deoxycitidine. (C) Twenty-four hours after transfection with indicated cDNAs HCT116s were treated with 1 μM 5-aza-2'-deoxydecitidine. Forty-eight hours later, RNA was collected and used for qPCR analysis to measure expression of indicated mRNAs.

CHAPTER VI: CONCLUSIONS AND FUTURE DIRECTIONS

Summary

Cancer Testis Antigens represent a unique opportunity in the study and treatment of cancer. Not only do they provide unique targets for immunotherapy, they potentially offer a vast array of biological insights into the process of tumorigenesis, insights that may provide unexpected opportunities for therapeutic intervention. The studies described above contribute greatly to both our understanding of CTA function within tumors and their potential mechanisms of activation.

In Chapter III, we completed the first comprehensive screen to assess the functional contribution of CTAs to tumorigenesis. Using a loss-of-function screening platform across a panel of 11 tumor-derived cell lines, we determined the impact of 135 individual CTAs on multiple aspects of tumor biology including: viability, survival, proliferation and activity of five tumorigenic signaling pathways (TGFβ, Wnt, NF-κB, HIF, and Retinoic Acid). These analyses revealed that numerous CTAs contribute to multiple aspects of tumorigenesis. Focusing on tumor cell viability we found that depletion of FATE1, a previously uncharacterized CTA, had a potent and highly penetrant impact on tumor cell fitness. We determined that FATE1 is a mitochondrial protein that interacts with MFF, a core component of the mitochondrial fission machinery. We also found that FATE1 expression is capable of altering mitochondrial morphology in a contrary manner to MFF, which coupled with their interaction suggests that FATE1 may antagonize MFF-induced mitochondrial fission.

We elaborated one of FATE1's mechanistic contributions to tumorigenesis in Chapter IV. Here, we found that FATE1 is required within the transformed cellular environment to prevent induction of apoptosis, the programmed cell death pathway. FATE1 interacts with and regulates an apical sensor in the apoptotic pathway, BIK. BIK is activated by a number of stress signals encountered in the tumor cell environment. By attenuating the accumulation of BIK, FATE1 may allow tumor cells to survive these otherwise fatal levels of stress signaling. Furthermore, we identified, RNF183, a previously uncharacterized E3-ligases as a post-translation regulator of BIK. Although definitive assays remain to be performed we found multiple lines of evidence supporting the hypothesis that FATE1 and RNF183 cooperate to support tumor cell viability.

In Chapter IV we demonstrated that FATE1 is a direct transcriptional target of the chimeric transcription factor EWS-FLI1, the oncogenic driver of Ewing sarcoma a pediatric bone and soft tissue tumor. We also found that expression of FATE1 supports Ewing sarcoma cell viability. By analyzing a previously published EWS-FLI1 ChIP-seq dataset and using gain- and loss-of function expression studies we identified 3 additional CTAs, BORIS, MAGE-A4, and SPATA19, whose expression is regulated by EWS-FLI1. Cell viability assays indicated that two members of this cohort, MAGE-A4 and SPATA19 are functionally required within the Ewing sarcoma cellular background opening the door for further investigations as to mechanistic contributions of CTAs to the tumorigenesis of Ewing sarcoma.

Future Directions

Although we identified one mechanism by which FATE1 supports tumor cell viability through its impact on protein levels of the pro-apoptotic BH-3-only protein BIK, additional mechanism are left to be elaborated especially within the Ewing sarcoma oncogenic background.

One possibility is that FATE1 cooperates with RNF183 to target other pro-apoptotic protein(s), such as BNIP3 and BNIP3L, two BH-3-only proteins identified as FATE1 binding partners in yeast 2-hybrid screens [143], or FATE1 may regulated additional E3-ligases such as MARCH2, MARCH5, or TRAF2. As we found that three of FATE1's E3-ligase interactors, RNF183, MARCH2, and TRAF2, support Ewing sarcoma cell viability, these would be ideal starting points to further characterize FATE1's function in this cellular background. In addition, investigating what, if any, impact expression of FATE1 may have on primary cell tolerance to expression of the EWS-FLI1 oncogene would be highly relevant to both the understanding of the initiation of Ewing sarcoma and the role played by CTAs in supporting tumorigenesis.

FATE1's effects on mitochondrial morphology and the mitochondrial fission machinery are also deserving of further study. We found that expression of FATE1 can alter mitochondrial morphology in both normal and cancer cell backgrounds and that FATE1 interacts with MFF, a core component of the mitochondrial fission pathway. Antagonism of this pathway would be expected to increase mitochondrial respiratory capacity and elevate the threshold of Bcl-2 family activity required for outer membrane premeabilization, both outcomes that would likely be beneficial to transformed cells [96, 188]. Clarification of FATE1's role in this process will likely involve identifying it impact on MFF's mitochondrial recruitment of Dynamin-Related Protein-1, the GTPase that physically severs the mitochondria and its possible effects mitochondrial respiration [189]. FATE1 may also regulate this pathway independently of MFF, for instance, MARCH5, an E3-ligase that is a FATE1 binding partner, is also required for Drp1-induced mitochondrial division [190].

FATE1 is a poor target for conventional small molecule drug approaches as it lacks any readily druggable domains. However, a 2003 study found a small percentage (7.3 %) of

hepatocellular carcinoma patients had sera reactive against recombinant FATE1 indicating that FATE1 has antigenic potential within patients [89]. The possibility that this number could be augmented by treatment with immunostimulatory agents or immune checkpoint inhibitors should be addressed. If FATE1 antigenicity can be augmented FATE1 would make an attractive immunotherapeutic target as it is required across a range of cancers *in vitro* and appears to support tumor cell viability through at least two unique mechanisms. Also, FATE1 has little sequence similar to other proteins, aside from a small portion of MFF, and thus FATE1-targeted therapy would be unlikely to have off-target cross-reactivity with other proteins.

In addition to increasing the immune response to FATE1, its role in tumorigenesis *in vivo* remains to be clarified before its full therapeutic potential can be determined. At the time of this dissertation xenograft studies are underway examining the impact of shRNA-mediated FATE1 depletion in multiple Ewing sarcoma cell lines. In addition to these traditional xenograft studies, looking at the requirement of FATE1 in a more physiologic setting such as muscle or bone orthotopic xenografts may shed further light on the role of FATE1 in Ewing sarcoma development. The study of FATE1 *in vivo* with mice is somewhat limited as FATE1's orthologue in mice is a pseudogene and therefore knockout studies are not possible; however, this does not preclude a knock-in model which could be crossbred with genetically engineered mouse models of cancer to determine if FATE1 promotes tumor initiation and development in these contexts.

In conclusion, the results of these studies lay the foundation for continued investigation into the role of FATE1 in support tumor cell viability. Expression of FATE1 affects fundamental cellular biological processes (mitochondrial dynamics) and provides mechanisms to deflect tumor-specific insults (accumulation of BIK protein). FATE1's unique regulation in Ewing

sarcoma make it a promising entry point to understanding the biology support the disease. The finding that additional CTAs may also be functionally activated by EWS-FLI1 strengthens the hypothesis that CTA make meaningful contributions to tumorigenesis. Further study of the functional contribution of CTAs within Ewing sarcoma and other tumor types will improve their use as immunotherapeutic targets and potentially open additional therapeutic avenues based on the biologic processes in which they are found to intercede.

REFERENCES

1. Moss, R.W., *The life and times of John Beard, DSc (1858-1924).* Integr Cancer Ther, 2008. **7**(4): p. 229-51.

2. Coulie, P.G., et al., *Tumour antigens recognized by T lymphocytes: at the core of cancer immunotherapy.* Nat Rev Cancer, 2014. **14**(2): p. 135-46.

3. Gillis, S. and K.A. Smith, *Long term culture of tumour-specific cytotoxic T cells.* Nature, 1977. **268**(5616): p. 154-6.

4. Cerottini, J.C. and K.T. Brunner, *Cell-mediated cytotoxicity, allograft rejection, and tumor immunity.* Adv Immunol, 1974. **18**: p. 67-132.

5. Rouse, B.T., M. Rollinghoff, and N.L. Warner, *Anti-theta serum-induced supression of the cellular transfer of tumour-specific immunity to a syngeneic plasma cell tumour.* Nat New Biol, 1972. **238**(82): p. 116-7.

6. De Plaen, E., et al., *Immunogenic (tum-) variants of mouse tumor P815: cloning of the gene of tum- antigen P91A and identification of the tum- mutation.* Proc Natl Acad Sci U S A, 1988. **85**(7): p. 2274-8.

7. Szikora, J.P., et al., *Structure of the gene of tum- transplantation antigen P35B: presence of a point mutation in the antigenic allele.* EMBO J, 1990. **9**(4): p. 1041-50.

8. Sibille, C., et al., *Structure of the gene of tum- transplantation antigen P198: a point mutation generates a new antigenic peptide.* J Exp Med, 1990. **172**(1): p. 35-45.

9. Van den Eynde, B., et al., *The gene coding for a major tumor rejection antigen of tumor P815 is identical to the normal gene of syngeneic DBA/2 mice.* J Exp Med, 1991. **173**(6): p. 1373-84.

10. van der Bruggen, P., et al., *A gene encoding an antigen recognized by cytolytic T lymphocytes on a human melanoma.* Science, 1991. **254**(5038): p. 1643-7.

11. Traversari, C., et al., *A nonapeptide encoded by human gene MAGE-1 is recognized on HLA-A1 by cytolytic T lymphocytes directed against tumor antigen MZ2-E.* J Exp Med, 1992. **176**(5): p. 1453-7.

12. Weon, J.L. and P.R. Potts, *The MAGE protein family and cancer.* Curr Opin Cell Biol, 2015. **37**: p. 1-8.

13. Boel, P., et al., *BAGE: a new gene encoding an antigen recognized on human melanomas by cytolytic T lymphocytes.* Immunity, 1995. **2**(2): p. 167-75.

14. De Backer, O., et al., *Characterization of the GAGE genes that are expressed in various human cancers and in normal testis.* Cancer Res, 1999. **59**(13): p. 3157-65.

15. Sahin, U., et al., *Human neoplasms elicit multiple specific immune responses in the autologous host.* Proc Natl Acad Sci U S A, 1995. **92**(25): p. 11810-3.

16. Tureci, O., et al., *The SSX-2 gene, which is involved in the t(X;18) translocation of synovial sarcomas, codes for the human tumor antigen HOM-MEL-40.* Cancer Res, 1996. **56**(20): p. 4766-72.

17. Tureci, O., et al., *Identification of a meiosis-specific protein as a member of the class of cancer/testis antigens.* Proc Natl Acad Sci U S A, 1998. **95**(9): p. 5211-6.

18. Chen, Y.T., et al., *A testicular antigen aberrantly expressed in human cancers detected by autologous antibody screening.* Proc Natl Acad Sci U S A, 1997. **94**(5): p. 1914-8.

19. Simpson, A.J., et al., *Cancer/testis antigens, gametogenesis and cancer.* Nat Rev Cancer, 2005. **5**(8): p. 615-25.

20. Hofmann, O., et al., *Genome-wide analysis of cancer/testis gene expression.* Proc Natl Acad Sci U S A, 2008. **105**(51): p. 20422-7.

21. Scanlan, M.J., A.J. Simpson, and L.J. Old, *The cancer/testis genes: review, standardization, and commentary.* Cancer Immun, 2004. **4**: p. 1.

22. Whitehurst, A.W., *Cause and consequence of cancer/testis antigen activation in cancer.* Annu Rev Pharmacol Toxicol, 2014. **54**: p. 251-72.

23. Dalerba, P., et al., *MAGE, BAGE and GAGE gene expression in human rhabdomyosarcomas.* Int J Cancer, 2001. **93**(1): p. 85-90.

24. Jungbluth, A.A., et al., *Monoclonal antibody MA454 reveals a heterogeneous expression pattern of MAGE-1 antigen in formalin-fixed paraffin embedded lung tumours.* Br J Cancer, 2000. **83**(4): p. 493-7.

25. Meinhardt, A. and M.P. Hedger, *Immunological, paracrine and endocrine aspects of testicular immune privilege.* Mol Cell Endocrinol, 2011. **335**(1): p. 60-8.

26. Guillaudeux, T., et al., *Expression of HLA class I genes in meiotic and post-meiotic human spermatogenic cells.* Biol Reprod, 1996. **55**(1): p. 99-110.

27. Griswold, M.D., *The central role of Sertoli cells in spermatogenesis.* Semin Cell Dev Biol, 1998. **9**(4): p. 411-6.

28. Cheng, C.Y. and D.D. Mruk, *Cell junction dynamics in the testis: Sertoli-germ cell interactions and male contraceptive development.* Physiol Rev, 2002. **82**(4): p. 825-74.

29. Meinhardt, A., et al., *Macrophage migration inhibitory factor production by Leydig cells: evidence for a role in the regulation of testicular function.* Endocrinology, 1996. **137**(11): p. 5090-5.

30. Abe, R., et al., *Regulation of the CTL response by macrophage migration inhibitory factor.* J Immunol, 2001. **166**(2): p. 747-53.

31. Apte, R.S., et al., *Cutting edge: role of macrophage migration inhibitory factor in inhibiting NK cell activity and preserving immune privilege.* J Immunol, 1998. **160**(12): p. 5693-6.

32. Anderson, M.S. and M.A. Su, *Aire and T cell development.* Curr Opin Immunol, 2011. **23**(2): p. 198-206.

33. Gotter, J., et al., *Medullary epithelial cells of the human thymus express a highly diverse selection of tissue-specific genes colocalized in chromosomal clusters.* J Exp Med, 2004. **199**(2): p. 155-66.

34. Pinto, S., et al., *Misinitiation of intrathymic MART-1 transcription and biased TCR usage explain the high frequency of MART-1-specific T cells.* Eur J Immunol, 2014. **44**(9): p. 2811-21.

35. Yang, X.A., et al., *Immunohistochemical analysis of the expression of FATE/BJ-HCC-2 antigen in normal and malignant tissues.* Lab Invest, 2005. **85**(2): p. 205-13.

36. Li, H., et al., *Immune regulation by low doses of the DNA methyltransferase inhibitor 5-azacitidine in common human epithelial cancers.* Oncotarget, 2014. **5**(3): p. 587-98.

37. Karpf, A.R., *A potential role for epigenetic modulatory drugs in the enhancement of cancer/germ-line antigen vaccine efficacy.* Epigenetics, 2006. **1**(3): p. 116-20.

38. Woloszynska-Read, A., et al., *Intertumor and intratumor NY-ESO-1 expression heterogeneity is associated with promoter-specific and global DNA methylation status in ovarian cancer.* Clin Cancer Res, 2008. **14**(11): p. 3283-90.

39. Link, P.A., et al., *Distinct roles for histone methyltransferases G9a and GLP in cancer germ-line antigen gene regulation in human cancer cells and murine embryonic stem cells.* Mol Cancer Res, 2009. **7**(6): p. 851-62.

40. Wischnewski, F., K. Pantel, and H. Schwarzenbach, *Promoter demethylation and histone acetylation mediate gene expression of MAGE-A1, -A2, -A3, and -A12 in human cancer cells.* Mol Cancer Res, 2006. **4**(5): p. 339-49.

41. Karpf, A.R., et al., *Limited gene activation in tumor and normal epithelial cells treated with the DNA methyltransferase inhibitor 5-aza-2'-deoxycytidine.* Mol Pharmacol, 2004. **65**(1): p. 18-27.

42. De Smet, C., et al., *Involvement of two Ets binding sites in the transcriptional activation of the MAGE1 gene.* Immunogenetics, 1995. **42**(4): p. 282-90.

43. Kang, Y., et al., *Dynamic transcriptional regulatory complexes including BORIS, CTCF and Sp1 modulate NY-ESO-1 expression in lung cancer cells.* Oncogene, 2007. **26**(30): p.

4394-403.

44. Hong, J.A., et al., *Reciprocal binding of CTCF and BORIS to the NY-ESO-1 promoter coincides with derepression of this cancer-testis gene in lung cancer cells.* Cancer Res, 2005. **65**(17): p. 7763-74.

45. Crosio, C., et al., *Mitotic phosphorylation of histone H3: spatio-temporal regulation by mammalian Aurora kinases.* Mol Cell Biol, 2002. **22**(3): p. 874-85.

46. Vatolin, S., et al., *Conditional expression of the CTCF-paralogous transcriptional factor BORIS in normal cells results in demethylation and derepression of MAGE-A1 and reactivation of other cancer-testis genes.* Cancer Res, 2005. **65**(17): p. 7751-62.

47. Smith, I.M., et al., *Coordinated activation of candidate proto-oncogenes and cancer testes antigens via promoter demethylation in head and neck cancer and lung cancer.* PLoS One, 2009. **4**(3): p. e4961.

48. Woloszynska-Read, A., et al., *DNA methylation-dependent regulation of BORIS/CTCFL expression in ovarian cancer.* Cancer Immun, 2007. **7**: p. 21.

49. Hoffmann, M.J., et al., *Epigenetic control of CTCFL/BORIS and OCT4 expression in urogenital malignancies.* Biochem Pharmacol, 2006. **72**(11): p. 1577-88.

50. Yawata, T., et al., *Enhanced expression of cancer testis antigen genes in glioma stem cells.* Mol Carcinog, 2010. **49**(6): p. 532-44.

51. Kholmanskikh, O., et al., *Expression of BORIS in melanoma: lack of association with MAGE-A1 activation.* Int J Cancer, 2008. **122**(4): p. 777-84.

52. Lam, I. and S. Keeney, *Mechanism and regulation of meiotic recombination initiation.* Cold Spring Harb Perspect Biol, 2015. **7**(1): p. a016634.

53. Bolcun-Filas, E., et al., *Mutation of the mouse Syce1 gene disrupts synapsis and suggests a link between synaptonemal complex structural components and DNA repair.* PLoS genetics, 2009. **5**(2): p. e1000393.

54. de Vries, F.A., et al., *Mouse Sycp1 functions in synaptonemal complex assembly, meiotic recombination, and XY body formation.* Genes Dev, 2005. **19**(11): p. 1376-89.

55. Shin, Y.H., et al., *Hormad1 mutation disrupts synaptonemal complex formation, recombination, and chromosome segregation in mammalian meiosis.* PLoS genetics, 2010. **6**(11): p. e1001190.

56. Yang, F., et al., *Mouse TEX15 is essential for DNA double-strand break repair and chromosomal synapsis during male meiosis.* J Cell Biol, 2008. **180**(4): p. 673-9.

57. Miki, K., *Energy metabolism and sperm function.* Soc Reprod Fertil Suppl, 2007. **65**: p. 309-25.

58. Mi, Y., Z. Shi, and J. Li, *Spata19 is critical for sperm mitochondrial function and male fertility.* Mol Reprod Dev, 2015. **82**(11): p. 907-13.

59. Suzuki-Toyota, F., et al., *Factors maintaining normal sperm tail structure during epididymal maturation studied in Gopc-/- mice.* Biol Reprod, 2007. **77**(1): p. 71-82.

60. Odunsi, K., et al., *Efficacy of vaccination with recombinant vaccinia and fowlpox vectors expressing NY-ESO-1 antigen in ovarian cancer and melanoma patients.* Proc Natl Acad Sci U S A, 2012. **109**(15): p. 5797-802.

61. Dhodapkar, M.V., et al., *Induction of antigen-specific immunity with a vaccine targeting NY-ESO-1 to the dendritic cell receptor DEC-205.* Sci Transl Med, 2014. **6**(232): p. 232ra51.

62. Mkrtichyan, M., et al., *Cancer-testis antigen, BORIS based vaccine delivered by dendritic cells is extremely effective against a very aggressive and highly metastatic mouse mammary carcinoma.* Cell Immunol, 2011. **270**(2): p. 188-97.

63. Hunder, N.N., et al., *Treatment of metastatic melanoma with autologous CD4+ T cells against NY-ESO-1.* N Engl J Med, 2008. **358**(25): p. 2698-703.

64. Robbins, P.F., et al., *Tumor regression in patients with metastatic synovial cell sarcoma and melanoma using genetically engineered lymphocytes reactive with NY-ESO-1.* J Clin Oncol, 2011. **29**(7): p. 917-24.

65. Morgan, R.A., et al., *Cancer regression and neurological toxicity following anti-MAGE-A3 TCR gene therapy.* J Immunother, 2013. **36**(2): p. 133-51.

66. Linette, G.P., et al., *Cardiovascular toxicity and titin cross-reactivity of affinity-enhanced T cells in myeloma and melanoma.* Blood, 2013. **122**(6): p. 863-71.

67. Park, J.H., G.H. Kong, and S.W. Lee, *hMAGE-A1 overexpression reduces TNF-alpha cytotoxicity in ME-180 cells.* Mol Cells, 2002. **14**(1): p. 122-9.

68. Cilensek, Z.M., et al., *A member of the GAGE family of tumor antigens is an anti-apoptotic gene that confers resistance to Fas/CD95/APO-1, Interferon-gamma, taxol and gamma-irradiation.* Cancer Biol Ther, 2002. **1**(4): p. 380-7.

69. Duan, Z., et al., *Overexpression of MAGE/GAGE genes in paclitaxel/doxorubicin-resistant human cancer cell lines.* Clin Cancer Res, 2003. **9**(7): p. 2778-85.

70. Whitehurst, A.W., et al., *Synthetic lethal screen identification of chemosensitizer loci in cancer cells.* Nature, 2007. **446**(7137): p. 815-9.

71. Whitehurst, A.W., et al., *Tumor antigen acrosin binding protein normalizes mitotic spindle function to promote cancer cell proliferation.* Cancer Res, 2010. **70**(19): p. 7652-61.

72. Ciro, M., et al., *ATAD2 is a novel cofactor for MYC, overexpressed and amplified in aggressive tumors.* Cancer Res, 2009. **69**(21): p. 8491-8.

73. Epping, M.T., et al., *The human tumor antigen PRAME is a dominant repressor of retinoic acid receptor signaling.* Cell, 2005. **122**(6): p. 835-47.

74. Doyle, J.M., et al., *MAGE-RING protein complexes comprise a family of E3 ubiquitin ligases.* Mol Cell, 2010. **39**(6): p. 963-74.

75. Pineda, C.T., et al., *Degradation of AMPK by a cancer-specific ubiquitin ligase.* Cell, 2015. **160**(4): p. 715-28.

76. Ahmed, A.A., et al., *SIK2 is a centrosome kinase required for bipolar mitotic spindle formation that provides a potential target for therapy in ovarian cancer.* Cancer Cell, 2010. **18**(2): p. 109-21.

77. Korch, C., et al., *DNA profiling analysis of endometrial and ovarian cell lines reveals misidentification, redundancy and contamination.* Gynecol Oncol, 2012. **127**(1): p. 241-8.

78. Almeida, L.G., et al., *CTdatabase: a knowledge-base of high-throughput and curated data on cancer-testis antigens.* Nucleic Acids Res, 2009. **37**(Database issue): p. D816-9.

79. Germain, M., J.P. Mathai, and G.C. Shore, *BH-3-only BIK functions at the endoplasmic reticulum to stimulate cytochrome c release from mitochondria.* J Biol Chem, 2002. **277**(20): p. 18053-60.

80. Ferguson, S.S. and M.G. Caron, *Green fluorescent protein-tagged beta-arrestin translocation as a measure of G protein-coupled receptor activation.* Methods Mol Biol, 2004. **237**: p. 121-6.

81. Schmittgen, T.D. and K.J. Livak, *Analyzing real-time PCR data by the comparative C(T) method.* Nat Protoc, 2008. **3**(6): p. 1101-8.

82. Pei, H., et al., *FKBP51 affects cancer cell response to chemotherapy by negatively regulating Akt.* Cancer Cell, 2009. **16**(3): p. 259-66.

83. Stearman, R.S., et al., *Analysis of orthologous gene expression between human pulmonary adenocarcinoma and a carcinogen-induced murine model.* Am J Pathol, 2005. **167**(6): p. 1763-75.

84. Cancer Genome Atlas, N., *Comprehensive molecular portraits of human breast tumours.* Nature, 2012. **490**(7418): p. 61-70.

85. Cancer Genome Atlas, N., *Comprehensive molecular characterization of human colon and rectal cancer.* Nature, 2012. **487**(7407): p. 330-7.

86. Cancer Genome Atlas Research, N., *Comprehensive molecular profiling of lung*

adenocarcinoma. Nature, 2014. **511**(7511): p. 543-50.

87. Olesen, C., et al., *Identification of human candidate genes for male infertility by digital differential display.* Mol Hum Reprod, 2001. **7**(1): p. 11-20.

88. Olesen, C., et al., *Human FATE is a novel X-linked gene expressed in fetal and adult testis.* Mol Cell Endocrinol, 2001. **184**(1-2): p. 25-32.

89. Dong, X.Y., et al., *Identification of two novel CT antigens and their capacity to elicit antibody response in hepatocellular carcinoma patients.* Br J Cancer, 2003. **89**(2): p. 291-7.

90. Gandre-Babbe, S. and A.M. van der Bliek, *The novel tail-anchored membrane protein Mff controls mitochondrial and peroxisomal fission in mammalian cells.* Mol Biol Cell, 2008. **19**(6): p. 2402-12.

91. Otera, H., et al., *Mff is an essential factor for mitochondrial recruitment of Drp1 during mitochondrial fission in mammalian cells.* J Cell Biol, 2010. **191**(6): p. 1141-58.

92. Liu, R. and D.C. Chan, *The mitochondrial fission receptor Mff selectively recruits oligomerized Drp1.* Mol Biol Cell, 2015. **26**(24): p. 4466-77.

93. Santel, A. and M.T. Fuller, *Control of mitochondrial morphology by a human mitofusin.* J Cell Sci, 2001. **114**(Pt 5): p. 867-74.

94. Bieche, I., et al., *Prognostic value of chorionic gonadotropin beta gene transcripts in human breast carcinoma.* Clin Cancer Res, 1998. **4**(3): p. 671-6.

95. Gomes, L.C., G. Di Benedetto, and L. Scorrano, *During autophagy mitochondria elongate, are spared from degradation and sustain cell viability.* Nat Cell Biol, 2011. **13**(5): p. 589-98.

96. Montessuit, S., et al., *Membrane remodeling induced by the dynamin-related protein Drp1 stimulates Bax oligomerization.* Cell, 2010. **142**(6): p. 889-901.

97. Youle, R.J. and M. Karbowski, *Mitochondrial fission in apoptosis.* Nat Rev Mol Cell Biol, 2005. **6**(8): p. 657-63.

98. Johnstone, R.W., A.A. Ruefli, and S.W. Lowe, *Apoptosis: a link between cancer genetics and chemotherapy.* Cell, 2002. **108**(2): p. 153-64.

99. Wang, X., *The expanding role of mitochondria in apoptosis.* Genes Dev, 2001. **15**(22): p. 2922-33.

100. Vaux, D.L., S. Cory, and J.M. Adams, *Bcl-2 gene promotes haemopoietic cell survival and cooperates with c-myc to immortalize pre-B cells.* Nature, 1988. **335**(6189): p. 440-2.

101. Levine, A.J., *p53, the cellular gatekeeper for growth and division.* Cell, 1997. **88**(3): p.

323-31.

102. Gandhi, L., et al., *Phase I study of Navitoclax (ABT-263), a novel Bcl-2 family inhibitor, in patients with small-cell lung cancer and other solid tumors.* J Clin Oncol, 2011. **29**(7): p. 909-16.

103. Rudin, C.M., et al., *Phase II study of single-agent navitoclax (ABT-263) and biomarker correlates in patients with relapsed small cell lung cancer.* Clin Cancer Res, 2012. **18**(11): p. 3163-9.

104. Knudson, C.M., et al., *Bax-deficient mice with lymphoid hyperplasia and male germ cell death.* Science, 1995. **270**(5233): p. 96-9.

105. Print, C.G., et al., *Apoptosis regulator bcl-w is essential for spermatogenesis but appears otherwise redundant.* Proc Natl Acad Sci U S A, 1998. **95**(21): p. 12424-31.

106. Coultas, L., et al., *Concomitant loss of proapoptotic BH3-only Bcl-2 antagonists Bik and Bim arrests spermatogenesis.* EMBO J, 2005. **24**(22): p. 3963-73.

107. Youle, R.J. and A. Strasser, *The BCL-2 protein family: opposing activities that mediate cell death.* Nat Rev Mol Cell Biol, 2008. **9**(1): p. 47-59.

108. Denault, J.B. and G.S. Salvesen, *Caspases: keys in the ignition of cell death.* Chem Rev, 2002. **102**(12): p. 4489-500.

109. Fernald, K. and M. Kurokawa, *Evading apoptosis in cancer.* Trends Cell Biol, 2013. **23**(12): p. 620-33.

110. Li, W., et al., *Star-PAP control of BIK expression and apoptosis is regulated by nuclear PIPKIalpha and PKCdelta signaling.* Mol Cell, 2012. **45**(1): p. 25-37.

111. Zhong, Q., et al., *Mule/ARF-BP1, a BH3-only E3 ubiquitin ligase, catalyzes the polyubiquitination of Mcl-1 and regulates apoptosis.* Cell, 2005. **121**(7): p. 1085-95.

112. Ishihara, Y., et al., *Dual regulation of hepatocyte apoptosis by reactive oxygen species: Increases in transcriptional expression and decreases in proteasomal degradation of BimEL.* J Cell Physiol, 2011. **226**(4): p. 1007-16.

113. Ravid, T. and M. Hochstrasser, *Diversity of degradation signals in the ubiquitin-proteasome system.* Nat Rev Mol Cell Biol, 2008. **9**(9): p. 679-90.

114. Mizushima, N. and D.J. Klionsky, *Protein turnover via autophagy: implications for metabolism.* Annu Rev Nutr, 2007. **27**: p. 19-40.

115. Neutzner, A., et al., *The ubiquitin/proteasome system-dependent control of mitochondrial steps in apoptosis.* Semin Cell Dev Biol, 2012. **23**(5): p. 499-508.

116. Zhu, H., et al., *Bik/NBK accumulation correlates with apoptosis-induction by bortezomib*

(PS-341, Velcade) and other proteasome inhibitors. Oncogene, 2005. **24**(31): p. 4993-9.

117. Nikrad, M., et al., *The proteasome inhibitor bortezomib sensitizes cells to killing by death receptor ligand TRAIL via BH3-only proteins Bik and Bim.* Mol Cancer Ther, 2005. **4**(3): p. 443-9.

118. Deshaies, R.J. and C.A. Joazeiro, *RING domain E3 ubiquitin ligases.* Annu Rev Biochem, 2009. **78**: p. 399-434.

119. Huibregtse, J.M., et al., *A family of proteins structurally and functionally related to the E6-AP ubiquitin-protein ligase.* Proc Natl Acad Sci U S A, 1995. **92**(7): p. 2563-7.

120. de Bie, P. and A. Ciechanover, *Ubiquitination of E3 ligases: self-regulation of the ubiquitin system via proteolytic and non-proteolytic mechanisms.* Cell Death Differ, 2011. **18**(9): p. 1393-402.

121. Sahtoe, D.D. and T.K. Sixma, *Layers of DUB regulation.* Trends Biochem Sci, 2015. **40**(8): p. 456-67.

122. Yu, H., et al., *Next-generation sequencing to generate interactome datasets.* Nat Methods, 2011. **8**(6): p. 478-80.

123. Rual, J.F., et al., *Towards a proteome-scale map of the human protein-protein interaction network.* Nature, 2005. **437**(7062): p. 1173-8.

124. Han, J., P. Sabbatini, and E. White, *Induction of apoptosis by human Nbk/Bik, a BH3-containing protein that interacts with E1B 19K.* Mol Cell Biol, 1996. **16**(10): p. 5857-64.

125. Chinnadurai, G., S. Vijayalingam, and R. Rashmi, *BIK, the founding member of the BH3-only family proteins: mechanisms of cell death and role in cancer and pathogenic processes.* Oncogene, 2008. **27 Suppl 1**: p. S20-9.

126. Boyd, J.M., et al., *Bik, a novel death-inducing protein shares a distinct sequence motif with Bcl-2 family proteins and interacts with viral and cellular survival-promoting proteins.* Oncogene, 1995. **11**(9): p. 1921-8.

127. Sturm, I., et al., *Loss of the tissue-specific proapoptotic BH3-only protein Nbk/Bik is a unifying feature of renal cell carcinoma.* Cell Death Differ, 2006. **13**(4): p. 619-27.

128. Bredel, M., et al., *High-resolution genome-wide mapping of genetic alterations in human glial brain tumors.* Cancer Res, 2005. **65**(10): p. 4088-96.

129. Castells, A., et al., *Mapping of a target region of allelic loss to a 0.5-cM interval on chromosome 22q13 in human colorectal cancer.* Gastroenterology, 1999. **117**(4): p. 831-7.

130. Reis, P.P., et al., *Quantitative real-time PCR identifies a critical region of deletion on 22q13 related to prognosis in oral cancer.* Oncogene, 2002. **21**(42): p. 6480-7.

131. Arena, V., et al., *Mutations of the BIK gene in human peripheral B-cell lymphomas.* Genes Chromosomes Cancer, 2003. **38**(1): p. 91-6.

132. Prieto-Remón, I., et al., *BIK (NBK) is a mediator of the sensitivity of Fanconi anaemia group C lymphoblastoid cell lines to interstrand DNA cross-linking agents.* Biochem J, 2012. **448**(1): p. 153-63.

133. Hur, J., et al., *The Bik BH3-only protein is induced in estrogen-starved and antiestrogen-exposed breast cancer cells and provokes apoptosis.* Proc Natl Acad Sci U S A, 2004. **101**(8): p. 2351-6.

134. Hur, J., et al., *Regulation of expression of BIK proapoptotic protein in human breast cancer cells: p53-dependent induction of BIK mRNA by fulvestrant and proteasomal degradation of BIK protein.* Cancer Res, 2006. **66**(20): p. 10153-61.

135. Mebratu, Y.A., et al., *The BH3-only protein Bik/Blk/Nbk inhibits nuclear translocation of activated ERK1/2 to mediate IFNgamma-induced cell death.* J Cell Biol, 2008. **183**(3): p. 429-39.

136. Jiang, A. and E.A. Clark, *Involvement of Bik, a proapoptotic member of the Bcl-2 family, in surface IgM-mediated B cell apoptosis.* J Immunol, 2001. **166**(10): p. 6025-33.

137. Campion, E.M., et al., *Repression of the proapoptotic cellular BIK/NBK gene by Epstein-Barr virus antagonizes transforming growth factor β1-induced B-cell apoptosis.* J Virol, 2014. **88**(9): p. 5001-13.

138. Real, P.J., et al., *Transcriptional activation of the proapoptotic bik gene by E2F proteins in cancer cells.* FEBS Lett, 2006. **580**(25): p. 5905-9.

139. García, N., et al., *A molecular analysis by gene expression profiling reveals Bik/NBK overexpression in sporadic breast tumor samples of Mexican females.* BMC Cancer, 2005. **5**: p. 93.

140. Lu, Y., et al., *A gene expression signature predicts survival of patients with stage I non-small cell lung cancer.* PLoS Med, 2006. **3**(12): p. e467.

141. Lopez, J., et al., *Src tyrosine kinase inhibits apoptosis through the Erk1/2- dependent degradation of the death accelerator Bik.* Cell Death Differ, 2012. **19**(9): p. 1459-69.

142. Rual, J.-F., et al., *Towards a proteome-scale map of the human protein-protein interaction network.* Nature, 2005. **437**(7062): p. 1173-1178.

143. Rolland, T., et al., *A proteome-scale map of the human interactome network.* Cell, 2014. **159**(5): p. 1212-26.

144. Colas, E., et al., *Molecular markers of endometrial carcinoma detected in uterine aspirates.* Int J Cancer, 2011. **129**(10): p. 2435-44.

145. Torres, E.M., et al., *Effects of aneuploidy on cellular physiology and cell division in haploid yeast.* Science, 2007. **317**(5840): p. 916-24.

146. Szatrowski, T.P. and C.F. Nathan, *Production of large amounts of hydrogen peroxide by human tumor cells.* Cancer Res, 1991. **51**(3): p. 794-8.

147. Abrams, J.M. and M.A. White, *Coordination of cell death and the cell cycle: linking proliferation to death through private and communal couplers.* Curr Opin Cell Biol, 2004. **16**(6): p. 634-8.

148. Fei, P., et al., *Bnip3L is induced by p53 under hypoxia, and its knockdown promotes tumor growth.* Cancer Cell, 2004. **6**(6): p. 597-609.

149. Chourasia, A.H. and K.F. Macleod, *Tumor suppressor functions of BNIP3 and mitophagy.* Autophagy, 2015. **11**(10): p. 1937-8.

150. Grier, H.E., et al., *Addition of ifosfamide and etoposide to standard chemotherapy for Ewing's sarcoma and primitive neuroectodermal tumor of bone.* N Engl J Med, 2003. **348**(8): p. 694-701.

151. Womer, R.B., et al., *Randomized controlled trial of interval-compressed chemotherapy for the treatment of localized Ewing sarcoma: a report from the Children's Oncology Group.* J Clin Oncol, 2012. **30**(33): p. 4148-54.

152. Bacci, G., et al., *Therapy and survival after recurrence of Ewing's tumors: the Rizzoli experience in 195 patients treated with adjuvant and neoadjuvant chemotherapy from 1979 to 1997.* Ann Oncol, 2003. **14**(11): p. 1654-9.

153. McTiernan, A.M., et al., *Improving Outcomes After Relapse in Ewing's Sarcoma: Analysis of 114 Patients From a Single Institution.* Sarcoma, 2006. **2006**: p. 83548.

154. Delattre, O., et al., *Gene fusion with an ETS DNA-binding domain caused by chromosome translocation in human tumours.* Nature, 1992. **359**(6391): p. 162-5.

155. Lessnick, S.L. and M. Ladanyi, *Molecular pathogenesis of Ewing sarcoma: new therapeutic and transcriptional targets.* Annu Rev Pathol, 2012. **7**: p. 145-59.

156. Aman, P., et al., *Expression patterns of the human sarcoma-associated genes FUS and EWS and the genomic structure of FUS.* Genomics, 1996. **37**(1): p. 1-8.

157. Bailly, R.A., et al., *DNA-binding and transcriptional activation properties of the EWS-FLI-1 fusion protein resulting from the t(11;22) translocation in Ewing sarcoma.* Mol Cell Biol, 1994. **14**(5): p. 3230-41.

158. Crompton, B.D., et al., *The genomic landscape of pediatric Ewing sarcoma.* Cancer Discov, 2014. **4**(11): p. 1326-41.

159. Arvand, A. and C.T. Denny, *Biology of EWS/ETS fusions in Ewing's family tumors.*

Oncogene, 2001. **20**(40): p. 5747-54.

160. Boeva, V., et al., *De novo motif identification improves the accuracy of predicting transcription factor binding sites in ChIP-Seq data analysis.* Nucleic Acids Res, 2010. **38**(11): p. e126.

161. Guillon, N., et al., *The oncogenic EWS-FLI1 protein binds in vivo GGAA microsatellite sequences with potential transcriptional activation function.* PLoS One, 2009. **4**(3): p. e4932.

162. Riggi, N., et al., *EWS-FLI1 utilizes divergent chromatin remodeling mechanisms to directly activate or repress enhancer elements in Ewing sarcoma.* Cancer Cell, 2014. **26**(5): p. 668-81.

163. Gangwal, K., et al., *Microsatellites as EWS/FLI response elements in Ewing's sarcoma.* Proc Natl Acad Sci U S A, 2008. **105**(29): p. 10149-54.

164. Worch, J., et al., *Racial differences in the incidence of mesenchymal tumors associated with EWSR1 translocation.* Cancer Epidemiol Biomarkers Prev, 2011. **20**(3): p. 449-53.

165. May, W.A., et al., *The Ewing's sarcoma EWS/FLI-1 fusion gene encodes a more potent transcriptional activator and is a more powerful transforming gene than FLI-1.* Mol Cell Biol, 1993. **13**(12): p. 7393-8.

166. Braunreiter, C.L., et al., *Expression of EWS-ETS fusions in NIH3T3 cells reveals significant differences to Ewing's sarcoma.* Cell Cycle, 2006. **5**(23): p. 2753-9.

167. Uren, A., et al., *Beta-platelet-derived growth factor receptor mediates motility and growth of Ewing's sarcoma cells.* Oncogene, 2003. **22**(15): p. 2334-42.

168. Tirode, F., et al., *Mesenchymal stem cell features of Ewing tumors.* Cancer Cell, 2007. **11**(5): p. 421-9.

169. Riggi, N., et al., *Development of Ewing's sarcoma from primary bone marrow-derived mesenchymal progenitor cells.* Cancer Res, 2005. **65**(24): p. 11459-68.

170. Riggi, N., et al., *EWS-FLI-1 expression triggers a Ewing's sarcoma initiation program in primary human mesenchymal stem cells.* Cancer Res, 2008. **68**(7): p. 2176-85.

171. DuBois, S.G., et al., *Comparative evaluation of local control strategies in localized Ewing sarcoma of bone: a report from the Children's Oncology Group.* Cancer, 2015. **121**(3): p. 467-75.

172. *Ewing Sarcoma Treatment (PDQ(R)): Health Professional Version*, in *PDQ Cancer Information Summaries*. 2002: Bethesda (MD).

173. Wagner, T.D., et al., *Combination short-course preoperative irradiation, surgical resection, and reduced-field high-dose postoperative irradiation in the treatment of*

tumors involving the bone. Int J Radiat Oncol Biol Phys, 2009. **73**(1): p. 259-66.

174. Krishnadas, D.K., et al., *A phase I trial combining decitabine/dendritic cell vaccine targeting MAGE-A1, MAGE-A3 and NY-ESO-1 for children with relapsed or therapy-refractory neuroblastoma and sarcoma.* Cancer Immunol Immunother, 2015. **64**(10): p. 1251-60.

175. Cho, D., et al., *Cytotoxicity of activated natural killer cells against pediatric solid tumors.* Clin Cancer Res, 2010. **16**(15): p. 3901-9.

176. Evans, C.H., et al., *EWS-FLI-1-targeted cytotoxic T-cell killing of multiple tumor types belonging to the Ewing sarcoma family of tumors.* Clin Cancer Res, 2012. **18**(19): p. 5341-51.

177. Berghuis, D., et al., *Reduced human leukocyte antigen expression in advanced-stage Ewing sarcoma: implications for immune recognition.* J Pathol, 2009. **218**(2): p. 222-31.

178. Patel, M., et al., *Tumor-specific retargeting of an oncogenic transcription factor chimera results in dysregulation of chromatin and transcription.* Genome Res, 2012. **22**(2): p. 259-70.

179. Prieur, A., et al., *EWS/FLI-1 silencing and gene profiling of Ewing cells reveal downstream oncogenic pathways and a crucial role for repression of insulin-like growth factor binding protein 3.* Mol Cell Biol, 2004. **24**(16): p. 7275-83.

180. McLean, C.Y., et al., *GREAT improves functional interpretation of cis-regulatory regions.* Nat Biotechnol, 2010. **28**(5): p. 495-501.

181. Mitsiades, N., et al., *Ewing's sarcoma family tumors are sensitive to tumor necrosis factor-related apoptosis-inducing ligand and express death receptor 4 and death receptor 5.* Cancer Res, 2001. **61**(6): p. 2704-12.

182. Kontny, H.U., et al., *Sensitivity of Ewing's sarcoma to TRAIL-induced apoptosis.* Cell Death Differ, 2001. **8**(5): p. 506-14.

183. Picarda, G., et al., *Preclinical evidence that use of TRAIL in Ewing's sarcoma and osteosarcoma therapy inhibits tumor growth, prevents osteolysis, and increases animal survival.* Clin Cancer Res, 2010. **16**(8): p. 2363-74.

184. Karl, I., et al., *TRAF2 inhibits TRAIL- and CD95L-induced apoptosis and necroptosis.* Cell Death Dis, 2014. **5**: p. e1444.

185. Doiguchi, M., et al., *Spergen-1 might be an adhesive molecule associated with mitochondria in the middle piece of spermatozoa.* Dev Biol, 2002. **252**(1): p. 127-37.

186. Nagao, T., et al., *MAGE-A4 interacts with the liver oncoprotein gankyrin and suppresses its tumorigenic activity.* J Biol Chem, 2003. **278**(12): p. 10668-74.

187. Sakurai, T., et al., *A cleaved form of MAGE-A4 binds to Miz-1 and induces apoptosis in human cells.* J Biol Chem, 2004. **279**(15): p. 15505-14.

188. Tondera, D., et al., *SLP-2 is required for stress-induced mitochondrial hyperfusion.* EMBO J, 2009. **28**(11): p. 1589-600.

189. Smirnova, E., et al., *Dynamin-related protein Drp1 is required for mitochondrial division in mammalian cells.* Mol Biol Cell, 2001. **12**(8): p. 2245-56.

190. Karbowski, M., A. Neutzner, and R.J. Youle, *The mitochondrial E3 ubiquitin ligase MARCH5 is required for Drp1 dependent mitochondrial division.* J Cell Biol, 2007. **178**(1): p. 71-84.